Blast Performance of Hollow Metal Steel Doors

Colton Keene

Thesis submitted to the
Faculty of Virginia Polytechnic Institute and State University
in partial fulfillment of the requirements for the degree of

Master of Science

in

Civil Engineering

Eric Jacques, Chair
Matthew Hebdon
Ioannis Koutromanos

August 16, 2019
Blacksburg, Virginia

Keywords: Hollow Metal Doors, Blast Doors, Shock Tube, Testing, Finite Element Analysis, SDOF Analysis, Dynamic, Blast Resistant Doors

Abstract

Blast Performance of Hollow Metal Steel Doors

Colton Keene

Recent terrorist attacks and accidental explosions have prompted increased interest in the blast resistant design of high-risk facilities, including government offices, private sector buildings, transportation terminals, sporting venues, and military facilities. Current blast resistant design standards prioritize the protection of the primary structural system, such as walls, columns, and beams, to prevent a disproportionate collapse of the entire structure. Secondary structural systems and non-structural components, such as blast resistant doors, are typically outside the focus of standard building design. Components such as blast resistant doors are designed and manufactured by private sector entities, and their details are confidential and considered proprietary business information. For this reason, scientific research on blast resistant doors is sparse and most test results are unavailable for public consumption. Nevertheless, the performance of blast doors is crucial to the survival of building occupants as they are relied upon to contain blast pressures and remain operable after a blast event to allow ingress/egress. These important roles highlight the critical need for further research and development to enhance the level of protection provided by components that are often not considered in any detail by protective design practice. This thesis presents a combined experimental and analytical research program intended to support the development of blast resistant hollow metal doors.

A total of 18 static beam-assembly tests were conducted, which consisted of the flexural four-point bending of door segments, to inform on the performance characteristics of full-sized blast resistant doors. Six tests were conducted to evaluate the effectiveness of three skin-core construction methodologies, which consisted of one epoxy and two weld attachment specifications, between door skins and their internal reinforcing structures. The remaining 12 tests were performed to evaluate the in-situ performance of hinge hardware typically installed on blast resistant door assemblies. The results of the skin-core construction tests demonstrated that closely spaced weld patterns would provide the best blast performance. The results of the hinge hardware

tests demonstrated that hinges which provided a continuous load-path directly into the primary structural core elements of the door frame and door were ideal; furthermore, robust hinges with fully-welded or continuous knuckles were best suited for limiting undesirable deformations.

A semi-empirical analytical methodology was developed to predict the global deformation response of full-sized hollow metal doors subjected to blast loading in the seated direction. The goal was to provide practicing engineers who are competent but non-expert users of high fidelity simulations with the flexibility to conduct in-house evaluation of the blast resistance of hollow metal doors without having to conduct live explosive or simulated blast tests. A finite element analysis was first performed to compute the door resistance function. Hollow metal door construction was idealized using a bulk material sandwiched between sheet metal skins and internally stiffened by stringers. The properties of the bulk material were calibrated such that the deformability of the idealized core reasonably approximated the global load-deformation behavior which occurs due to loss of composite action when welds fail. The resistance curves were then used in a single-degree-of-freedom dynamic analysis to predict the displacement response of the door subjected to blast loading. The proposed methodology was first validated against the static beam-assembly flexural tests. It was then extended to the case of a full-sized door subjected to shock tube blast testing using results published in the literature. The proposed methodology was found to reasonably approximate the out-of-plane load-deformation response of beam-assemblies and full-size doors, provided the bulk material properties of the idealized core are calibrated against experimental data.

Finally, the new Virginia Tech Shock Tube Testing Facility was introduced. A description of the facility, including an overview of the shock tube's location, construction, main components, instrumentation, and key operating principles, were discussed. Operating guidelines and procedures were outlined to ensure safe, controlled, and repeated blast testing operations. A detailed calibration plan was proposed, and future work pertaining to the development of blast resistant hollow metal doors was presented.

General Audience Abstract

Blast Performance of Hollow Metal Steel Doors

Colton Keene

Recent terrorist attacks and accidental explosions have motivated an increase in the demand for blast protection of critical infrastructure. Secondary components, such as doors, play a pivotal role in the protection of occupants as they ensure blast pressures are contained and ingress/egress is possible after a blast event. Experiments have been conducted to characterize the performance of several door construction methodologies (i.e., epoxy, reduced weld requirements) and the in-situ performance of hinge hardware through quasi-static testing of beams whose construction closely mimics that of a full-size door. Results of door construction testing indicated that, whenever possible, blast resistant doors should be constructed with full weld attachment (maximum specification with weld spaced every 3") as these doors were found to provide the greatest resistance. Due to inconsistent and sudden failure mode, epoxy skin-core construction is not recommended for use in blast resistant doors at this time. Hinge testing determined that hinge mounting plates (which hinge hardware leaves are attached to) should be integrally connected to the frame and door internal reinforcing elements to provide adequate strength and that hinges with fully welded knuckles should be used for blast applications to limit deformation and facilitate post-blast operability. An ABAQUS finite element analysis methodology utilizing a "skins and stringers" approach to generate a beam-assembly model resulted in an adeauate prediction of load-deflection results recorded during beam-assembly testing after calibration of the model. An extension of this modeling approach was used to model full-size doors and adequately captured their dynamic performance when subjected to blast loading. Finally, preparation of the Virginia Tech Shock Tube Testing Facility, which is currently in progress, is summarized with regards to its calibration and the first round of testing which will focus on providing more data for comparison with the analysis methodology developed in this research.

Acknowledgments

I want to thank my advisor, Dr. Eric Jacques, and my two committee members, Dr. Koutromans and Dr. Hebdon for direction and support throughout the research and development presented in this thesis. I would like to also thank a fellow undergraduate student, Luis Hernandez, for his help with the testing and data processing.

I want to also extend my gratitude to my fellow research peers, faculty, and staff at the Thomas M. Murray Structures Lab at Virginia Tech, as well as the faculty and staff of the SEM program at Virginia Tech for their constant willingness to help and provide support throughout this research project.

I would finally like to thank AMBICO for funding this research and donating specimens for testing.

Table of Contents

Chapter 1. Introduction 13

1.1. General 13

1.2. Previous Research of Blast resistant Steel Doors 14

1.3. Applicable Codes and Standards 23

1.4. Research Needs 27

1.5. Objective 27

1.6. Scope 28

Chapter 2. Beam-Assembly Tests 29

2.1. General 29

2.2. Test Specimens 29

2.2.1 Door Construction Specimens 31

2.2.2 Hardware Capacity Specimens 33

2.2.3 Material Properties 40

2.3. Experimental Program 41

2.3.1 Test Fixture 41

2.3.2 Instrumentation 43

2.3.3 Procedure 44

2.4. Experimental Results 45

2.4.1 Door Construction Specimens 45

2.4.2 Hardware Capacity Specimens 52

2.5. Discussion 66

2.6. Recommendations 73

Chapter 3. Analytical Modeling of Blast Doors 75

3.1. General 75

3.2. Beam Assembly Modeling 75

3.2.1 Modeling Strategy 76

3.2.2 Modeling Procedure 76

3.2.3 Model Calibration 78

3.2.4 Discussion of Model 82

3.3. Full-Sized Hollow Metal Blast Door Modeling 83

3.3.1 Overview 83

3.3.2 Review of Previous Full-size Door Tests 83

3.3.3 Analysis 87

Chapter 4. Conclusions and Recommendations 94

4.1. Conclusions 94

4.2. Recommendations 96

4.3. Recommendations for Future Research 98

References 99

Appendix A: VT Shock Tube Testing Facility 103

A1. General 103

A2. Facility Description 103

A2.1 Overview 103
A2.2 Shock Tube Construction 105
A2.3 Location 111
A2.4 Instrumentation and Control 112
A2.5 Operating Procedure 113

A3. Calibration Plan 117

A3.1 Simulator Calibration Curves 117
A3.2 Determination of Planarity of the Shock Wave 118

A4. Sample Test Data 121

A5. Future Work 122

List of Figures

Figure 1.1: Typical door cross-section and blast resistant mechanism (Anderson et al. 2003). ...15
Figure 1.2: Photographs from typical shock tube door assembly test (Lowak et al. 2011). 18
Figure 1.3: Typical door specimen configuration and failure modes (Jacques, et al. 2015).....21
Figure 1.4: Typical specimens and failure modes (Shen et al. 2010) 23
Figure 2.1: Typical beam-assembly door panel construction details. 30
Figure 2.2: Beam-assembly frame construction details. 31
Figure 2.3: *6″* PBB Stainless Hinges (Series 4).....34
Figure 2.4: Hinge Pins & 4.5" Hinges (Series 5). 35
Figure 2.5: Hinge Retainer & 4.5" Hinges (Series 6). 36
Figure 2.6: Pin & Barrel Hinge (Series 7). 37
Figure 2.7: Surelock S2HA7 Mortised 5.75" Hinge (Series 8). 38
Figure 2.8: Integrally connected hinge mounting plate configuration for Series 8 Surelock Hinges. 38
Figure 2.9: Series 9A Gallery Hinges 39
Figure 2.10: 6" PBB Mild Steel Hinges (Series 9B). 40
Figure 2.11: Average representative stress-strain behavior for *14*-gauge and *16*-gauge sheet metal. 41
Figure 2.12: Test fixture schematic for door construction and hardware capacity tests. 42
Figure 2.13: Photographs of the beam-assembly test fixture. 43
Figure 2.14: Comparison of load-deflection behavior of Series 1: Epoxy Attachment beam-assembly specimens. 45
Figure 2.15: Post-test photographs taken of specimens from Series 1: Epoxy Attachment. 46
Figure 2.16: Photographs of epoxy and weld failures observed during Series 1 tests. 47
Figure 2.17: Comparison of load-deflection behavior of Series 2: Partial Weld Attachment beam-assembly specimens 48
Figure 2.18: Post-test photographs of Series 2 door panels. 49
Figure 2.19: Photographs of typical failure modes observed during Series 2 tests. 50
Figure 2.20: Comparison of load-deflection behavior of Series 3: Plug Weld Attachment (100% spec) beam-assembly specimens. 51
Figure 2.21: Post-test photographs taken of Series 3: Full weld attachment. 51
Figure 2.22: Comparison of load-deflection behavior of Series 4: 6” PBB Stainless Steel Hinges. 53
Figure 2.23: Typical door stop HSS frame-skin weld failure. 54
Figure 2.24: Post-test Series 4 frame deformation photos. 54
Figure 2.25: Post-test damage Series 4 photos. 55
Figure 2.26: Comparison of load-deflection behavior of Series 5: Frame-Pins & 4.5" Hinges. ...56
Figure 2.27: Post-test photos of Series 5 (Frame-Pins and 4.5" hinges). 57
Figure 2.28: Comparison of load-deflection behavior of Series 6: Hinge retainer & 4.5" Hinges. 58
Figure 2.29: Series 6 post-test frame deformations. 59
Figure 2.30: Series 6 post-test overall frame-skin deformations. 59

Figure 2.31: Series 6 post-test hinge deformations. 59
Figure 2.32: Comparison of load-deflection behavior of Series 7: Pin & Barrel Hinges. 60
Figure 2.33: Series 7 post-test hinge deformations. 61
Figure 2.34: Comparison of load-deflection behavior of Series 8: S2HA7 Mortised 5.75" Hinge. 62
Figure 2.35: Series 8 post-test deformations. 62
Figure 2.36: Comparison of load-deflection behavior of Series 9: Gallery Hinges. 63
Figure 2.37: Series 9A post-test deformations. 64
Figure 2.38: Comparison of load-deflection behavior of Series 9B: 6” PBB Mild Steel Hinges. 65
Figure 2.39: Series 9B post-test deformations. 66
Figure 2.40: Comparison of load-deflection behavior for the three door construction methodologies. 68
Figure 3.1: Partitioning and core elements of skins and stringers beam-assembly ABAQUSmodel. 77
Figure 3.2: Boundary conditions and mesh discretization of the skins and stringers for beam-assembly ABAQUS model. 78
Figure 3.3: Beam-assembly model resistance curve predictions with elastic-plastic bulk materials. 79
Figure 3.4: Generalized stress-strain curve prescribed to bulk materials of Series 2 and 3 beam-assemblies for modeling resistance curve unloading. 80
Figure 3.5: Beam-assembly resistance curves predictions with unloading stress-strain relations for bulk material. 80
Figure 3.6: Deformed shape of the model showing both vertical and horizontal (flexural shortening) deformation. 81
Figure 3.7: Flexural shortening analysis comparison with specimen 3B of the beam-assembly tests. 82
Figure 3.8: Conceptual door construction details for ST-9A blast resistant door (Jacques et al. 2015). 84
Figure 3.9: University of Ottawa shock tube fixture for full-size door testing (Jacques et al., 2015). 85
Figure 3.10: Experimental results for ST-9A blast test 1. 86
Figure 3.11: Reflected pressure, impulse, and displacement-time history for Test 2 of ST-9A. ..86
Figure 3.12: Boundary conditions and deformed mesh for full-size door assembly FEA. 88
Figure 3.13: FEA model resistance curves with varying bulk material properties. 89
Figure 3.14: Dynamic SDOF solutions for three iterations of bulk material properties compared with ST-9A test 1 and test 2 shock-wave displacement-time histories 92
Figure A.1: Overview of the Virginia Tech Shock Tube Testing Facility. 104
Figure A.2: Photograph of Virginia Tech Shock Tube Testing Facility. 105
Figure A.3: Detonation Chamber of Virginia Tech Shock tube. 106
Figure A.4: Detonation Chamber components. 107
Figure A.5: Volume of gas in detonation chamber as a function of the distance from the rear wall of the detonation chamber. 108
Figure A.6: Photograph of the transition section of the shock tube. 109
Figure A.7: Photograph of the reaction frame of the Virginia Tech Shock Tube. 110
Figure A.8: Site layout of the Virginia Tech Shock Tube Testing Facility. 111
Figure A.9: Instrumentation and operations schematic for shock tube facility. 113

Figure A.10: *10'×10'* Steel Calibration Plate Reflecting Surface with Gauge Mount Locations (Shown from Inside shock-tube). 119
Figure A.11: Pressure and impulse-time histories for test shot 1 using the Virginia Tech Shock Tube. 121
Figure A.12: Shock tube test fixture for full-size door assembly testing. 122

List of Tables

Table 1-1 Door Response Categories and Descriptions (ASTM 2012). 25
Table 2-1: Test matrix for the skin construction beam-assembly tests. 32
Table 2-2: Test Matrix for Hardware Capacity Testing 33
Table 3-1: Summary of experimental and predicted results for door test ST-9A 87
Table A-1: Sample calibration data for Peak Reflected Pressure, Impulse, and Cart Movement Calibration Curve Values 118
Table A-2: Properties for Analysis of Shock Wave Planarity on the Reflecting Calibration surface. 120

Notations

Acronym		Definition
SDOF	=	Single Degree of Freedom
LVDT	=	Linear Variable Displacement Transducer
FEA	=	Finite Element Analysis
DIF	=	Dynamic Increase Factor

Symbol		Definition
P	=	Load, the total load used in load-deflection curves
δ	=	Deflection, used in load-deflection curves
R	=	Resistance, used to represent total load resistance
P_r	=	Reflected pressure
I_r	=	Reflected impulse
t_d	=	Positive phase duration
t_a	=	Relative time of arrival
v_o	=	Arrival velocity of shock wave
L	=	Length
k_{ML}	=	Load transformation factor
$u(t)$	=	Time-varying displacement of an SDOF
$\ddot{u}(t)$	=	Time-varying acceleration of an SDOF
m_t	=	The total mass of an SDOF system

Chapter 1. Introduction

1.1. General

Blast protection of structural and non-structural building components has become a high priority considering recent terrorist attacks and accidental explosions. This type of protective design, concerning non-nuclear level blast pressures, is a primary concern for high-risk government facilities, private sector buildings, transportation terminals, sporting venues, military installations, and other critical facilities or high-value targets. According to (ASCE 2011), blast resistant buildings are designed to ensure the primary structural system (i.e., load-bearing walls, columns, and beams, etc.) are designed to maintain the building envelope and minimize flying debris. Standard protective design practice is typically focused on the primary structural system and the exterior cladding, while blast resistant doors are proprietary and outside the typical practice for building design (ASCE 2011). Typical performance objectives for the design of blast resistant doors include: (i) no blast pressure leakage before, during or after the blast event; (ii) no structural damage or permanent deformations; (iii) maintaining operability and egress after the event.

Hollow metal blast resistant doors are commonly used in commercial and government buildings for emergency egress, equipment access, delivery areas, and utility rooms (ASCE 2011). They are relied upon to compartmentalize a facility during a blast event and, if designed correctly, remain operable to allow occupants to evacuate after the blast. Operability allows the safe ingress and egress of emergency personnel and building occupants. Typical sizes of blast resistant doors range from around *3'×7'*to *4'×8'* for single doors, and up to *8'×8'* for double doors, with thicknesses in the range of *1-3/4"* to *2"* being typical. Doors are constructed using *14* gauge to *20* gauge cold rolled steel sheets as external skins that are internally stiffened with sheet metal stiffeners or polystyrene or honeycomb materials. Internal HSS tubes are often added to increase the flexural strength and stiffness of door panels. Specified blast pressure resistance of these doors typically ranges from *1 psi* up to *20 psi*, depending on client-specific needs. Special hinge and latch hardware are installed to ensure the door remains operable after a blast event and does not become dislodged or generate flying debris. Doors subjected to blast pressures that tend to close

the door are said to be seated, meaning the door is in contact at all points with the frame during the inbound response. The unseated response, which occurs when the door is loaded in such a way that it tends to open, is more critical than seated response as the load path from the door to the frame is directly through the hinge/latch hardware. Seated doors often fail when the door pushes past the stop due to a lack of internal structural integrity, while the failure of hardware is the primary concern during the unseated response.

Blast resistant doors are designed and manufactured by a variety of companies that have capitalized on the need for this market. Some of these companies include: AMBICO Limited, a Canadian manufacturer of steel blast resistant doors, blast resistant windows and window frames, US Aluminum, which focuses on blast resistant storefronts, Overly Door Company, a manufacturer of blast resistant and bullet-proof doors and Chem-Pruf Door Company which focus is on blast resistant doors. Performance qualification of blast resistant doors can either be performed through (i) full-scale blast testing of replicate doors subjected to the specified airblast pressure-impulse combination; (ii) equivalent static uniform pressure loading; (iii) analysis and design using finite element methods and other means provided such techniques have been validated against experimental data. It is important to note that a blast door is a series of components – the door, frame, hardware, anchorage, and other accessories – which often necessitates consideration of system-level behavior to ensure the specified performance objectives can be achieved for a given design pressure-impulse combination. As a result, door manufacturers typically qualify the entire assembly (doors, frames, and hardware) per the ASTM F2927 (ASTM 2012) or ASTM F2247 (ASTM 2018), which will be discussed later, to validate the blast resistant performance of their products.

1.2. Previous Research of Blast resistant Steel Doors

Anderson and Dover (2003)

Anderson and Dover of the Air Force Research Laboratory (AFRL) tested lightweight, blast resistant doors used to contest increasing terrorist threats. The doors tested were lightweight Accordion-Flex doors. As the name suggests, the surface of these doors was composed of a repeating fold, much like an accordion, as shown in Figure 1.1 (a). The design of their surface area allowed the doors the ability to expand over twice their original surface area during a blast event while remaining mostly elastic (Anderson et al. 2003).

The doors were designed to satisfy the following three performance objectives: (i) they had to be lightweight enough to be used in general purpose and allow for easy entry; (ii) the doors were to withstand the required blast-pressure and (iii) the doors were to be contained in a frame that would prevent them from becoming a projectile. The doors were intended to serve as both an option for retrofit or new construction.

The doors were tested and achieved desired results under the specified reflected pressures of *50 psi*. These doors resisted blast loading through the use of membrane action, a damping chamber, and air vents. Membrane action refers to the replacement of the door skin with a flexible non-rigid element that allows maximum elasticity during a blast event. The damping chamber and air vents work together to achieve a damping effect. As the blast wave contacts the surface of the door, the damping chamber (space between the front and back door panel) decreases in volume as air is allowed to exit the chamber through venting on the door sides, as illustrated in Figure 1.1 (b). During testing, the primary mode of failure was determined to be damage to the mounting hardware. Minimal damages to the doors and frames themselves were observed.

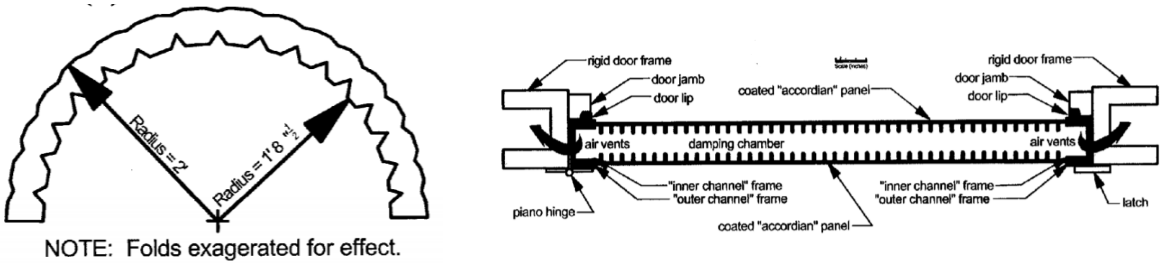

(a) Accordion door membrane. (b) Typical cross-section of the door.

Figure 1.1: Typical door cross-section and blast resistant mechanism (Anderson et al. 2003).

<u>Salomoni and Mazzuco (2013)</u>

Salomoni and Mazzuco conducted a study to model the non-linear behavior of nineteen different steel blast resistant door configurations under dynamic loads from explosive hazards. Window specimens were also analyzed. Door specimen sizes ranged from *39.4"* by *78.7"* to *138"* by *177"*. Peak pressures analyzed ranged with door sizes from *0.4 psi* to *4.4 psi* (Salomoni et al. 2013).

Finite element analysis was conducted on all door specimens; only one was reported; however, the *39.4"* by *82.7"*. The door analyzed was internally braced with seven horizontal beam stiffening elements. The analysis concluded the maximum stress and displacements in both the

internal steel frame and external steel plating. These results were predicted for the peak phase and the rebound phase of the blast event.

Experimental testing was conducted to validate the numerically determined results of the peak phase analysis. The explosive blast wave was dynamically reproduced through the use of a mass impact on the door's surface. A result of this test method was that the rebound phase of the design blast could not be accurately validated.

A key observation resulting from testing was that the door frame and counter-frame behaved as springs in series, thus creating a desirable dampened behavior for blast resistance. The structural significance of this indicated that the door was able to withstand around *1.5* to *2.0* times its design loading. It was concluded from this study that door frame deformations should be accounted for during analysis as they are desirable behaviors.

Veeredhi and Rao (2015)

Veeredhi and Rao utilized the finite element software ABAQUS to predict the damage to a stiffened steel plate door resulting from blast loading. The analysis was performed assuming peak pressures that ranged from *20 psi* to *71 psi* imposed onto the stiffened door. Three different shapes of stiffening reinforcement were analyzed (T, I, and HAT shaped). The stiffeners thicknesses were varied from *0.217"* to *0.335"* for all specimens. Mid-point displacement was the focus of the analysis (Veeredhi et al. 2015)

Stiffeners were arranged such that there were four vertical and two horizontal spaced evenly across the respective spans of the door. Results indicated for all thicknesses and peak pressures, HAT stiffeners were the most efficient, and T shaped stiffeners were the least efficient for blast resistance. The deflections of HAT stiffened doors were around half of those deflections of T stiffened doors for every scenario. The I-shape stiffener performance was determined to be between HAT and T shapes.

Validation was provided through a comparison with previously conducted experiments. The result of the comparison indicated that displacements were within *2%* to *8%* of the reference values. It is mentioned, however, that there are few experimental or numerical studies to reference results for comparison, indicating a need for more research in this area.

Yuen and Nurick (2005)

Yuen and Nurick studied the effect of varying stiffener patterns on mild steel plates subjected to uniform blast loading. Stiffener configurations were as follows: unstiffened control plate, single vertical stiffener, double vertical stiffeners, two perpendicular stiffeners, and two verticals crossed by one horizontal stiffener (Yuen et al. 2005).

The experimental blast was replicated utilizing a plastic explosive (PE 4). The experiment metal for all plate configurations for a range of impulses from *6.97 lbs-s* to *9.1 lbs-s*. The conclusion of the experimental results indicated, for a given impulse, configurations with more stiffeners displayed the least deflection.

More interestingly, the results also indicated that the configurations with more stiffeners were more susceptible to tearing for any given impulse. This was determined to be because the stiffeners were inhibiting plastic deformations that would otherwise cause larger deflections for an un-stiffened plate (allowing energy dissipation). The results of finite element analysis agreed with the results of the experiment only when the temperature-dependent properties of the mild steel were considered.

Lowak et al. (2016)

Research was conducted by Baker Engineering and Risk Consultants to determine the effectiveness of using load-deflection data from the static testing of doors as input to a single degree of freedom analysis tool to predict the blast response of doors. The doors, which were the focus of the research were light-gauge metal doors considered of high use in governmental facilities not specifically designed to withstand blast loading (Lowak et al. 2011). A photograph of a typical door specimen after shock tube testing is illustrated in Figure 1.2 (a).

Doors were statically tested to failure and dynamically tested utilizing a shock tube. Static testing provided resistance functions to predict dynamic behavior using SDOF analysis, while dynamic testing was done to validate this analysis method. Door panels ranged from *14* gauge to 16 gauge in thickness. A variety of stiffening configurations were represented in the door specimens (i.e., vertically stiffened or polystyrene core). Blast loading ranged from *4.8 psi* to *12.6 psi*. A typical load-deflection curve obtained from static testing of sealed door assemblies can be referenced in Figure 1.2 (b). From this load-deflection curve, it can be seen that there is an initial yielding of the door and subsequent regaining of strength before final failure.

It was concluded that using load-deflection data from resistance functions and SDOF analysis yielded accurate models for the dynamic behavior of light-gauge hollow metal door systems. It was also discussed that finite-element analysis models could be used to predict dynamic behavior as well. Both static and dynamic load tests determined that frame stiffness and anchorages play a large role in the performance of the doors tested (see latch strike plate failure in Figure 1.2 (c)); as such, this research places emphasis on considering these components of a door system for future evaluations (Lowak et al. 2011).

(a) Door assembly after dynamic testing.

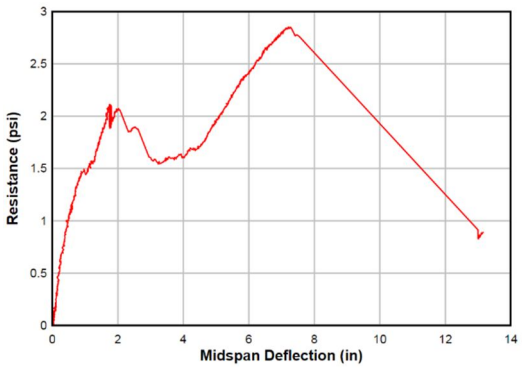

(b) Typical static door resistance curve.

(c) Typical latch strike plate failure via dynamic testing.

Figure 1.2: Photographs from typical shock tube door assembly test (Lowak et al. 2011).

Chen and Hao (2014)

This thesis conducted at the University of Western Australia presented the analysis of three forms of protective blast resistant steel paneling: (i) multi-arched double-layered panels, (ii) stiffened multi-arched double-layered panels and (iii) sandwich panels with rotational friction dampers. For types i. and ii., the arched panels were configured such that the arched surface was

exterior convex towards the blast wave. For type (iii) panels, rotational dampers were sandwiched between two steel panels. The dynamic response and energy absorption were studied for each panel type using experimental and numerical methods. Parametric studies were conducted for each panel type to determine the best configuration (i.e., placement of dampers, number/dimensions of arched segments, etc.).

The finite element analysis program LS-DYNA was utilized to analyze the performance of the double-layered arched-panel. It was determined that the double-layered arched panel performed better than flat panels, which were used as a control, for a given blast load. The parametric analysis determined that performance increased (less deflection and reduced boundary force reactions) as the arch height increased and the ratio of external panel thickness (the arched panel) to internal panel thickness increased.

Experimental validation was conducted on the double-layered arched panel by imitating blast loadings with a pendulum impact test system wherein a pendulum was used to strike an air-bag which transferred the force as planer stress to the surface of arched panels. The experimental tests validated the results acquired for double-layered arched panels using the LS-DYNA analysis. Results indicated both a reduction in deflection and boundary reaction forces as the ratio of outer panel thickness to internal thickness increased and as the arch height increased for the arches on the external steel panel.

Results analyzed of the rotational friction dampers were obtained using theoretically derived and numerical simulations. It was determined that the addition of friction dampers between two steel panels greatly reduced peak deflections and boundary forces for a given blast load. The efficiency of this reduction in unwanted effects depended on the pre-loading of the dampers as well as the coefficient of friction of the steel used for the dampers.

Like the analysis of rotational stiffened (type iii. panels), only numerical simulations were carried out for the stiffened version of the double-layered arched panels (type ii. panels). It was determined that the placement of stiffeners further improved the effectiveness of the panels to resist blast loading deflections over that of the un-stiffened panels; however, stiffeners increased boundary loading. This research highlighted the parametric properties of a surface, such as a door could play a pivotal role in the resistance of dynamic forces (Chen et al. 2014).

Jacques, Lloyd, Berry, Saatcioglu, and Shinder (2015)

(Jacques et al. 2015) worked with the specialty door manufacturer AMBICO to develop steel blast resistant doors to meet the requirements associated with the minimum anti-terrorism marketplace. The research was conducted at the University of Ottawa's Shock Tube Testing Facility.

Ten door specimens, *84"* tall, and *36"* wide were tested. Door paneling consisted of *14* gauge galvanneal steel sheet metal. Four stiffening configurations were tested: specimens with stiffened rigid insulation cores, vertical hat stiffeners, horizontal hat stiffeners and a specimen with a stiffened insulation core and a single horizontal HSS horizontal stiffener. Typical door specimens listed above can be referenced in Figure 1.3 (a).

The specimens were tested in the seated direction (bearing against the door frame) aside from one specimen tested in the unseated to measure the capacity of the door latch. Both high-pressure and low-pressure frames were tested on four (4) and six (6) specimens, respectively. Small *5"* by *20"* and larger *24"* by *36"* windows were tested on three and two-door specimens respectively.

Doors with stiffened rigid insulation were observed to fail along the bottom edge in such a way that caused them to push past the door stop and become unseated (Figure 1.3 (b)). Testing of vertically stiffened doors highlighted the critical importance of the number of welds that attach the vertical HAT stiffeners to the bottom HSS horizontal stiffener; as the failure of this connection between the two adjacent framing members caused this specimen to push past the doorstop. Figure 1.3 (c) shows the failure mode of this specimen.

Horizontally stiffened specimens out-performed vertically stiffened specimens, with the only failure occurring in several bolts near the hinge after about *11 psi* of blast loading. The best performance observed came from the fourth specimen type (structural rigid insulation core). The only damage was that of deformation of the external door skin due to the failure of several plug welds.

For several of both the seated and unseated tests, latch performance was an issue of concern. Latches failed through rupture of the bolting mechanism for unseated direction, rendering the door useless. The latch failed during the seated tests causing the doors to become open during the rebound phase of the blast.

Smaller window configurations discussed above performed quite well across the board. Larger windows were discovered to fail catastrophically, sending large projectiles (up to *8.8 lbs*) flying away from the door. See a comparison of window failures in Figure 1.3 (d).

The research conducted provided several recommendations utilized by the manufacturer AMBICO Ltd. It is determined that doors should be stiff enough to resist shortening in laterally and vertically not to become unseated. Latches and any connecting components should be designed to meet and exceed forces required to hold the door in place. Doorstops should be designed to accommodate anticipated door shortening to stop possible unseating. The research also highlighted the importance of redundant load paths and frame connection points for the internal structure of the door.

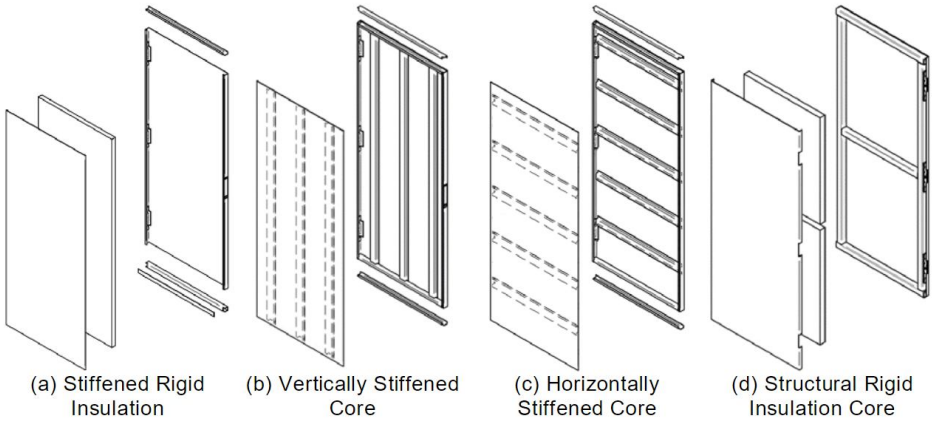

(a) Typical door stiffener configurations.

(b) Failure along the bottom of the rigid insulation specimen

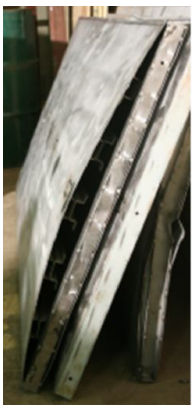

(c) Failure mode (vertical stiffeners)

(d) Comparison of small and large window failures

Figure 1.3: Typical door specimen configuration and failure modes (Jacques, et al. 2015)

Hsieh et al. (2008)

Finite element analysis determined the dynamic response of blast resistant doors. The door analyzed was *202"* by *100.8"* stiffened with I-shaped stiffeners. The stiffeners were arranged vertically and horizontally within the door panels. The analysis was conducted to determine the effects of varying web thicknesses within the stiffening elements. Peak over-pressures ranged from *30 psi* to *99 psi*, and stiffener web thicknesses ranged from *0.22"* to *0.33"* (Hsieh et al. 2008).

The results determined that increasing the web thickness of the stiffeners and the depth of the stiffeners greatly reduces the principal stresses in the stiffening elements and the deflections of the doors themselves. Static experiments and numerical analysis validated the results; however, no actual blast testing or imitated blast testing was carried out on the specimens for validation. This lack of actual experimental validation happened to be the case for many studies encountered during the review of the current literature.

Shen et al. (2010)

Experiments were conducted on blast resistance of curved aluminum sandwich panels consisting of two aluminum face sheets and an aluminum foam core. Specimens were tested under two radius values *11.81"* and *23.6"*. Core thicknesses were varied from *0.413"* to *1.19"*. The thickness of the inner plate and outer plates were also varied from *0.0197"* to *0.063"*. Typical test specimens can be referenced below in Figure 1.4 (a).

The specimens were tested over a range of impulses *4.5 lbs-s* to *9.7 lbs-s*. During the experiments, the effects of the above varying parameters were observed as deflections and deformation types (core deformation, deboning of the core from the panels and deformation of the front and back aluminum panels). See typical failure modes below (Figure 1.4 (b)) (Shen et al. 2010).

The main factors found to be of most influence in the determination of blast resistance were: the impulse, the thickness of the front and back panel, and the thickness of the core. Under a given impulse, the thickness of the core and face sheet thicknesses were the controlling factors of the final deformation. It was discovered that switching the thickness of the front and back panels had little to no correlation to this deflection. The larger radius panels and core were observed to reduce the impulse transferred to the shell and its support components.

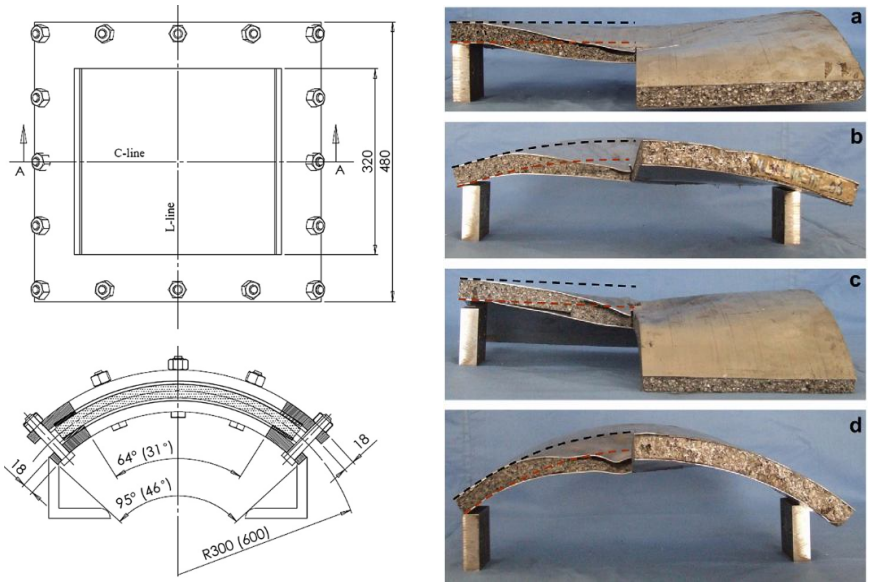

(a) Typical plate test assembly (b) Typical failure modes

Figure 1.4: Typical specimens and failure modes (Shen et al. 2010)

1.3. Applicable Codes and Standards

ASTM F2927-12 Standard Test Method for Door Systems Subject to Airblast Loadings

The ASTM F2927 is a test method that provides the necessary testing requirements regarding the specimens, testing apparatus and procedures to assign a given blast resistant door assembly a certain damage category, such as those listed below in Table 1-1, after being subjected to a specified blast pressure. The results of these tests may be used to declare an assembly is capable of withstanding a certain pressure/time loading and provide an appropriate damage level to be expected. Details of this test standard are discussed on the following pages.

The method applies to all types of swinging doors when testing for blast capacity using a shock tube or open-air explosion. The method is intended to test complete door assemblies. Door assemblies refer to door panels, frame and frame connections to a rigid reaction structure, latches, hinges, and door hardware. The test accommodates the use of vision lights (windows) as well. A minimum standoff distance of *3 meters (9'-10")* is required to prevent punching effects.

A test frame is required to emulate the opening which the door assembly will be installed. The required opening is to be *1/8"* to *1"* larger than the dimensions of the door frame. The maximum displacement of the test frame is held to the standard of *L/360* and should remain elastic

during this deflection. The door frame should be installed such that it is no more than *6"* recessed from the test frame anchored according to the specifications of the manufacturer.

Requirements are also set out for pressure transducers, strain gauges, data acquisition systems (DAS), photographic equipment, force gauges, and temperature measuring devices (TMD). Transducers are required to be capable of defining the blast pressure history with enough resolution to capture the entire pressure/time event. Strain gauges can be placed at the discretion of the test conductor. The DAS must be capable of (possess enough channels) accommodating all pressure transducers and any other measuring devices by either digital or analog means for recording.

A sufficient camera must be supplied to allow the visual recording of testing through still photography or video footage. A force gauge must be adequate to measure the force required to operate the door (open and close). This force gauge must be accurate to *1 lbs* and have the capacity to measure twice the suspected operation forces. The TMD is required so that the ambient temperature may be measured before each test.

A witness panel shall be mounted at the back wall and consist of two layers. The back layer (furthest from the door system) is to be *1"* thick polystyrene foam. The front layer is to be *½"* rigid foam plastic thermal insulation board bonded to a white matte non-glare aluminum facer and reflective reinforced aluminum facer (towards the door assembly).

It is discussed that careful consideration must be given to ensure that the door assembly and its components are as tested. A design specification can not be made from the results of testing unless the performance of the door assembly, the wall, and all components are as tested. As such, all specimens must be supplied as a complete door assembly.

The use and storage of explosive materials must be handled and overseen by a professional qualified by a U.S. government agency to handle explosives. All federal statutes are applicable during testing with such materials. Door specimens must adhere to requirements for a blast resistant door. No certain manufacturer is required. It is simply required that the door's design is adequate for the test load it will undergo. Testing will then prove its adequacy for a given load. The typical door assembly is *3*-sided supported in the seated direction. It may also be considered *4*-sided simply supported if the door assembly is intended to have a bottom threshold. All specimens are to be numbered and permanently marked as such.

When instrumenting test specimens for shock tube testing, a minimum of two pressure transducers are to be mounted on the front surface of the test frame or bulkhead (one on the vertical center-line and one on the horizontal center-line). Such extensive explanation of F2927 has been employed as this is the test method that will be adhered to in future studies at the Virginia Tech Shock Tube Testing Facility.

Table 1-1 Door Response Categories and Descriptions (ASTM 2012).

Damage Rating	Description of Door / Frame Response	Damage Level Category
Undamaged	After the blast, the door remains mostly unchanged. Permanent deformations are to remain within 1/8". The door must be proven operable by being completely open and closed again. No damage should be evident on any components (i.e., frame anchorage, latches, hinges, etc.). Any recorded stresses should remain within specifiers "acceptable limits."	I
Damaged but Openable	Deformation and damage remain in an acceptable range while the door remains operable. The door must be proven openable by unlatching and opening wide enough to allow ingress and egress.	II
Non-catastrophic Failure	The door may become lodged in the opening or swung open by the blast. Acceptable damage and deformation are determined by the specifier based on door use. The door is not to become detached, and the frame must remain attached to the wall.	III
Limited Hazard Failure	The door leaf and/or its frame and frame anchorage may fail and become detached and/or thrown into the test structure witness area. The door leaf/assembly must not be thrown more than 120". No components may be observed to strike the witness panel on the back wall of the test structure.	IV
High Hazard Failure	The door leaf separates from the frame and/or the frame anchorage fails. Either the door leaf and/or frame is separated from the wall and thrown into the witness panel above the "High Hazard Threshold." No hardware may strike the witness panel above the High Hazard Threshold."	V

ASTM F2247 Standard Test Method for Metal Doors used in Blast Resistant Applications

This test method seeks to test metal doors for their structural integrity against blast loading and to categorize the doors according to their performance much like ASTM 2927 discussed above. The method uses equivalent static loading to replicate a predetermined blast pressure, in place of

actual blast testing with a shock tube. The loading is selected based upon the characteristics of the blast pressure given and the structural behavior of the door itself (ASTM 2018).

The use of the test data is limited in terms of size. Results can not be extrapolated for specimens larger than those tested; however, results can be extrapolated for smaller specimens than those tested. The principals of pressure, deflection as well as strain gauge measurement are used within this test method. This method is not to be applied when forces are applied from explosive charges, forced air or a shock tube apparatus.

Specimens may be tested to their ultimate capacity or tested to a predetermined static loading. Two procedures exist in this method. The first, procedure A, is used when load-deflection curves are not required and when a single load is applied. The second, procedure B, is applied when load-deflection curves are required, and multiple static loadings are applied. After static testing under this method, specimens are categorized using an analogous system, as summarized above in Table 1-1.

Other Applicable Standards

The Unified Facilities Criteria by the DoD Minimum Antiterrorism Standards for Buildings is a document that implies the commitment of the DoD to minimize casualties and injury due to a terrorist attack on DoD employees. It provides standards that provide minimum levels of protection against terrorist attacks. Its use is meant for design teams to help determine the minimum requirements that must be incorporated to design for said minimum standards. The standard references the ASTM F2247 for the design of doors. Door hazard rating levels are taken from ASTM F2247 and thus are analogous to Table 1-1 above (DoD 2018).

The SDI 133-16 is a specifying guideline for steel doors and frames meant to resist blast loading. This document references the ASTM F2927 and ASTM F2247 and others that will not be discussed here; as such, it is an excellent reference document for review of all applicable standards necessary to design blast resistant steel doors (SDI 2016).

1.4. Research Needs

The necessity for blast resistance of non-structural components, such as blast resistant doors, has become increasingly more apparent. Though generally not considered to be structurally significant, doors are critically important in the event of a blast for several reasons. First, doors not adequately designed may become fatal projectiles in the event of an explosion. In addition, if a door does survive the blast but becomes damaged beyond operation, it may trap survivors within the building or prevent emergency responders from entering the structure during an emergency. Finally, a door is a system of components, consisting of a door panel, door frame, latch and hinge hardware, and anchorage, that must possess sufficient strength, ductility, and redundancy to survive the applied blast loading. Loss of one component in the system can lead to a cascading failure of the entire system.

Published research pertaining to light gauge blast resistant doors is sparse and detailed design guidelines governing the construction requirements and best practices for this class of components are generally non-existent. The lack of published research is attributed to the proprietary nature of hollow metal blast doors, which are outside of standard structural design practice. Therefore, non-proprietary information or purposefully obfuscated details are often published to ensure private manufacturers maintain a competitive advantage. Therefore, proprietary design details, engineering, and testing typically necessitate confidentiality on the part of the manufacturer. Non-proprietary research reviewed pertained to monitoring blast performance of hot rolled steel plates (both stiffened and un-stiffened) and finite element analysis without experimental test validation. Combined, these research needs motivate further research to understand the behavior of hollow metal blast doors and develop much-needed design information required for these often-overlooked components.

1.5. Objective

The objectives of this thesis are to (i) characterize the performance of several configurations of skin-core construction (*i.e.*, epoxy, reduced weld requirements) methodologies and in-situ hardware capacities of typical hinges through quasi-static flexural testing of beams whose internal construction closely mimics that of a full-size door. The second objective is (ii) develop and validate a reduced-order finite element analysis methodology to generate resistance curves of full-size blast doors for use in single-degree-of-freedom dynamic analysis. The third

objective is (iii) introduce and describe the Virginia Tech Shock Tube Testing Facility, a unique research installation equipped with a large-scale gas-detonation blast simulator that can safely and accurately simulate pressure waves generated by accidental explosions and terrorist bombings.

1.6. Scope

The scope of this research program is as follows:

1. Review of previous research regarding the design, construction, testing, and analysis of blast resistant hollow metal doors;
2. Perform static testing of component-scale beam-assembly specimens to evaluate the effectiveness of alternative skin-core construction methodologies at achieving composite action to inform on the construction of future full-size blast doors;
3. Perform static testing of component-scale beam-assembly specimens to evaluate the in-situ capacities of typical hinge hardware to inform on the construction of future full-size blast doors;
4. Development of a finite element analysis methodology to generate resistance curves for beam-assemblies to be validated with the resistance curves measured during static testing;
5. Extend the finite element analysis methodology developed under Task 4 to full-size doors and validate the model with previously tested door data from Jacques et al. (Jacques et al. 2015);
6. Provide an introduction to the new Virginia Tech Shock Tube Testing Facility which covers testing capabilities, instrumentation, operation, and a calibration plan;
7. Discuss future work to be completed at the Virginia Tech Shock Tube Testing Facility.

Chapter 2. Beam-Assembly Tests

2.1. General

This chapter presents the experimental results obtained from quasi-static testing of 18 beam-assemblies performed to (i) evaluate the effectiveness of alternative skin-core construction methodologies at achieving composite action, and (ii) evaluating the in-situ capacities of typical hinge hardware when installed into the door and frame assemblies. The outcomes of these tests will be used to inform on the construction of full-sized doors evaluated during subsequent blast tests.

Door construction details, material properties, load-deflection curves, and overall behavior are discussed. Whenever possible, load-deflection curves for each companion series of beam-assembly tests have been grouped together to facilitate a direct comparison of test parameters. The influence of key parameters affecting beam-assembly response is discussed, and recommendations are made to enhance the blast resistance of full-sized hollow metal doors.

2.2. Test Specimens

All test specimens were prepared by the manufacturer following their typical construction practices and shipped to Virginia Tech for testing. The overall dimensions and materials used to construct the door panels and frame segments were nominally identical, with varying skin-core attachment details and hinge hardware depending on the aims of each test series. As illustrated in Figure 2.1 (a), the door panels were each *42”* long × *24”* wide × *2-5/32”* thick and consisted of a central *2×2×1/8* HSS tube sandwiched between *14*-gauge Galvanneal sheet metal skins. The ends of the central HSS tube were welded to perpendicular *2×2×1/8* HSS tubes which normally form the perimeter frame around an actual door. The configuration of the HSS tubes and sheet metal skins and stiffeners used in the door panels was based on typical full-sized hollow metal door construction.

As is common practice to simplify fabrication, the central and perimeter tubes were only welded along their depth through the thickness of the door panel, as shown in Figure 2.1 (b). The

external sheet metal skins were formed (bent) around the perimeter HSS tubes to create the necessary profile required for proper door function. Cut-outs in the skin on the hinge side, highlighted in Figure 2.1 (c), aligned with pre-tapped inserts for installation of hinge hardware. Door latch hardware was not considered in the quasi-static tests at the request of the sponsor. *16*-gauge Galvanneal sheet metal C-shaped stiffeners spanning perpendicular to the central HSS tube spacing were provided to support the sheet metal skins every *7-3/32”*.

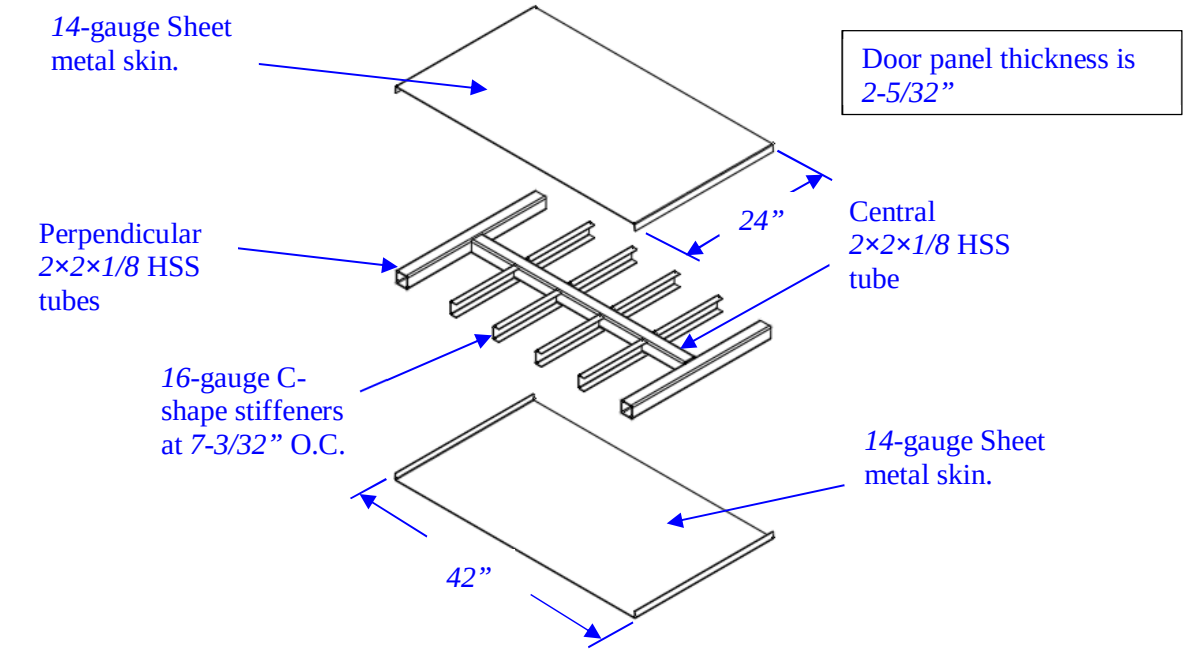

(a) Overview of door panel components.

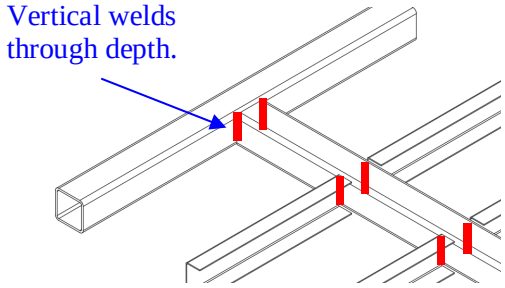

(b) Vertical weld through depth connecting two perpendicular *2×2×1/8* HSS Tubes.

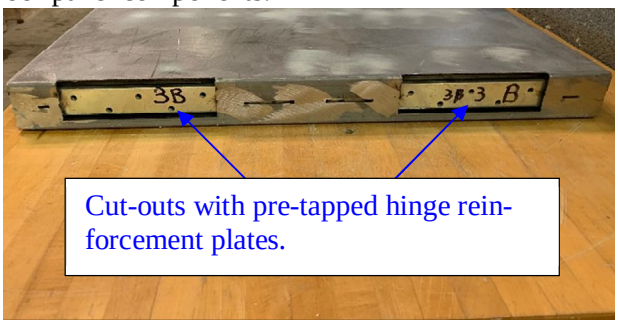

(c) Cut-outs aligned with pre-tapped inserts for installation of hinge hardware.

Figure 2.1: Typical beam-assembly door panel construction details.

The beam-assembly specimens were mounted into two-door frame segments representative of the manufacturers’ typical installation practices. As illustrated in Figure 2.2, the “latch frame” refers to the frame segment where the door rests upon the door jamb and where latch hardware

would normally be installed. The "hinge frame" refers to the frame segment containing the hinges. The construction of the frames was nominally identical, except for the placement of through-holes used for attachment of the specimens to the test fixture and whether pre-tapped inserts were provided for installation of hinge hardware.

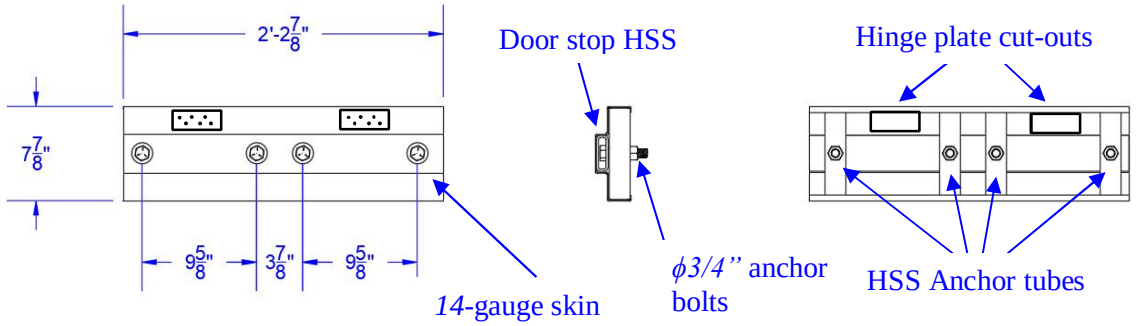

(a) "Hinge frame" dimensions and components.

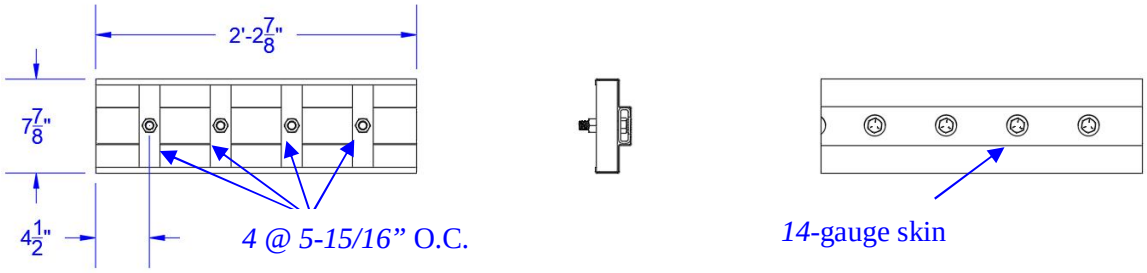

(b) "Latch frame" dimensions and components.

Figure 2.2: Beam-assembly frame construction details.

The frame segments were constructed of four *1-3/4×1-3/4×1/8* anchor HSS tubes as shown in Figure 2.2, a *1×3×3/16* HSS tube to reinforce the door jamb, and a *14*-gauge sheet metal skin forming the outer covering. Each frame was connected to the test fixture using *4* ea. *ϕ¾"* anchor bolts installed through ϕ*7/8"* clearance holes drilled through the anchor tubes. The doorstops were *1"* high which provided a 3/4" seating width for the doors in the closed positioned when properly installed with a *1/8"* stop gap and accounting for *1/8"* bevel.

2.2.1 Door Construction Specimens

The test matrix for door construction specimens is provided in Table 2-1. A total of six nominally identical door panels divided into three companion pairs of skin-core construction methodologies were tested. The panels were designed to evaluate the effectiveness of alternate skin-core construction methodologies (*e.g.*, epoxy, reduced weld requirements, full weld requirements) at achieving skin-core composite action suitable for blast-resistance. The overall

dimensions and boundary conditions of all door construction tests were the same. The boundary conditions of door construction tests and hinge hardware tests will be discussed in Section 2.3.1. All door construction specimens were attached to the frame with two *6"* PBB stainless steel hinges (discussed in Section 2.2.2). The following provides a detailed description of the three types of door construction specimens.

Table 2-1: Test matrix for the skin construction beam-assembly tests.

Test No.	Construction Details	Hinge Type	Replicates
1A/1B	Skins epoxied to tubes.	*6"* PBB Stainless Hinges	2
2A/2B	Skins welded to tubes with normal spec (*1/8"* × *1"* fillets every *6"* or *5/16"* plugs every *6"*).		2
3A/3B	Skins welded to tubes with max. spec (*1/8"* × *1"* fillets every *3"* or *3/8"* plugs every *3"*).		2

Series 1: Epoxy Construction

The door panels of Series 1 were constructed using Tri-Tex Co. Inc. 0379A adhesive epoxy (Tri-Tex Co. Inc. 2009) to fasten the door skins to the internal frame. The specially formulated 0379A adhesive is designed for use with metal doors. Assembly of epoxied door panels consisted of surface preparation through mechanical cleaning, followed by application of the epoxy resin to the HSS and C-shape stiffeners. The sheet metal skins were then laid onto the adhesive-coated steel core, and the epoxy was allowed to cure at room temperature. Compared with traditional welded construction, epoxy construction is relatively simple and offers the potential to reduce labor costs and speed up production time and eliminates the heat involved with welding which often causes distortion.

Series 2: Normal Weld Specification Construction

The manufacturers' normal weld specification used for hollow metal blast doors consists of a combination of *1/8"* × *1"* fillet welds and *5/16"* plug welds spaced every *6"*. The assembly process consists of placing the assembled core on the back door skin and applying the fillet welds at *6"* spacing along with all components of the frame. Subsequently, the front skin is then placed on top of the assembly and plug welded every *6"*. This method of construction is more labor-intensive than comparable epoxy construction.

Series 3: Maximum Weld Specification Construction

The door panels of Series 3 were constructed using a combination of *1/8" × 1"* fillet welds and *3/8"* plug welds spaced at *3"*. The assembly process follows the same procedure as Series 2 but employed a tighter weld pattern. This method of construction is the most labor-intensive requiring the longest fabrication time but is assumed to be the most robust in terms of strength and stiffness.

2.2.2 Hardware Capacity Specimens

The test matrix for hardware capacity specimens, provided in Table 2-2, comprises a total of *12* identical beam-assembly specimens with various hinge hardware. The door panels used in the hardware capacity tests were the same as those tested in Series 3, comprising the maximum weld specification of *3"* spacing. The dimensions and boundary conditions of all hardware capacity tests were the same. The following describes the door hardware specimens.

Table 2-2: Test Matrix for Hardware Capacity Testing

Test No.	Hinge Details	Door Construction	Hinge Reinforcement	Replicates
4A/4B	*6″* PBB Stainless Hinges	Heavy weld spec	Floating	2
5A/5B	Hinge Pins & *4.5″* Hinges			2
6A/6B	Hinge Retainer & *4.5″* Hinges			2
7A/7B	Pin & Barrel Hinge			2
8A/8B	Surelock S2HA7 Mortised *5.75″* Hinge		Integral	2
9A	Gallery Hinges		Floating	1
9B	*6″* PBB Mild Steel Hinges			1

Series 4: 6" PBB Stainless Steel Hinges

Series 4 consisted of two replicate test specimens (4A and 4B) mounted to the hinge frame with *6"* PBB model 4B60 Stainless Steel Hinges (PBB 2003). These hinges, shown in Figure 2.3, are of PBB's heavy weight line and are intended for use on heavy weight doors receiving high-frequency service. Each hinge leaf is fastened to the door/frame using five stainless steel FHMS - *1/4-20 × 1/2"* screws (a total of *10* screws per hinge). The gauge thickness of the hinge is *0.2"*.

Per the door manufacturer, this type of hinge is intended to provide sufficient performance while remaining relatively easy to install.

It should be noted that the hinge reinforcement plates where the hinge leaves are attached to the frame and door panel are not welded directly to the anchor tubes or internal HSS structure for the frame and door panel respectively. The hinge reinforcement plates are essentially only connected to the sheet metal skin of the door panel and frame; this mounting configuration is referred to as *floating* in the subsequent discussion.

Figure 2.3: *6″* PBB Stainless Hinges (Series 4).

Series 5: Frame-Pins & 4.5" Hinges

Series 5 consisted of two replicate test specimens (5A and 5B) mounted to the hinge frame with a set of *4.5”* hinges attached to floating hinge reinforcement plates and reinforced with an externally-mounted interlocking frame-pin system. A pair of pins protruding from an HSS attached to the door fit into a set of holes in the frame which provides an additional load path to supplement the out-of-plane capacity of the hinges. The frame-pin interlock system, illustrated in Figure 2.4, consists of an HSS *1×1×1/8* welded along the hinge side of the door specimen with seven *1-1/8” × 1/8”* fillet welds along each side spaced at *3”* on center. Two *1”* long *ϕ½*” steel pins are welded to the HSS and align with *ϕ3/4”* holes drilling into the frame. The hinges are Hager Companies *4-1/2” × 4-1/2”* five knuckle ball bearing heavy weight hinges type BB1168 (Hager Companies 1996). They are connected to the frame and door with a total of eight *12-24 × ½”* screws (four screws per hinge leaf). They have a gauge thickness of *0.18”* and comply with all specifications and requirements set forth by (SDI 2014).

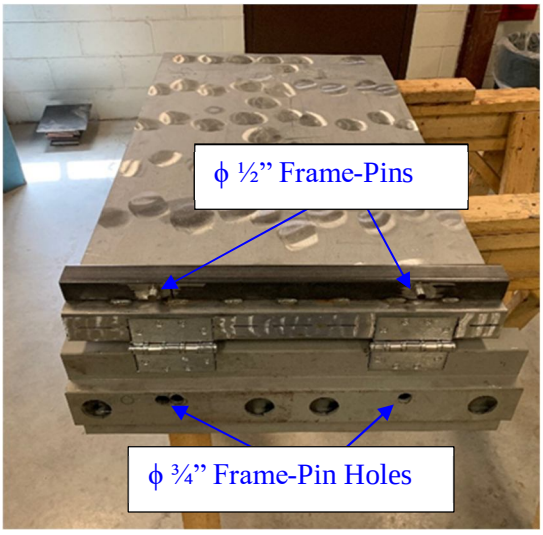

(a) Overall view of hinge and frame.

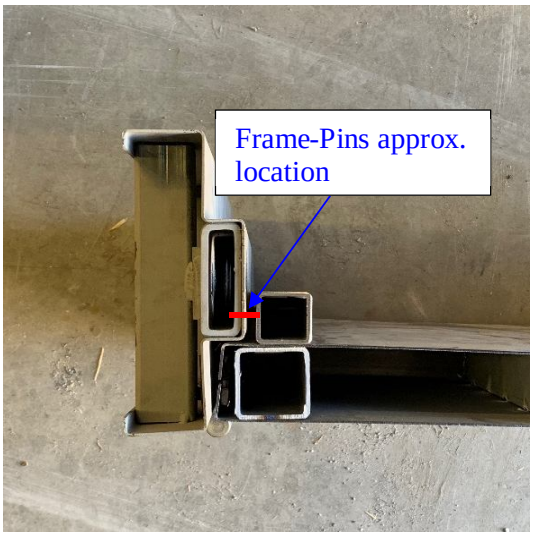

(b) Frame pins functionality.

Figure 2.4: Hinge Pins & 4.5" Hinges (Series 5).

Series 6: Hinge Retainer & 4.5" Hinges

Series 6 consisted of two replicate test specimens (6A and 6B) mounted with a set of *4.5”* Hager Companies heavy weight hinges (type BB1168) (Hager Companies 1996) reinforced with an externally-mounted interlocking hinge retainer system. Just as with the hinges in Series 5, the hinge reinforcement plates were also floating. As shown in Figure 2.5, the hinge retainer was composed of two *1”×1”×1/8”* angles welded to the frame segment which interlocked with a *2”×1”×1/4”* channels welded along the hinge side of the door panels. The angles were tack welded to the frame segment directly while the channel was welded to the door panel using eight *1-1/8” × 1/8”* fillet welds along each side. The hinge retainer was designed to provide an additional load path to supplement the out-of-plane capacity of the hinges.

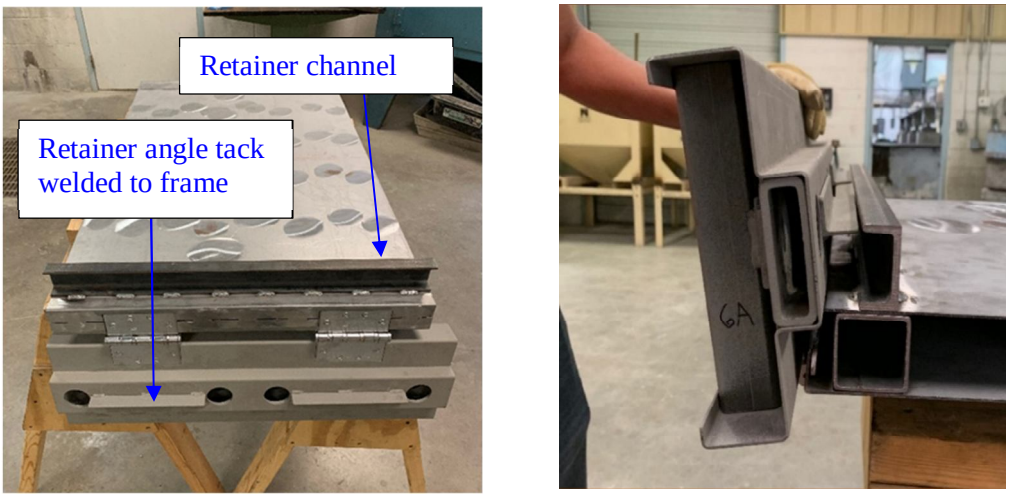

(a) Overall view of hinge and frame. (b) Hinge retainer functionality.

Figure 2.5: Hinge Retainer & 4.5" Hinges (Series 6).

Series 7: Pin & Barrel Hinge

Series 7 consisted of two replicate test specimens (7A and 7B) mounted with a pin and barrel hinge attached along the length of the door panel, as shown in Figure 2.6. The hinge was a Select Hinges SL200 Concealed Pin & Barrel Hinge (Select Hinges, 2015) that was *24”* long with *4-1/2”* leaf width. The hinge was made from *14*-gauge 1012 cold-rolled steel with a zinc plated carbon steel finish and a *3/16”* 304 stainless steel rod serving as the pin. The hinge was attached to floating hinge reinforcement plates using four *10-24* × *7/8”* zinc plated Phillips flathead undercut self-drilling Tek screws per leaf. Attachment of hinges is labor-intensive on the contractor’s end as the doors and frames must be measured, pre-drilled and threaded on-site for installation of hinges. The design of this hinge distributes the connection points along the length of the door, which provides better weatherproofing compared with discrete hinges. This design is also touted as being more efficient for heavy weight doors used in high-frequency openings.

Figure 2.6: Pin & Barrel Hinge (Series 7).

Series 8: Surelock McGill S2HA7 Mortised 5.75" Hinge

Series 8 consisted of two replicate test specimens (8A and 8B) mounted to the hinge frame with a pair of Surelock S2HA7 mortised *5.75"* × *4.0"* hinges (Surelock McGill, 2016). A photograph of these hinges installed prior to testing is shown in Figure 2.7. S2HA7 hinges are designed for heavy-duty security, blast and ballistic doors. The hinges have a thickness of *0.39"*, and each leaf is connected to the door and frame hinge reinforcement through four screws. The center pin of the hinge which runs along the knuckles is *0.5"* in diameter. The hinge and hinge pin are both 316 stainless steel. The overall robust design and ease of installation is a major proponent for the S2HA7. Mortised shear pinholes can be noticed in Figure 2.7, below, but were not tested per the manufacturers' request. The hinge reinforcement plates for each hinge leaf of Series 8 were welded directly to the anchor tubes of the frame as can be seen below in Figure 2.8. This was the only hinge tested in the hardware-capacity tests which employed integrally connected hinge reinforcement.

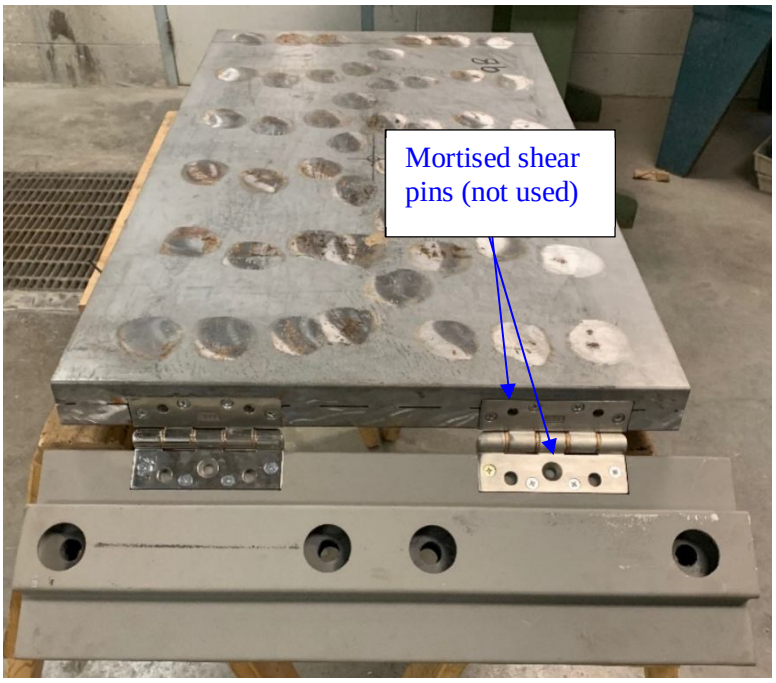

Figure 2.7: Surelock S2HA7 Mortised 5.75" Hinge (Series 8).

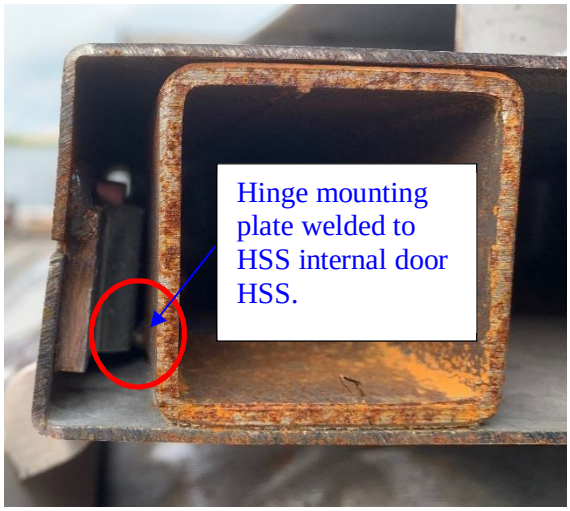

(a) Beam-assembly hinge mounting plate.

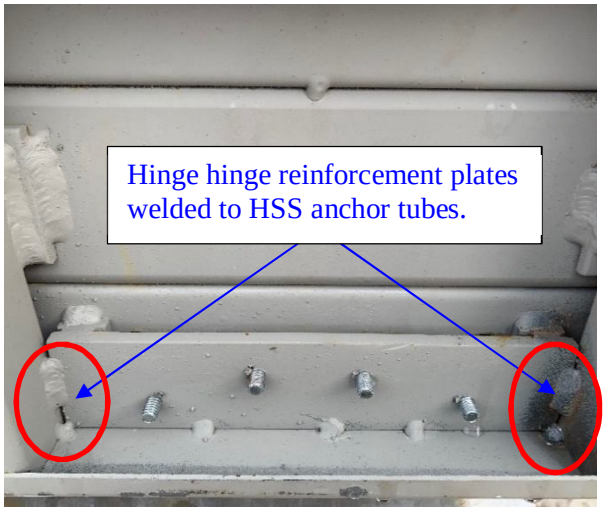

(b) Frame hinge mounting plate configuration.

Figure 2.8: Integrally connected hinge mounting plate configuration for Series 8 Surelock Hinges.

Series 9A: Gallery Hinges

Series 9A consisted of a *4-1/2"* a GSH 918 full mortise butt hinge with a shear resistant stud (Gallery, 2014). The hinges, shown in Figure 2.9, are heavy-duty hinges with a completely sealed and inaccessible center pin designed for use in prisons. The hinges connect to floating hinge reinforcement plates of both the door panel and the frame with four *¼"-20* Torx type machines screws, totaling eight screws per hinge. The machine screws are supplemented by a ϕ *½", ¼"* long pin which protrudes from each hinge mounting plate into holes drilled into the receiving door or frame. The integral hinge pin is intended to augment the resistance provided by the machine screws and increase the connection strength provided by this configuration of the hinge. The gauge thickness of the hinge is *0.188"*.

(a) Overview of Gallery hinges installed on specimen 9A.

(b) Series 9A Gallery Hinges.

(c) Mortise pin which interlocks with frame and door hinge mount plates.

Figure 2.9: Series 9A Gallery Hinges

Series 9B: 6" PBB Mild Steel Hinges

Series 9B consisted of hinge specimens mounted to the hinge frame with *6”* PBB 4B60 Mild Steel Hinges (PBB 2003). These hinges, shown in Figure 2.10, are of PBB’s heavy weight line and are intended for use on heavy weight doors receiving high-frequency service. Each hinge leaf is fastened to the floating hinge reinforcement plates of the door panel/frame using five stainless steel FHMS - *1/4-20 × 1/2”* screws (a total of 10 screws per hinge). The gauge thickness of the hinge is *0.2”*.

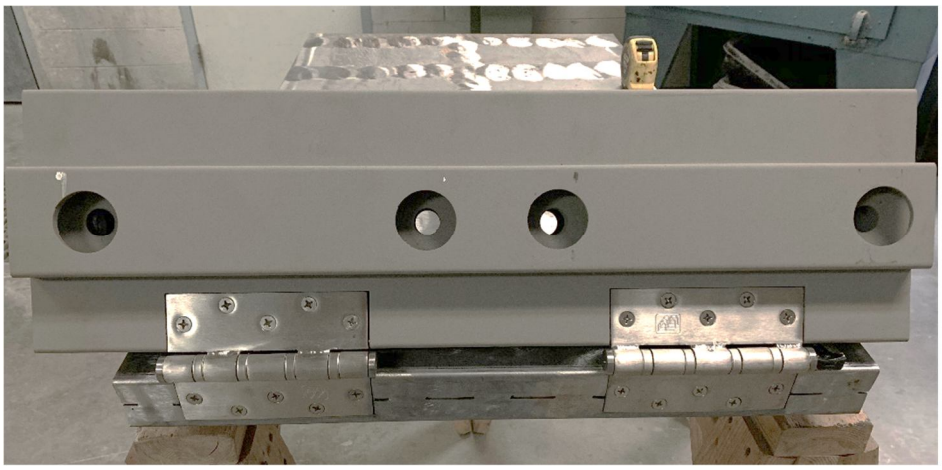

Figure 2.10: 6" PBB Mild Steel Hinges (Series 9B).

2.2.3 Material Properties

Coupon tests were performed in accordance with the ASTM E8-16a (ASTM 2016) to establish the tensile stress-strain properties of the sheet metal materials. Material tests were conducted on the *14*-gauge and *16*-gauge Galvanneal sheet metal used to fabricate the door skins and C-shape stiffeners. Three replicate standard dog-bone coupons were tested for each material, with each coupon having a gauge length of *2”*. The width of all coupons was *½”*, and thicknesses were nominally *1/14”* and *1/16”* (the gauge thickness of the door panels and stiffeners respectively).

Figure 2.11: shows a representative stress-strain curve for the *14*-gauge Galvanneal sheet metal. The yield strength was determined to be *35.9 ksi* with a corresponding modulus of elasticity of *27,171 ksi*. The ultimate strength was found to be *54.3 ksi*. Figure 2.11: also shows the representative stress-strain relationship for the *16*-gauge Galvanneal sheet metal. The yield strength was determined to be *42.3 ksi* with an ultimate strength of *53.3 ksi*. The modulus of elasticity was determined to be *27,250 ksi*. Tension coupon tests were conducted on the dogbone-

shaped specimens prepared from the *2×2×1/8"* HSS steel members. The results of the coupon tests indicated that the HSS had a yield strength of *60 ksi*.

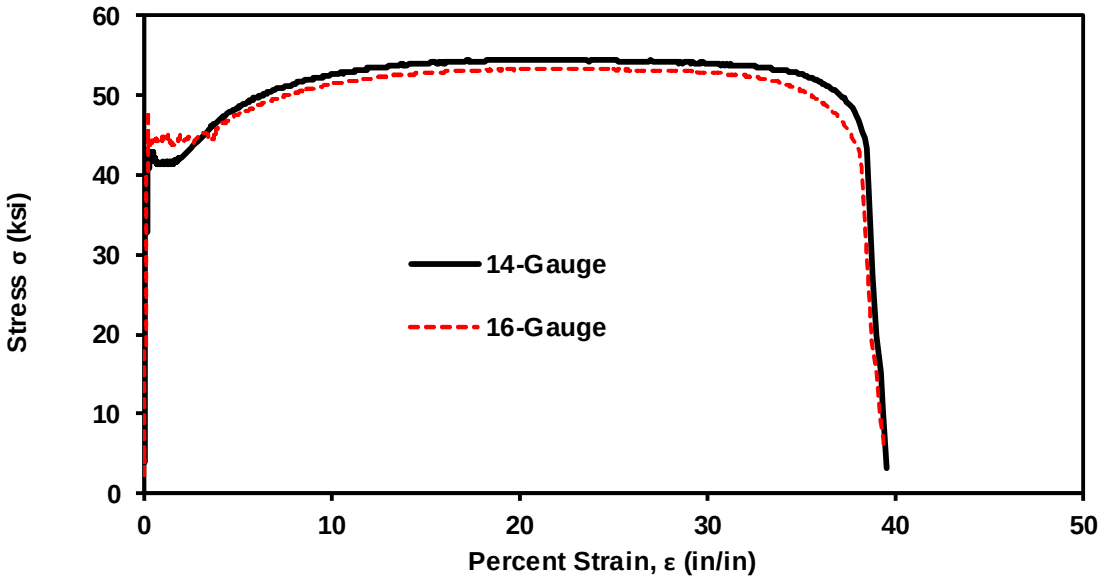

Figure 2.11: Average representative stress-strain behavior for *14*-gauge and *16*-gauge sheet metal.

2.3. Experimental Program

Details of the test fixture, instrumentation, and test procedure are described in the following sections.

2.3.1 Test Fixture

The door construction and hinge capacity tests were performed using a self-reacting steel fixture mounted in an MTS machine. The self-reacting frame, shown in Figure 2.12, consisted of two HSS*10×10×1/4* reaction frame ends stiffened with *¼"* steel plates to which the frame segments were bolted. The HSS reaction ends were attached to two *W8×18* flexural members which rested on the base reaction frame of the MTS machine. Design calculations demonstrated that these flexural members had sufficient rigidity to support the test fixture.

The MTS machine was used to apply two point loads to the top of the beam-assembly door specimen through a spreader. The spreader was composed of two *ϕ2"* steel rods welded to a center-mounted HSS *3×3×1/4* member. A roller release was attached to the top of the load spreader to avoid unnecessary moments at the load cell.

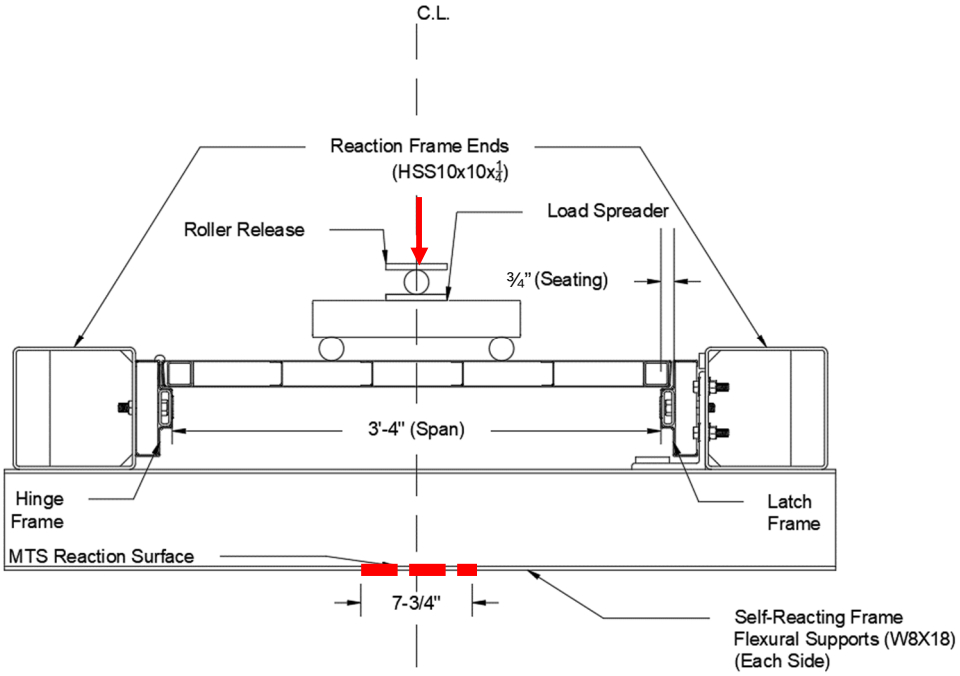

(a) Test fixture for door construction tests (seated configuration).

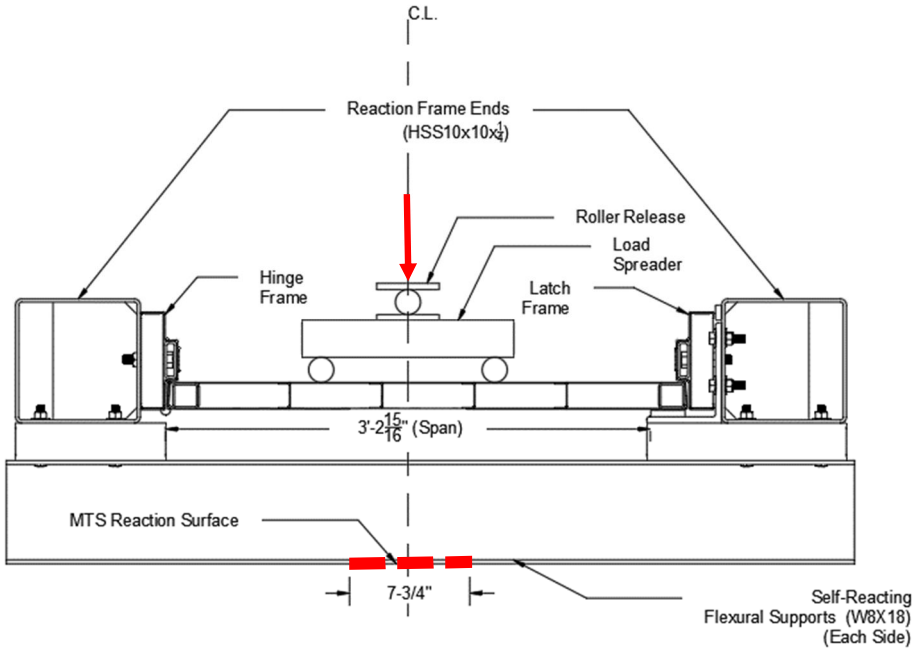

(b) Test fixture for hardware capacity tests (unseated configuration).

Figure 2.12: Test fixture schematic for door construction and hardware capacity tests.

Seated configuration for door construction tests

(a) View from hinge side.

(b) View from latch side.

Unseated configuration for hardware capacity tests

(c) View from hinge side.

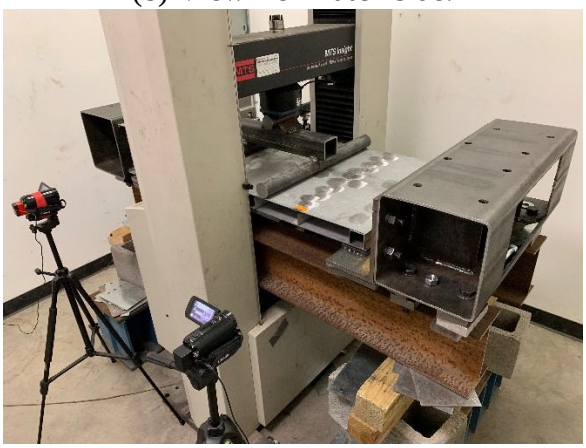

(d) View from latch side.

Figure 2.13: Photographs of the beam-assembly test fixture.

2.3.2 Instrumentation

Experimental data, consisting of applied load and mid-span deflection, was recorded by the MTS Test Works Version 4.0 data acquisition software recording at *10* samples per second. The data acquisition system was manually triggered at the beginning of the test. Data were recorded for the duration of the test and terminated manually once the specimen had failed. The applied load was measured using a *33.7 kip* Electromechanical load cell integral to the MTS uniaxial testing frame. Specimen displacements were monitored using a single Celesco PT101 cable extension position transducer with a stroke of *10"* that was calibrated prior to the testing. The displacement transducer was mounted at member mid-span using a magnetic attachment.

Three high definition video cameras were used to record member response to out-of-plane static loading. For door construction specimens (Series 1, 2 and 3), two cameras were placed to record the interaction of the door, frame, and test fixture at the hinge and latch side of the

specimens, while the third was oriented to provide an overall view of the sample from above. For hinge hardware tests (Series 4 through 9), two cameras were placed on each side of the hinge frame, and one camera was placed at the latch end of the specimen. The video cameras were manually operated at the beginning and end of each test.

2.3.3 Procedure

Pre-test activities followed a standard procedure. The test specimens were first photographed, and any damage or defects were noted. The test fixture was then checked for proper alignment relative to the MTS machine. The latch-side door frame was bolted into the test fixture. The hinge leaves were screwed to the door and then screwed into the hinge-side door frame, and the hinge-side frame and door were then bolted to the test fixture. Sheet metal shims were used as necessary to maintain a *1/8"* door gap on the latch side.

The alignment of the beam-assembly was then checked and adjusted to ensure it was centered in the test fixture and that it was installed square and level. All bolts between the frame and test fixture were tightened, and the spreader beam was placed on the specimen and centered relative to the MTS machine. The mid-span displacement transducer was installed, and the data acquisition was checked to ensure proper functionality. The load and displacement measurements were zeroed, and the crosshead was then lowered until it just contacted the spreader beam.

Finally, specimens were photographed in the fixture prior to testing. The video cameras were manually turned on and the specimens were loaded until failure at a constant crosshead speed of *0.1 inches/min.* Failure was generally defined at a consistent displacement and loading which far exceeded the flexural capacity of the beam-assembly, however, as will be described in the experimental results, loading was continued for some tests until the door slipped out of the stop on the latch side or to acquire as much hinge damage as possible per the manufacturer's request. After testing, the experimental data was saved, photographs were taken, and the video footage processed.

2.4. Experimental Results

The following sections describe the experimental results obtained from the static testing of the beam-assembly specimens.

2.4.1 Door Construction Specimens

Series 1: Epoxy Attachment

The load-deflection curves for Specimen 1A and 1B, having epoxy skin attachment, are shown in Figure 2.14. The elastic limit was identified from the load-deflection curve by the point beyond which significant non-linearity of the load-deflection curve was observed. The elastic limit for both specimens occurred at an approximate mid-span displacement $\delta = 0.20\ in$ and load $P = 5{,}800\ lbs$.

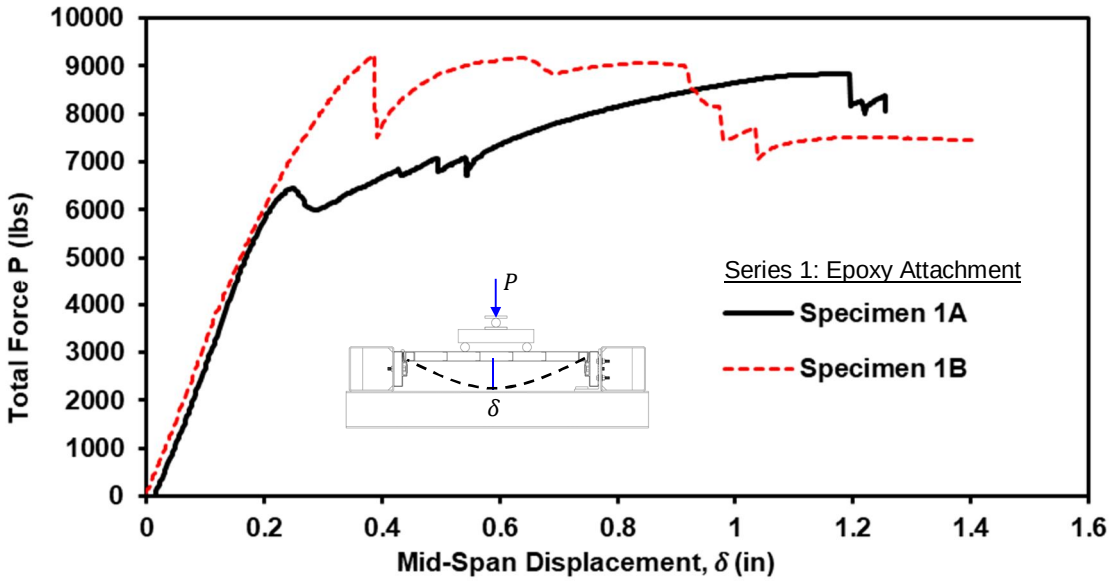

Figure 2.14: Comparison of load-deflection behavior of Series 1: Epoxy Attachment beam-assembly specimens.

Cracking and popping sounds could be heard during both tests prior to the onset of member yield resulting from what was believed to be local failures of the epoxy composite. Failure of the epoxy bond between the compression skin and the central HSS initiated the failure in both specimens of Series 1. The first significant failure of epoxy occurred in specimen 1A at $\delta = 0.24$" and $P = 6{,}400\ lbs$ and in specimen 1B at $\delta = 0.38\ in$ and $P = 9{,}200\ lbs$. The epoxy failure of specimen 1B occurred while testing was paused. These points of first significant epoxy failure were the last point at which loading was resisted by the fully composite action of the door panel.

Redistribution was achieved by both specimens tested; however, only specimen 1A was able to reach an ultimate load higher than it achieved with fully composite action at $\delta = 1.19"$ and an ultimate load of $P = 8{,}800\ lbs$. Once failure of the epoxy was initiated, de-bonding propagated instantaneously throughout the entire region of initial failure, including along the C-shape stiffeners, resulting in buckling of the skins shown in Figure 2.15.

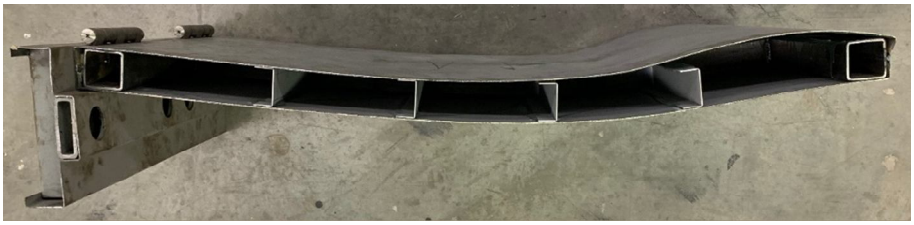

(a) Specimen 1A, epoxy failure on latch side.

(b) Specimen 1B, epoxy failure on hinge side.

Figure 2.15: Post-test photographs taken of specimens from Series 1: Epoxy Attachment.

After testing, the skins of the Series 1 doors were cut away in regions where epoxy failure occurred. As can be observed in Figure 2.16: (a), the application of the epoxy resin was observed to not cover all possible contact surfaces between the sheet metal skins and the internal core elements. It appeared as though the epoxy was already partially set and did not cover all possible contact surfaces, thus reducing potential bond capacity. The failure mode was ultimately a bond failure between the epoxy and the steel. It was also noted that, once epoxy failed and composite action was lost, the weld between the central HSS and perpendicular HSS failed on the exact side which composite action was lost and the skin buckled as shown in Figure 2.16: (b). Ensuring full epoxy coverage and perimeter fillet welds are used all the way around the HSS framing members.

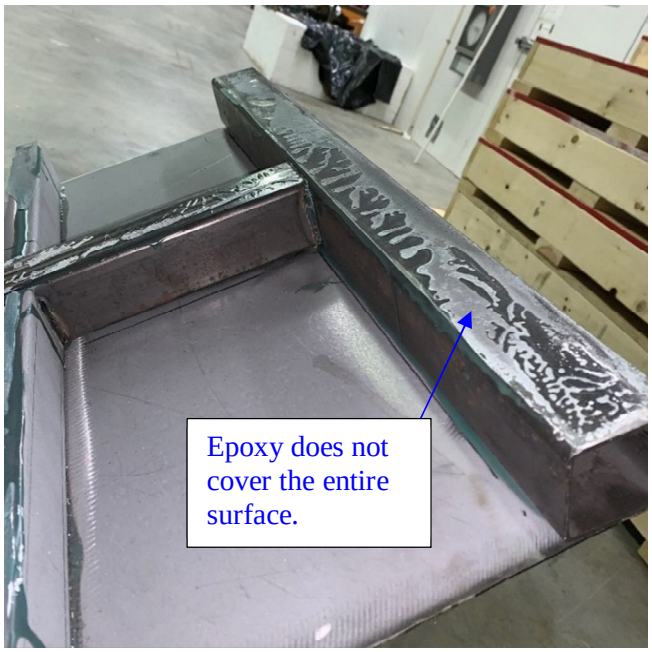

(a) Epoxy surface coverage.

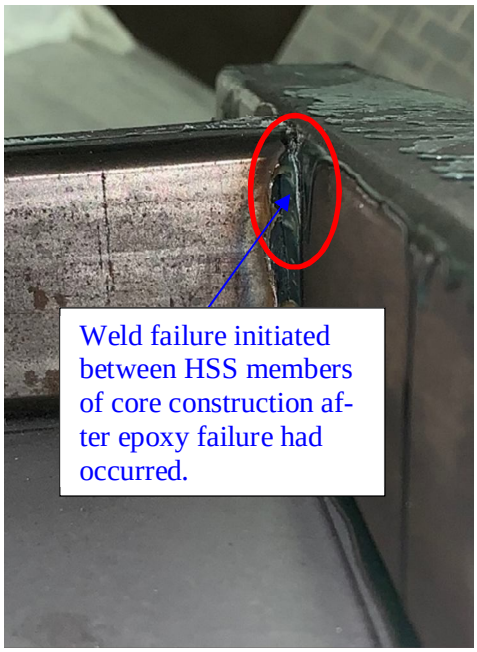

(b) Vertical weld failure at abutting perpendicular HSS members

Figure 2.16: Photographs of epoxy and weld failures observed during Series 1 tests.

Series 2: Partial Weld Attachment (Normal, 50% Plug Weld Specification)

The load-deflection curves for specimen 2A and 2B are shown in Figure 2.17. Both specimens exhibited very comparable load-deflection performance, indicating a high level of repeatability afforded by construction using *6"* weld spacing. The slope of the initial ascending portion of the curve was the same for both specimens with the elastic limit being reached at similar levels of displacement ($\delta = 0.3$*"*) and applied load ($P = 7000$ lbs).

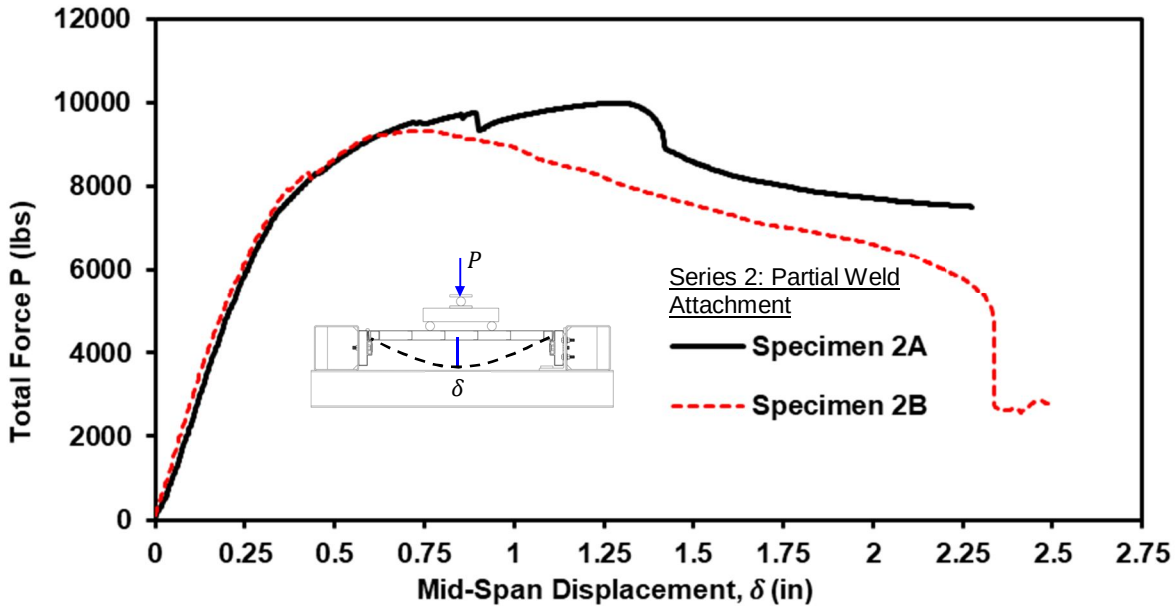

Figure 2.17: Comparison of load-deflection behavior of Series 2: Partial Weld Attachment beam-assembly specimens

Intermittent cracking sounds emanating from the door could be heard leading up to the elastic limit and throughout the entire test. Loss of plug weld attachment to the central HSS initiated failure in both specimens. An extremely loud pop, attributed to local plug weld failure and instantaneous buckling of the compression skin, was heard during both tests once the elastic limit was reached, as shown in Figure 2.19 (a).

For specimen 2A, the first plug weld failed on the compression side in the constant moment region at $\delta = 0.70$" *and* $P = 9500\ lbs$ at mid-span along the central HSS, while the first plug weld failed on the compression side in the shear span nearest the latch side for specimen 2B at $\delta = 0.358$" and $P = 7{,}845\ lbs$. These points correspond to the peak load carried by the door panels due to fully composite action between the skin and core. Figure 2.18 (a) and (b) show post-test photographs of specimens 2A and 2B, respectively, which highlight the deformed

configuration of the samples which first became evident once composite action between the skin and core was lost during testing.

(a) Specimen 2A, plug weld failure, and skin buckling on the compression skin at mid-span.

(b) Specimen 2B, plug weld failure, and skin buckling in the shear span on the latch side.

Figure 2.18: Post-test photographs of Series 2 door panels.

Once peak load had been attained, the skins on the compression sides exhibited significant buckling due to loss of multiple consecutive plug welds, as can be seen in Figure 2.19: (a). Specimen 2A and 2B resisted a peak load of *9,740 lbs* and *9,310 lbs*, respectively. Plug welds continued to fail incrementally as the mid-span deflection increased past peak load. Specimen 2A, after plug weld failure in the constant moment region, was able to carry additional load up to *9,980 lbs* due to redistribution. Specimen 2B, with plug weld failure in the shear span, began to unload after loss of composite skin-core action.

The ultimate load of specimen 2A was higher and occurred at a larger displacement of $\delta = 1.30"$ and $P = 9{,}980\ lbs$ compared with specimen 2B at ($\delta = 0.752"$ and $P = 9{,}310\ lbs$). When plug weld failure initiated in the outer span (as in 2B), the plastic moment capacity of the central HSS and subsequent buckling occurred under the point load closest to the loss of composite action. Figure 2.19: (b) shows a photograph of typical flexural yielding of central HSS tubes after loss of composite action. When plug welds were lost at mid-span (as in 2A), the loss of composite action caused the plastic moment capacity and failure of the central HSS to occur under the point load

closest to the hinge frame. It is also notable that, when the hinges did not deform as in 2B, the door slipped past the stop.

Test 2A was terminated once the door panel reached 2.25" deflection, while test 2B was continued until the door slipped off the door jamb on the latch side due to flexural shortening.

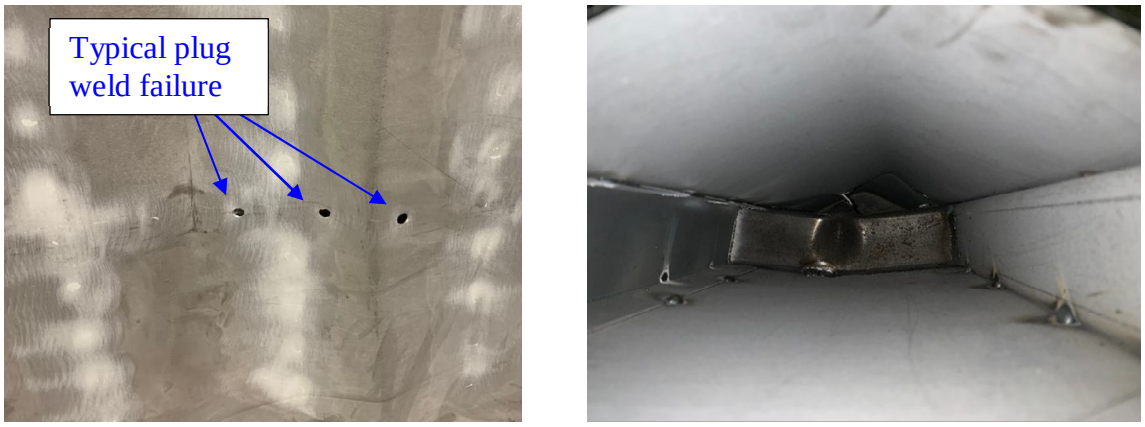

(a) Typical plug weld failure observed on the compression skin.

(b) Typical flexural yielding of central HSS tube after loss of composite action.

Figure 2.19: Photographs of typical failure modes observed during Series 2 tests.

Series 3: Full Weld attachment (Max, 100% Plug Weld Specification)

The load-deflection curves for specimen 3A and 3B, shown in Figure 2.20, were very consistent. This confirms a high degree of repeatability in the behavior of door panels constructed using welded construction, regardless of weld spacing. The elastic limit for the two specimens of Series 3 occurred at similar displacements ($\delta = 0.252$") and an applied load of ($P = 6{,}820\ lbs$).

As was observed during Series 2 tests, intermittent cracking could be heard emanating from the door leading up to this elastic limit. Loss of plug welds along the central HSS tube, characterized by the discontinuities in the load-deflection curves shown in Figure 2.20, initiated failure. Both specimens of Series 3 lost composite action at mid-span due to skin-core weld failure. The first weld failures occurred at $\delta = 0.57$" and $P = 10{,}230\ lbs$ for specimen 3A and $\delta = 0.844$" and $P = 10{,}720\ lbs$ for specimen 3B, the points at which full composite action was lost. Significant buckling of the skins on the compression side occurred, which can be seen in the post-damage photographs shown in Figure 2.20.

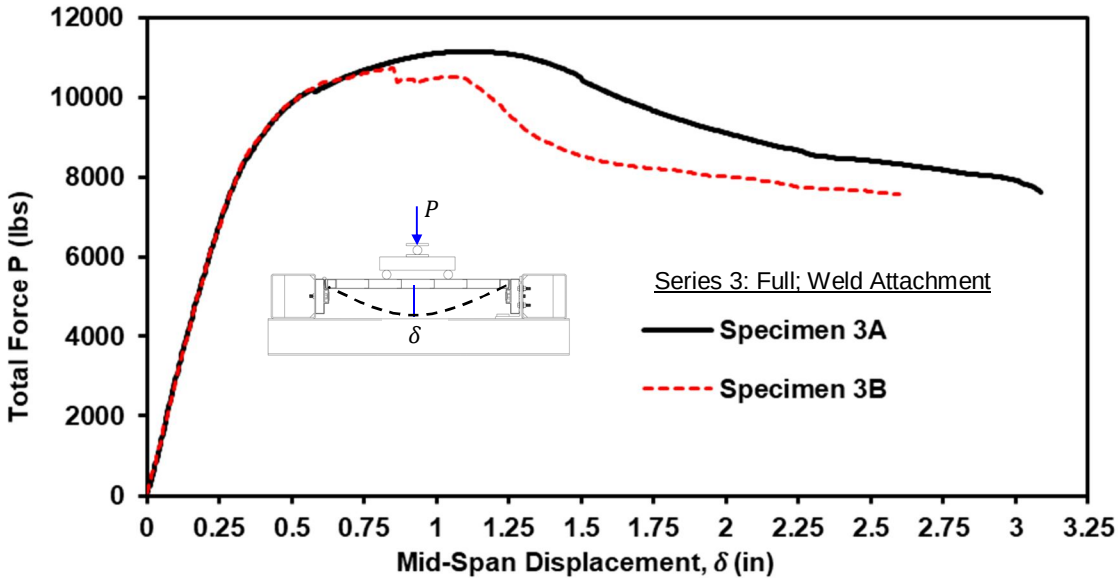

Figure 2.20: Comparison of load-deflection behavior of Series 3: Plug Weld Attachment (100% spec) beam-assembly specimens.

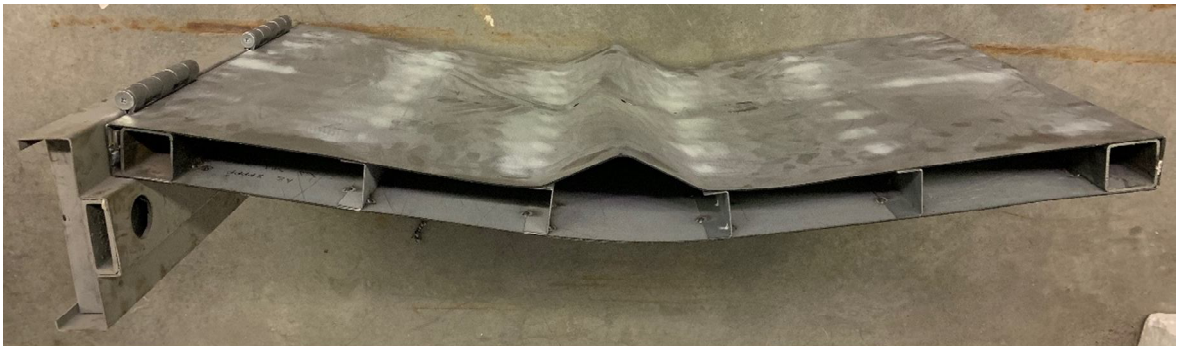

(a) Specimen 3A, plug weld failure, and skin buckling on the compression skin at mid-span.

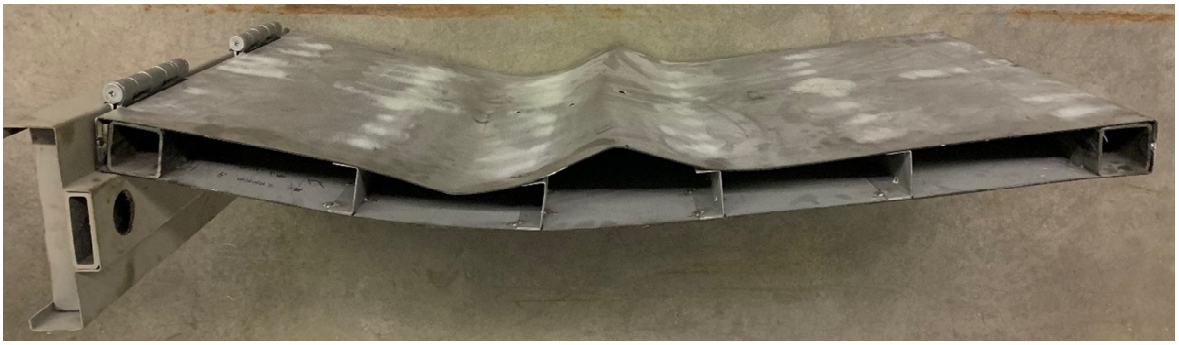

(b) Specimen 3B, plug weld failure, and skin buckling on the compression skin at mid-span.

Figure 2.21: Post-test photographs taken of Series 3: Full weld attachment.

Both specimens were able to achieve some level of redistribution; Specimen 3A achieved an ultimate load at $\delta = 1.08"$ and $P = 11{,}140\ lbs$. Specimen 3B was unable to achieve a higher load after re-distribution than before composite action was lost.

Specimen 3A and 3B had the most consistent elastic limit of all doors tested in of the first three series of tests at $\delta = 0.252"$ and $P = 6{,}820"$. The ultimate load of specimen 3A occurred at a larger displacement and load at $\delta = 1.08"$ and $P = 11{,}140\ lbs$ than specimen 3B at $\delta = 0.844"$ and $P = 10{,}720\ lbs$. Specimen 3B underwent a much more drastic loss in load due to its plugs weld loss at mid-span; which also occurred at high displacement and load than the first plug weld loss of 3A. It was again noted within Series 3 (as within series 2) that the hinge did not deform during testing of specimen 3A, and the door slipped past the door stop of the latch frame.

2.4.2 Hardware Capacity Specimens

In the following sections; the results of the hinge hardware tests are discussed. As a pre-cursor to the reading, it should be mentioned that Series 7 Pin & Barrel hinges were the only hinge specimens to reach capacity. In all other cases, the flexural capacity of the beam-assembly was reached with a plastic hinge developing under the point load closest to the latch-side of the specimen prior to hinge failure. This failure mode is likely different than what would be observed had both hinges and latches been tested at once, as the latch would have provided a less boundary response on the latch side during testing. The subtle differences in performance of all other specimens are discussed and arise, primarily, from the way in which the hinges were connected to the beam-assemblies and door frames.

Series 4: 6" PBB Stainless Hinges

Both hinge specimens of series 4 had consistent load-deformation behavior, as seen in Figure 2.22. During the loading portion of the test, several weld failures were observed between the door stop HSS and the frame-skin, which can be observed as sudden drops in the load-deflection curve in both samples of Figure 2.22. A typical photograph of these weld failures is indicated in Figure 2.23. In both tests of Series 4, a maximum load of approximately $P = 14{,}100\ lbs$ was reached. Test 4A was terminated after peak load had been reached, while all subsequent tests were performed until maximum specimen deformation capacity of the test fixture was attained (approximatey *4"*).

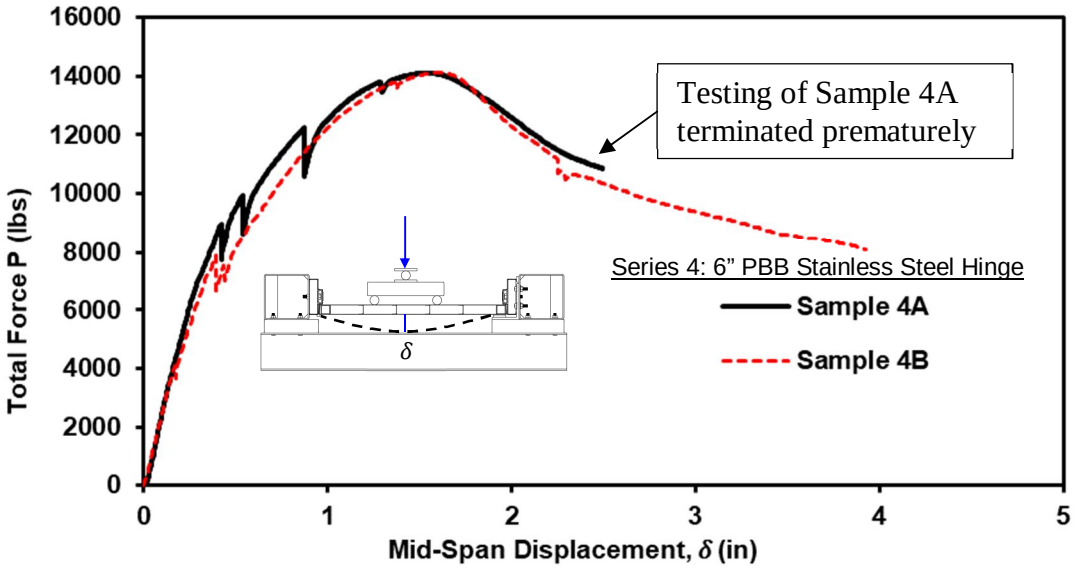

Figure 2.22: Comparison of load-deflection behavior of Series 4: 6" PBB Stainless Steel Hinges.

Figure 2.24: shows photographs of damage to the door and frame skin for both Series 4 specimens. Significant deformation of the sheet metal skin covering both the frames and the door panels occurred as the hinge reinforcement plates were only welded to the skin, rather than to the internal framing elements. As a result, the hinges were essentially "floating" with only a few welds between the hinge reinforcement plates and sheet metal responsible for providing a load-path through the beam-assembly. The deformation of the specimens in the area of the hinge attachment, shown in Figure 2.24, would be substantially reduced if the hinge reinforcement plates were mounted to the internal core components. Such enhancements would also lead to improvements in overall blast resistance.

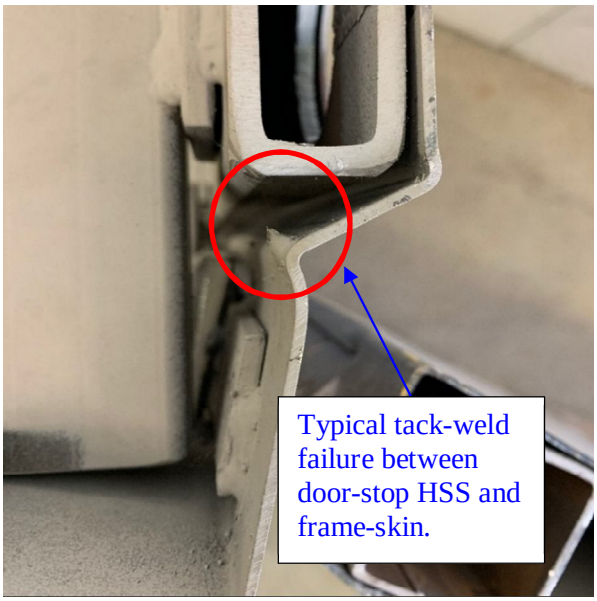

Figure 2.23: Typical door stop HSS frame-skin weld failure.

(a) Test 4A skin deformation.

(b) Test 4B skin deformation.

Figure 2.24: Post-test Series 4 frame deformation photos.

The hinge reinforcement plates also experienced significant deformation, as illustrated in Figure 2.25 (a). The Specimen 4B hinge reinforcement plates were so badly deformed that the hinges could not be removed after the test and negatively affected door swing. Despite significant deformation to the components surrounding the hinges, the hinges themselves performed well, and no damage was observed in Figure 2.25 (b and c).

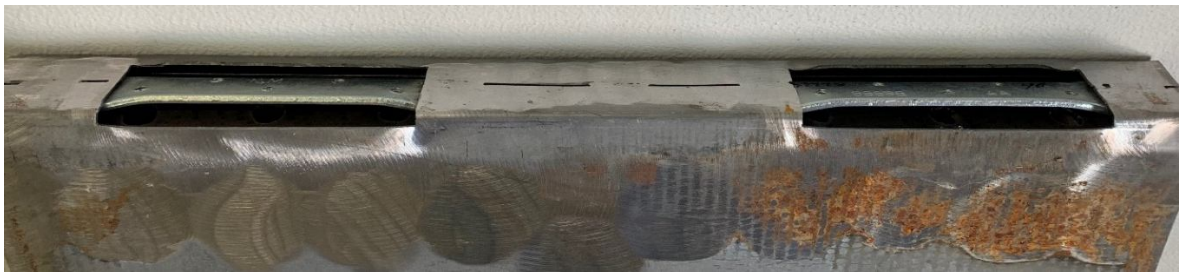

(a) Typical hinge mount plate deformation observed for Test 4A/4B.

(b) Close-up of Test 4A hinges.

(c) Close-up of Test 4B hinges.

Figure 2.25: Post-test damage Series 4 photos.

Series 5: Frame-Pins with 4.5" Hinges

Both hinge specimens of Series 5 had comparable load-deflection behavior through the linear portion of the loading curve as seen in Figure 2.26. No weld loss was observed between the frame skin and door-stop HSS; as a result, the curves for both specimens shown in Figure 2.26 are relatively smooth and free of discontinuities typically observed when welds failed. Test 5A achieved a maximum load of $P = 12{,}560\ lbs$ and test 5B achieved a maximum load of $P = 13{,}840\ lbs$.

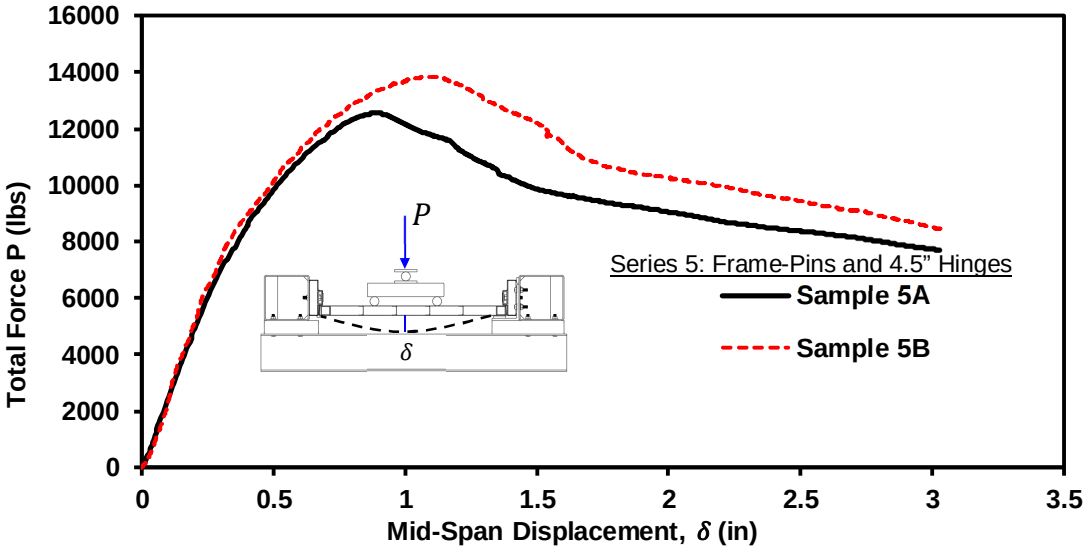

Figure 2.26: Comparison of load-deflection behavior of Series 5: Frame-Pins & 4.5" Hinges.

Visible damage was noted in the actual hinges of both tests in Series 5; most notable, was hinge deformation in the hinge knuckles as seen below in Figure 2.27 (a). The hinge knuckles for Series 5 hinges were not welded or integrally attached to the hinge leaf as indicated in Figure 2.27 (a), which allowed the hinge knuckle to begin to "unroll" during testing. The hinge leaves of the hinges were also observed to slide along their respective hinge reinforcement before the pins came into contact with their interlocking holes within the frame, as indicated in Figure 2.27 (b). No significant frame-skin deformation or weld failure (as previously mentioned) was evident throughout testing shown in Figure 2.27 (b and c).

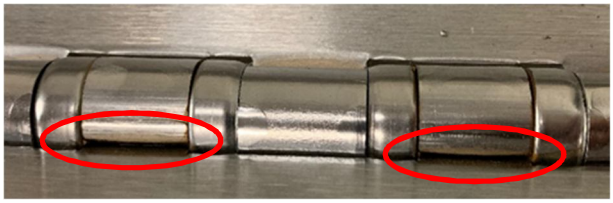

(a) Typical hinge knuckle deformation.

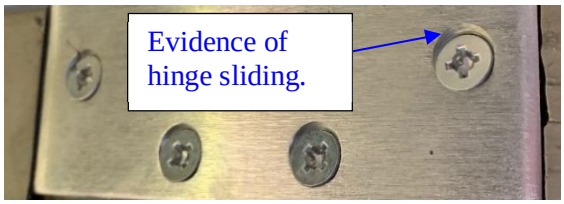

(b) Typical hinge-leaf sliding at screw/hinge interface.

(c) Test 5A frame-skin deformation.

(d) Test 5B frame-skin deformation.

Figure 2.27: Post-test photos of Series 5 (Frame-Pins and 4.5" hinges).

Series 6: Hinge Retainer & 4.5" Hinges

Both hinge specimens of Series 6 had consistent load-deflection behavior as can be observed in Figure 2.28. Weld failures in the door panel and frame components, characterized in the load-deflection response, were observed throughout testing. The maximum loads recorded during testing were $P = 13{,}670\ lbs$ for test 6A and $P = 14{,}000\ lbs$ for test 6B.

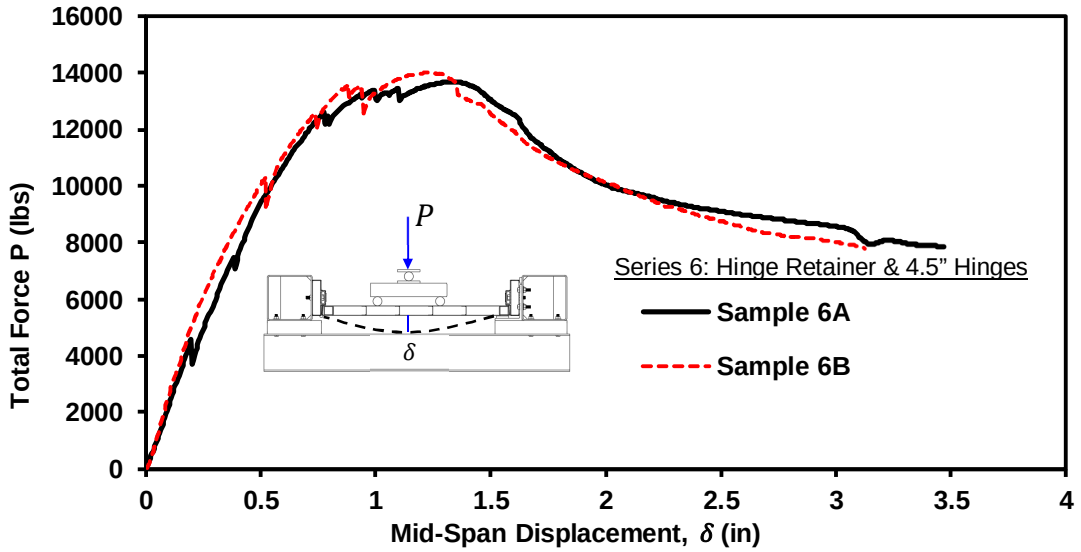

Figure 2.28: Comparison of load-deflection behavior of Series 6: Hinge retainer & 4.5" Hinges.

The hinge retainer system did not perform as expected, as early weld failure left the hinges to carry the applied loads. The previously mentioned weld failures were observed at (i) the two tack welds at each corner of the retainer angles necessary to fix the retainer to the frame (Figure 2.29), and (ii) along the door stop HSS and frame skin (Figure 2.30). Substantially more robust fillet welds along the retainer angle would improve the performance of the system at minimal overall additional labor.

Hinge knuckle deformation, shown in Figure 2.31 (a), was observed after testing. As was the case for Series 5 hinge hardware, the hinge knuckles for Series 6 hinges were not welded, which allowed the hinge knuckle to effectively unroll after the retainer angle had failed. Hinge leaf sliding was, again, observed during testing of both sets of hinges as shown in Figure 2.31 (b). It is important to note that damage to the hinges would not have occurred.

(a) Retainer angle weld failure and deformation (from test 6A).

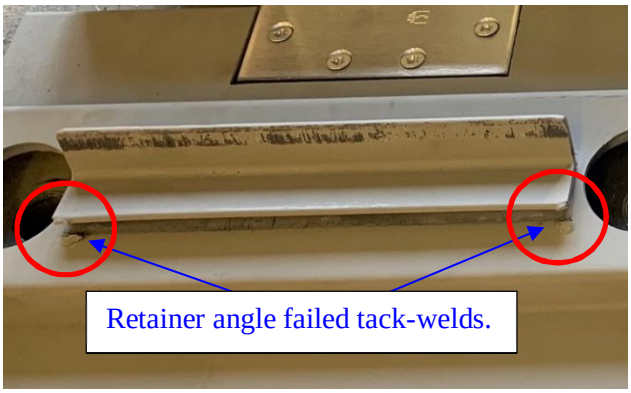

(b) Retainer angle weld failure and rotation.

Figure 2.29: Series 6 post-test frame deformations.

(a) Test 6A frame-skin deformation.

(b) Test 6B frame-skin deformation.

Figure 2.30: Series 6 post-test overall frame-skin deformations.

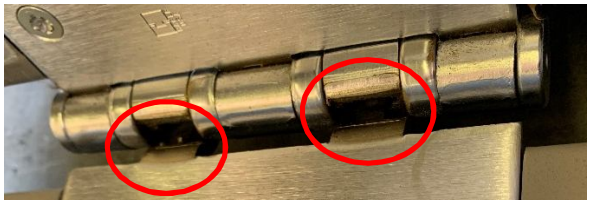

(a) Typical Series 6 hinge knuckle deformation.

(b) Typical hinge leaf slip observed.

Figure 2.31: Series 6 post-test hinge deformations.

Series 7: Pin & Barrel Hinge

The pin & barrel hinge of Series 7 demonstrated poor performance. Both hinges of Series 7 had consistent load-deflection performance as can be observed in Figure 2.32. The failure mode for Series 7 was by shear failure of the hinge screws, as shown in the photographs in Figure 2.33. Specimen 7A experienced screw shear failure at a load $P = 10{,}000\ lbs$ and Specimen 7B at a load $P = 8{,}260\ lbs$. These sudden shear failures occurred before any substantial permanent deformation was realized in the skin of the beam-assembly or the frame. During test 7A, the four screws which attached the hinge leaf to the door failed simultaneously. During test 7B, a single screw connecting the hinge leaf to the frame failed (characteristics by the sudden drop in loading at $\delta = 0.40$" for specimen 7B in Figure 2.32, with the three remaining screws failing after the application of additional load. Other than failure of the fasteners and minor global door panel deformation, there was no other notable damage observed to the hinge or panel.

It is expected that pin & barrel hinges would exhibit better performance when installed in a full-sized door assembly, owing to the greater total number of fastener screws distributed over entire hinge side, coupled with the overall reduced level of load on a full-size door compared with the beam-assembly component. However, full-size blast door tests of this type of hinge is recommended to confirm in-situ behavior.

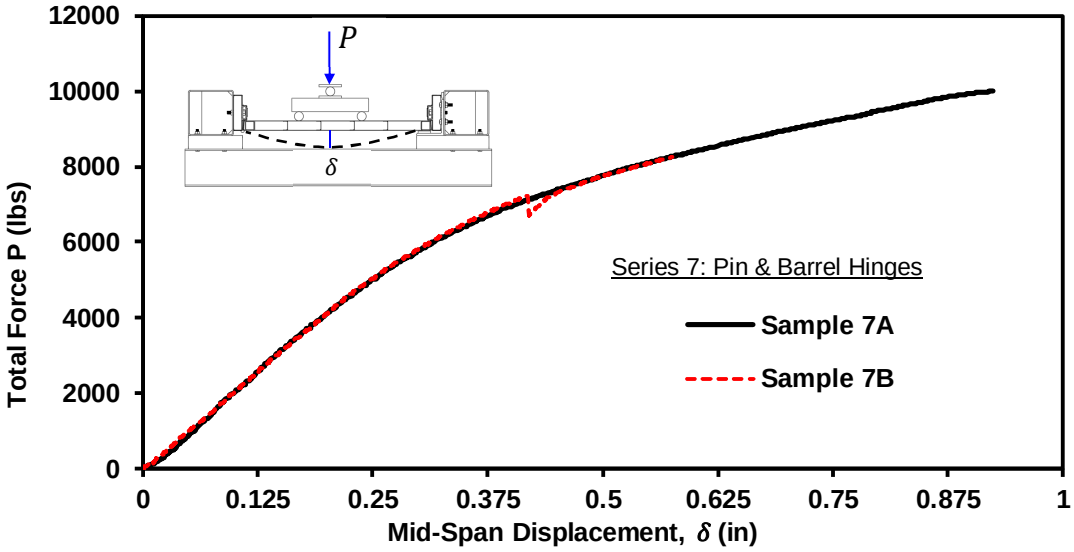

Figure 2.32: Comparison of load-deflection behavior of Series 7: Pin & Barrel Hinges.

(a) Typical Series 7 screw shear failure (on frame side).

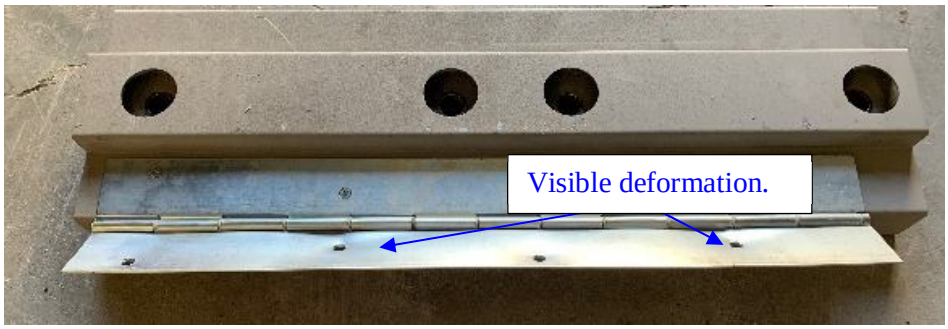

(b) Test 7A hinge deformation around screw holes.

Figure 2.33: Series 7 post-test hinge deformations.

Series 8: S2HA7 Mortised 5.75" Hinge

The hinge specimens of Series 8 demonstrated consistent load-deflection behavior as can be observed in Figure 2.34. The mortised hinges demonstrated excellent performance. No screw failures nor weld failures were observed; thus, no sudden drops in loading were noted in the load-deflection diagram. A maximum load of $P = 13{,}230\ lbs$ was achieved during test 8A and $P = 13{,}110\ lbs$ during test 8B.

No visible damage to the hinge hardware or hinge attachment was noted during or after testing. The frame segment performed well and remained undeformed after testing for both specimen 8A and 8B as can be observed below in Figure 2.35. The hinges themselves, as well as their hinge reinforcement within the frame and door remained undeformed, and the hinges were completely operable. This was attributed to the robust mounting configuration of the hinge reinforcement plates which were mounted directly to the internal structural components of the

frame and door components. Based on the experimental results, good blast performance would be expected from Series 8 hinge hardware.

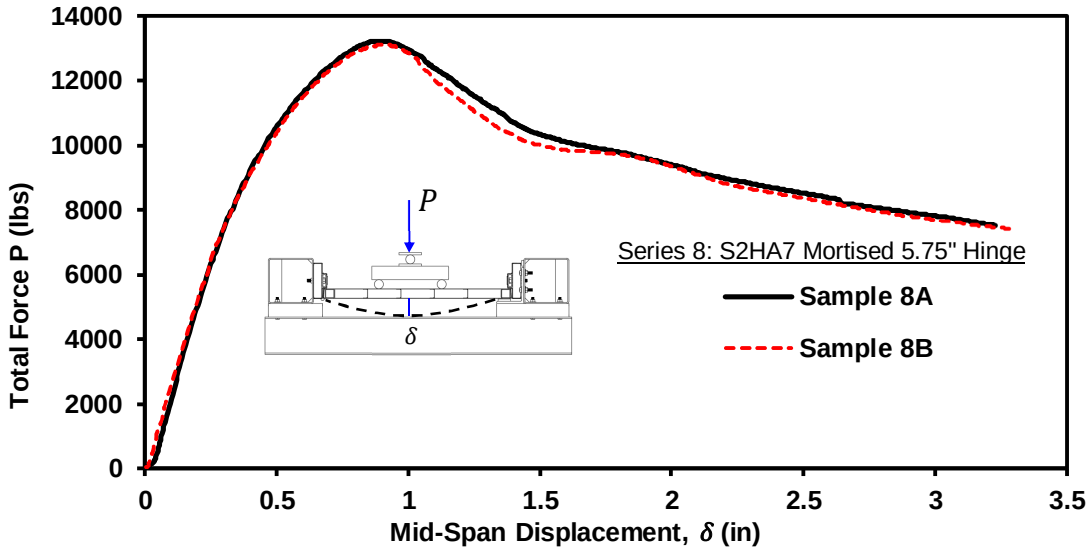

Figure 2.34: Comparison of load-deflection behavior of Series 8: S2HA7 Mortised 5.75" Hinge.

(a) Test 8A undeformed frame-skin.

(b) Test 8B undeformed frame-skin.

Figure 2.35: Series 8 post-test deformations.

Series 9A: Gallery Hinges

During the testing of 9A hinges, weld failures between the door-stop HSS and frame-skin were observed, similar to the tests of Series 4 and 6. Again, this can be observed below in Figure 2.36 as the sudden jump discontinuities in the loading curve. A maximum load of $P = 13{,}500\ lbs$ was achieved during test 9A.

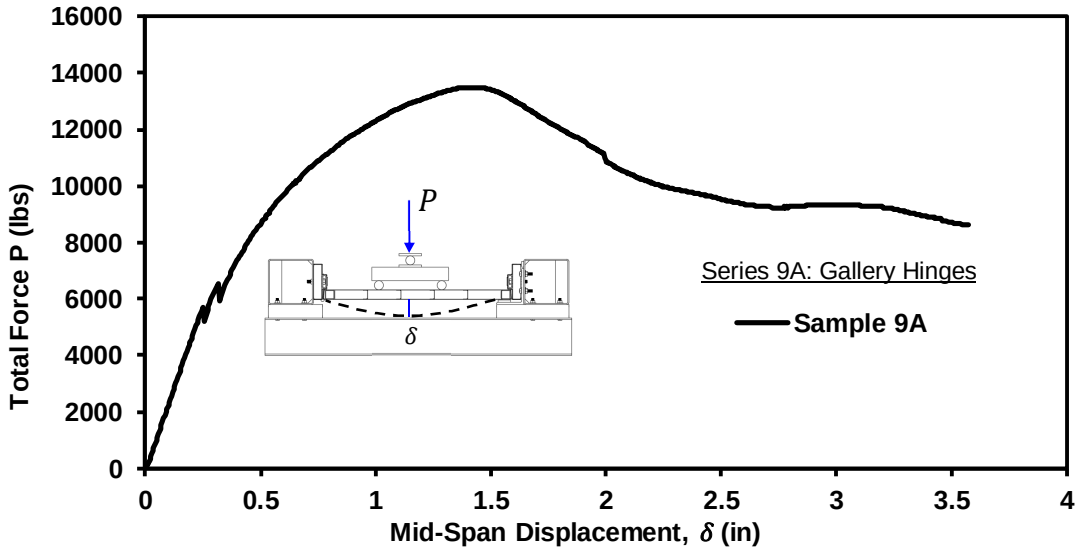

Figure 2.36: Comparison of load-deflection behavior of Series 9: Gallery Hinges.

The weld failures and subsequent deformation of the frame skin can be referenced below in Figure 2.37 (a). Significant deformation was observed in the components surrounding the hinge leaf connection points as well, shown in Figure 2.37 (b, c, and d). Figure 2.37 (d) specifically shows deformation in the door-skin. Both the hinge reinforcement plates in the door and frame allowed for movement of the hinge leaves during loading. It can also be observed from all photos included in Figure 2.37 that the hinge remained relatively undeformed.

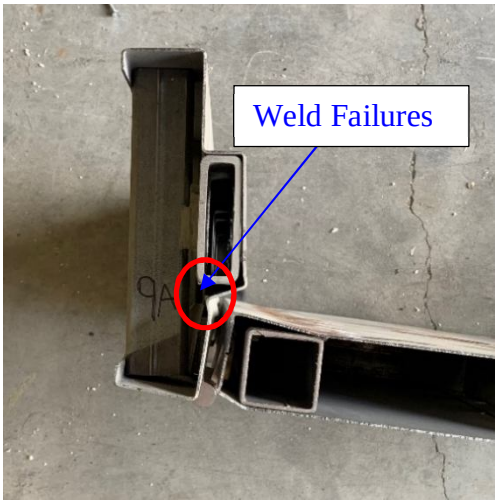

(a) Series 9A weld failure and frame-skin deformation.

(b) Series 9A typical hinge attached to deformed hinge reinforcement plates.

(c) Series 9A deformed hinge plates from bottom of the specimen.

(d) Series 9A deformed hinge plates and deformation in door-skin.

Figure 2.37: Series 9A post-test deformations.

Series 9B: 6" PBB Mild Steel Hinges

During the testing of 9B hinges, weld failures were observed between the door-skin and the door-stop HSS as seen as jump discontinuities in Figure 2.38. A maximum load of P = 12,890 lbs was achieved during test 9B.

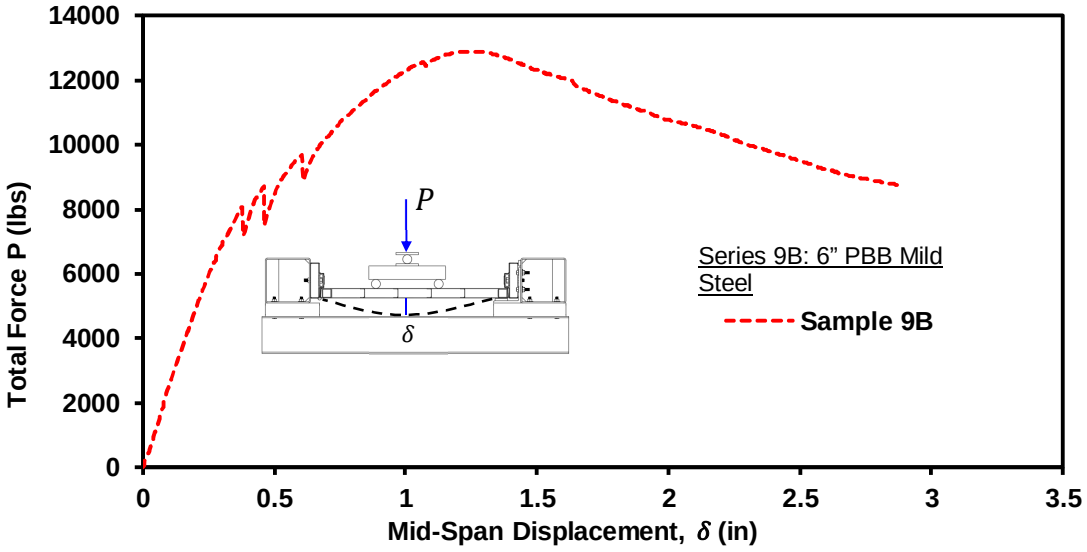

Figure 2.38: Comparison of load-deflection behavior of Series 9B: 6" PBB Mild Steel Hinges.

Visible damage was observed as weld failures, skin deformations, and screw failure. The weld failures (between the door-stop HSS and frame-skin) and subsequent deformation of the frame-skin and door-skin can be referenced below in Figure 2.39 (a). The screw failure is indicated in Figure 2.39 (b).

(a) Series 9B weld failure and frame-skin deformation.

(b) Series 9A deformed hinge plates and deformation in door-skin.

Figure 2.39: Series 9B post-test deformations.

2.5. Discussion

The objective of this phase of research was to leverage the results of the beam-assembly tests to inform on the design of full-size hollow metal doors to achieve optimal blast resistance. Accordingly, the beam-assembly tests were analyzed and discussed within the context of ASTM F2927-12, the standard test method for door systems subject to air blast loadings. ASTM F2927-

12 provides quantitative damage descriptions for various door levels of protection (discussed previously in Section 1.3 and summarized in Table 1-1). These damage descriptions can be used to identify beneficial (or detrimental) door construction and hinge behaviors observed during the static tests that can be used to infer information about probable blast performance in a full-size door assembly.

Door Construction Methodology

The three door construction methodologies were compared based on their ability to maintain composite action between the skin and core, and on the basis of their ability to resist large out-of-plane loads. According to ASTM F2927-12, resistance to deformations is an important consideration in blast performance because: (i) excessive deformations may cause the door to become lodged in place, rendering it unusable after the blast event; (ii) excessive deformation may cause the door to slip from its door-stop seating and open when loaded in the seated direction, allowing pressures and flying fragments to enter the protected space; and, (iii) excessive deformations may lead to the door becoming unlatched during rebound, leading to the door becoming opened during the blast event.

All three door construction methodologies shared similar load-deflection behavior prior to the loss of composite action between the sheet metal skins and internal HSS tubes. This similarity in behavior is evident in Figure 2.40, which shows the initial slope of all specimens having nominally identical stiffness. Therefore, it can be said that prior to loss of composite action, the door construction methodology exerts no influence on the response of the door construction specimens.

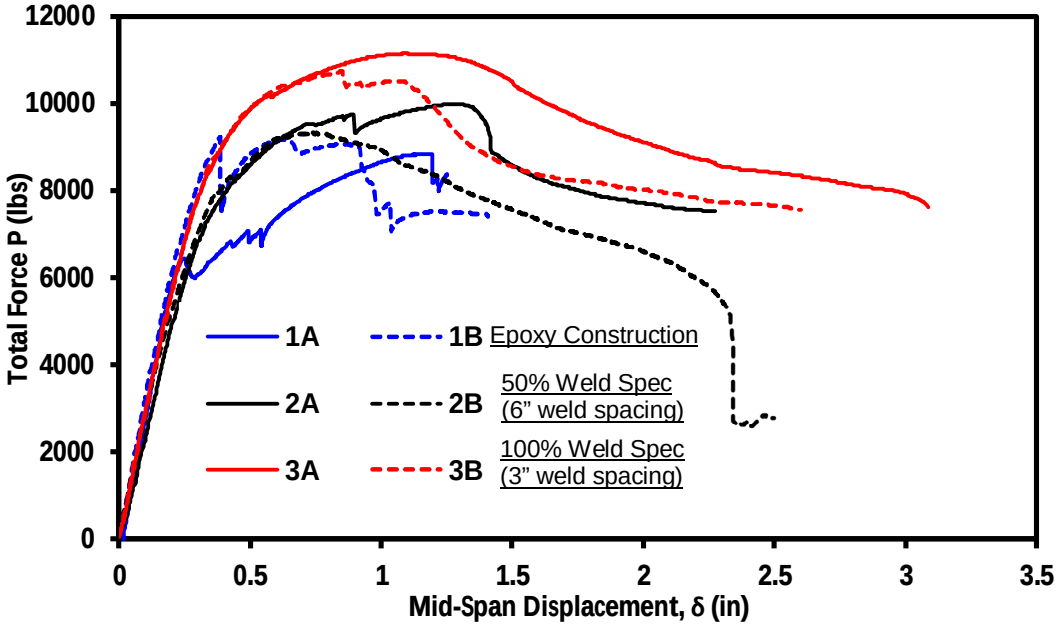

Figure 2.40: Comparison of load-deflection behavior for the three door construction methodologies.

However, the manner in which the skins were attached to the internal tubes was a critical design parameter influencing the peak strength and ductility of the beam-assembly samples. The epoxy-constructed specimens (Series 1) demonstrated the lowest and most variable load-deformation response after composite action was lost compared with the welded construction (Series 2 & 3). The variability in the load-deformation response of the two epoxy samples (Test 1A and Test 1B in Figure 2.40) poses potential challenges for design since the inconsistent responses would require penalizing the design capacity for epoxy doors to account for high resin variability. This would likely require determination of some critical stress between the skins and internal core or limiting overall deflection, after which, all composite action should be ignored.

In addition, the failure mechanism of the epoxy specimens was both sudden and catastrophic as compared with the localized and gradual failure observed for the welded specimens. Once the interfacial stresses at the skin-tube interface exceeded the capacity of the epoxy adhesive, an unstable and instantaneous failure occurred whereby the entire epoxy adhesive failed within the shear span, and the skin became entirely disengaged from the core. It was later noticed that weld cracks occurred within the vertical welds connecting the perpendicular HSS members of the core. These cracks only occurred in the epoxy-constructed specimens. It is likely that the cracks developed as a result of the transfer of stress due to the immediate loss of composite action.

Because the localized failure of the epoxy adhesive causes a cascading loss of composite action along the entire skin (*i.e.*, failure propagates following a "zipper effect"), there is a strong possibility that a full-sized door constructed with epoxy could exhibit high hazard failure (ASTM, 2012) at even modest pressure-impulse combinations. However, a close examination of the epoxy installation quality control of Series 1 showed that the epoxy resin was not applied over the entire surface of core elements in contact with the sheet metal door-skin. This can be seen in Figure 2.16, where the epoxy coverage is roughly *50%* of the total skin-core contact surface. Improved epoxy application procedures could potentially remedy some of the inconsistency issues noticed during the beam-assembly tests, although additional testing with improved resin installation would be required to confirm this belief.

It was observed that the welded specimens (Series 2 and 3) exhibited similar behavior to each other after reaching peak loading. Failures were observed to be incremental and localized to an area over one or two failed plug welds. It was determined that the plug welds essentially arrested the propagation of failure which would otherwise occur over a large area of skin and core attachment. This localization focused on the plastic response to the unbonded region. This allowed the door specimens to retain composite action over larger deformations. The specimens which had closer and more frequent welds between the skins and core (Series 3) achieved the highest loads during testing.

It can be considered that, under blast loading, the higher strength and more gradual failure of the *100%* weld spec (Series 3) doors would allow for better performance than *50%* weld spec (Series 2) when considering performance characteristics of ASTM F2927-12. It is certainly apparent that the closer weld specification achieved higher loads and greater ductility, as can be seen in Figure 2.40. However, it is our opinion that the level of deformation required to realize the difference in performance between the partial and full weld skin construction methodologies would not likely be achieved in a blast loading scenario. It may be more efficient to focus the additional labor costs of applying more closely spaced welds in more key areas rather than apply closers welds over the entire specimen. For instance, it is likely more important to employ closely spaced welds on the central and side HSS beams of the doors rather than along the stiffeners. This would lower costs without sacrificing most of the extra capacity that is gained in specifying the maximum weld pattern. A further observation of the welded specimens of Series 2 and 3 was that failure was always initiated on the compression surface, which was attached via plug welds in

every case. It may be worth testing specimens with stronger filet welds on the compression skin in the future to determine if this would provide better composite action. Full-scale blast testing or additional static tests are recommended to confirm and validate the hypothesized enhancements.

Hinge Hardware Testing

The seven hinge hardware types were qualitatively evaluated based on their potential ability to ensure the door remained operable after a blast event to allow occupants to safely evacuate the structure. In addition, their performance was qualitatively assessed on the possibility that a catastrophic failure of the hinge hardware could result in the entire door or the hardware components becoming a projectile and posing a hazard to occupants. These performance requirements are two of the key criteria for blast resistant door construction per ASTM F2927-12 (ASTM 2012).

The *6"* PBB hinges of Series 4 demonstrated good performance under static loading. The knuckles of the hinges were welded; thus, "unrolling" [*i.e.*, as can be seen in Figure 2.27 (a)] was not observed. No deformation was observed to affect the screws, and no detrimental damage to either hinge leaf was observed; however, substantial deformation was observed in the skins of the frame and door panels due to the floating hinge reinforcements for each hinge leaf. Despite this deformation, the beam-assembly remained operable after static testing. Thus, the *6"* PBB hinge performed well, but its overall performance could be substantially improved if integrally connected hinge reinforcements were incorporated into the design. Therefore, based on static tests, the *6"* PBB hinges are recommended for blast resistance provided integral hinge reinforcements are used.

The Hager Companies *4.5"* Hinges and frame-pin interlocking system of Series 5 demonstrated good capability in withstanding load while avoiding deformation in the sheet metal skin of the beam-assembly and frame. This was attributed to the frame-pin interlocking system, which provided a load path through the internal core components of the frame and door panel skin into the supports. Initially, the hinges resisted load only until the frame-pin interlocking system engaged, although some minor deformation of the hinges was observed. For example, the hinges slid with respect to their original mounting position due to the lack of resistance provided by the screws (this was similar to the screw deformation noted for the same hinges tested in Series 6). Furthermore, the unwelded hinge knuckles were observed to deform during loading. Based on the overall static performance of the system, this type of hinge is recommended for blast performance design. However, hinges with welded knuckles and integrally connected hinge reinforcement

plates would greatly improve performance and reduce the likelihood that the door becomes inoperable during a blast.

The Hager Companies hinges and channel retainer system of Series 6 were similar in function to Series 5, as they both employed retainer systems in tandem with a pair of *4.5"* hinges. However, the performance of Series 6 under static loading was poor. Significant skin deformation was observed around the hinge reinforcement plates during testing. This was attributed to inadequate tack welds used to attach the retainer angles to the frame skin, and the use of floating hinge reinforcements. Once failure of the tack welds initiated, the retainer angles rotated and disengaged from the retainer channel and dumped all the load into the hinges instantaneously. As was discussed in the test results, the hinge knuckles of the hinges were not welded and began to unroll, similar to what was observed in Series 5, only to a more severe extent. Therefore, based on the static test results, the use of this particular hinge and retainer system for blast protection is not recommended as the significant damage could result in inoperability of the door or detachment of components during a blast event. The performance of Series 6 could be improved if the retainer angles were fully welded, hinges with welded knuckles were used, and integrally connected hinge reinforcement plates were installed.

Both tests 7A and 7B of Series 7, which evaluated the performance of SL200 Pin and Barrel hinges, failed catastrophically at significantly less load than all other hinges. Shearing failure of the screws resulted in a loss of load-carrying capacity. As such, the loading achieved during each of the Series 7 tests was not sufficient to develop any permanent deformation in the frame-skin or beam-assembly skin around the hinge leaf attachments, despite the use of floating hinge reinforcement plates. Based on the sudden and catastrophic screw failure displayed by Series 7 hinges, it is determined that the blast performance of SL200 Pin & Barrel Hinge would be highly hazardous as the doors or any hardware components are likely to become detached during a blast event. However, full-size blast door testing of this hinge type is recommended to confirm performance.

The Surelock McGill S2HA7 hinges of Series 8 did not exhibit significant deformation around the areas of hinge attachment and demonstrated the best performance during loading of all hinges tested. This was attributed to the integrally connected hinge mounting plate connection configuration (shown previously in Figure 2.8). After flexural failure of the door, during both tests of Series 8, the hinges simply rotated open, just as they would under typical operation. Based on

the excellent performance observed during static tests, the S2HA7 hinges with integral hinge reinforcement plates are recommended for use in blast applications.

The Gallery GSH 918 Prison hinges of Series 9A demonstrated adequate performance during static loading. The hinge knuckles were welded and did not deform, allowing adequate operability after testing. Shear studs supplemented the capacity of the screws attaching the hinges to the hinge reinforcements; thus, no hinge plate sliding was observed. However, the hinge reinforcement plates were floating, which caused significant door panel and frame-skin deformation. Deformation around the hinges could be substantially reduced if integrally connected hinge reinforcement plates were used. Use of the Gallery GSH 918 Prison hinges for blast application is recommended, contingent on the use of integrally connected hinge reinforcement plates.

The *6"* PBB Mild steel hinges of Series 9B were very similar in performance to Series 4. The welded knuckles, just as in Series 4 testing, performed well and maintained rotation capability throughout testing. Hinge leaves performed well during loading, as no deformation was observed. As with other hinges, aside from the S2HA7 hinges of Series 8, floating hinge reinforcement plates contributed to significant frame and door panel skin deformations. Thus, PBB Mild steel hinges are recommended for blast applications, provided the more robust hinge reinforcement plate configuration is used.

Considering the performance of all hinges tested; it is apparent that the Surelock S2HA7 hinges of Series 8 were most well-suited for blast applications. The hinges exhibited virtually no deformation and were integrally connected to the internal core of both the frame and the door panel. The frame-pin retainer and hinges of Series 5 would likely provide the next highest level of protection during a blast event due to the continuous load path provided by the integrally connected frame-pin interlocking retainer system. The relative performance of the hinges from Series 4 and Series 9A and 9B were virtually indistinguishable from each other and exhibited similar performance characteristics and suffered from similar weaknesses related to their inadequate attachment configuration to the beam-assembly and frame. However, the blast performance of Series 4 and Series 9A and 9B would substantially improve if integral hinge reinforcement plates were used. The retainer angle and channel interlocking system of Series 6 rely too much on the tack welds of the retainer angles and, as such, performed worse than frame-pins of Series 5. The

pin and barrel hinge of Series 7 was determined to have the most undesirable blast performance characteristics as the hinges failed suddenly and catastrophically.

2.6. Recommendations

Based on the results and observations from the door construction and hinge hardware beam-assembly tests reported in this document, the following are recommendations to enhance the blast resistance of full-size hollow metal doors:

- Whenever possible, door panels fabricated with full weld attachment spaced at *3"* should be used for blast door construction as they were found to provide the greatest out-of-plane load capacity and ductility. However, door panels fabricated with partial weld attachment spaced at *6"* may be suitable for modest blast pressure-impulses provided full-scale door tests are performed to confirm resistance.
- Doors constructed using epoxy resin are not recommended for blast applications at this time due to highly variable loss of composite action observed during beam-assembly tests.
    - Epoxy resin should be applied following the manufacturer directions over the entire contact surface between the internal core and sheet metal skin to improve composite action and flexural resistance of the doors.
    - Additional static testing should be performed to evaluate the capacity of door panels fabricated using improved epoxy application.
- A full penetration weld provided around the perimeter of all intersecting HSS framing elements would substantially increase the strength and stiffness of door panels, particularly benefiting performance after composite action is lost.
- Skin attachment via filet welds on the compression skin (rather than on the tension side as tested) would provide for a stronger connection and potentially provide better restraint to the compression skin again buckling, thus leading to an overall improvement in the performance of all welded attachment specimens.
- "Floating" hinge reinforcement plates should be avoided for blast applications due to large deformations concentrated in the skins at the hinge locations which can potentially lead to catastrophic failure of the door.

- “Integrally connected” hinge reinforcement plates should be used whenever possible for blast applications as they provide a rigid, continuous load path from the door panel through the hinge to the frame and into the surrounding substrate.
- Hinges with fully welded or continuous knuckles should be used whenever possible for blast applications to limit undesirable hinge deformations and improve the post-blast functionality of the doors.
- Based on the static test results, the Surelock S2HA7 hinges of Series 8 are believed to offer the most robust blast protection, followed by, in decreasing order: the externally-mounted interlocking frame-pin system of Series 5; a tie between the *6”* PBB hinges of Series 4, the gallery hinges of Series 9A, and the 6” mild steel hinges of Series 9B; the hinge retainer and *4.5”* hinges of Series 6; and, the pin & barrel hinge of Series 7.
- Full-length fillet welds, rather than tack welds which are prone to premature failure, should be used to attach the hinge retainer angles to the frame skin for the Series 6 hinge system.
- The pin and barrel hinges of Series 7, which underwent unpredictable and catastrophic failure during static tests, should not be used for blast resistant applications.
- Full-scale blast tests are recommended to confirm the recommendations made as a result of the static tests performed during this phase of the project.

Chapter 3. Analytical Modeling of Blast Doors

3.1. General

One of the significant limitations of blast testing is that there is an infinite number of pressure-impulse combinations that produce the same level of response/displacement in a component. Testing all possible combinations is not economical or technically feasible. Therefore, engineers often rely on various analytical methods to benchmark and extend what limited blast test data is available to predict component behavior for pressure-impulse combinations outside of those tested. This chapter describes a semi-empirical analytical methodology developed to predict the global deformation response of full-sized hollow metal doors subjected to blast loading in the seated direction. The methodology, developed based on previous work by Jacques et al. (2015) and Jacques (2016), consists of a combined FEM-SDOF procedure tailored to provide practicing engineers with a relatively simple tool to quickly and efficiently evaluate the blast performance of hollow metal doors. An empirical finite element model of the doors was developed based on an idealized bulk material stiffened internally by stringers and externally by skins. This model was found to reasonably approximate the out-of-plane load-deformation response of a full-size door provided the bulk material properties are calibrated against experimental data. The goal was to provide competent but non-expert practicing engineers with the flexibility to conduct in-house evaluation of the blast resistance of hollow metal doors without having to conduct live explosive or simulated blast tests. The proposed methodology was first validated against the beam-assembly test data described in Chapter 2 and then extended to the results of full-sized door tests published in the literature.

3.2. Beam Assembly Modeling

The experimental results of Series 2 and Series 3 beam-assembly tests, described in Chapter 2, were used to validate the resistance curves generated by the proposed semi-empirical finite element analysis methodology.

3.2.1 Modeling Strategy

Resistance curves describing the global load-deformation response of doors, suitable for SDOF analysis, were generated using a semi-empirical finite element analysis. The "skins and stringers" feature of ABAQUS version 6.13-1 (ABAQUS 2013) was used to create a model of the beam assemblies based on an idealized bulk material stiffened internally by stringers and externally by skins. The internal beams and stiffeners and external skins each share a mesh with the bulk material, rather than being discretely connected through finite weld locations. By eliminating the need to discretely consider individual weld connectors from the overall analysis, the simplified model does away with complexities associated with defining the strength, stiffness, and failure characteristics of welded connections. In this manner, the deformability of the idealized core material is relied upon to approximate the loss of composite action which occurs when welds fail and also describe the non-linearity which occurs during extreme loading. However, the semi-empirical approach requires that the idealized properties of the bulk material be calibrated against experimental data.

Therefore the model captures, in a simplified manner, the following global response mechanisms: (i) the strength provided by the core beams and stiffeners, (ii) the strength provided by the skins, and; (iii) the equivalent connection between the skins and the core which provides composite action, as represented by their shared mesh with the deformable bulk material.

3.2.2 Modeling Procedure

A 3D-deformable solid was first created with the same overall dimensions as the beam-assemblies shown in Figure 2.1. The 3D solid was then partitioned to create reference planes at the appropriate locations required to assign the internal HSS and C-shape stiffening members, as shown in Figure 3.1 (a). Two additional partitions were created to define the locations where the point loads were applied through the load spreader as described in Figure 2.12. The edges spanning along mid-depth of the partitioned solid were then assigned beam elements with cross-sectional properties equal to those of the HSS tubes and C-shape stiffeners. These internal beam elements, known as the "stringers," are shown in Figure 3.1 (b). Skins were next assigned to the top and bottom surfaces of the solid with the appropriate thickness of *1/14"*. Elastic-plastic material properties were assigned to the skins and core stiffening elements based on the experimental coupon tests described in 2.2.3. The material properties of the HSS core elements were assigned

58 ksi plastic yield strength and a modulus of elasticity of *29,000 ksi* as material tests were not available at the time of modeling. The properties of the bulk material were initially assumed to be elastic-plastic with a modulus of elasticity of *3 ksi* and a plastic strength of *65 psi*. The bulk material properties were then empirically selected to calibrate the model based on experimental data. The Poisson's ratio of the bulk material was taken as a constant value of *0.4* based on similar simulations (Jacques et al. 2015).

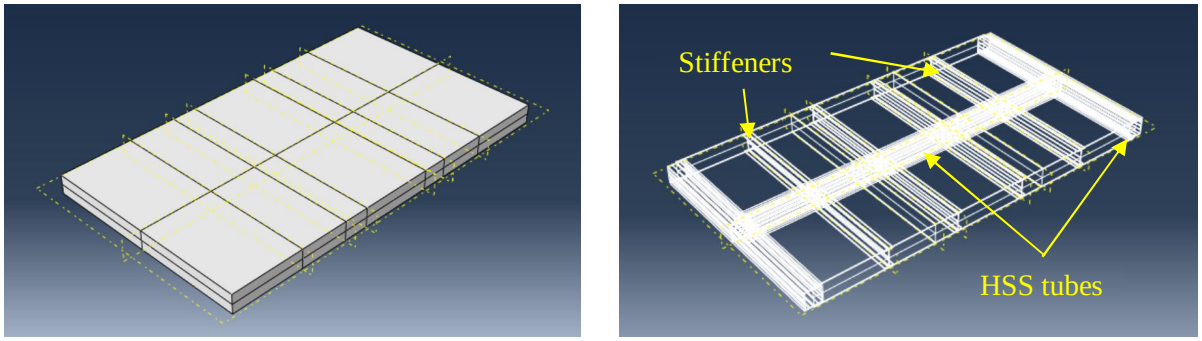

(a) 3D solid partitioning (b) Rendering of beam elements

Figure 3.1: Partitioning and core elements of skins and stringers beam-assembly ABAQUS-model.

The model was loaded in displacement control mode by applying a displacement boundary condition to the nodes on the top sheet metal skin at the locations of the load spreader. The nodes at the location of the load spreader were subjected to a progressively increasing displacement from *0"* to *3"*. The boundary conditions defined for the supports were consistent with a typical door undergoing seated response. The hinge edge of the door was assumed to be completely fixed against translation but free to rotate, which reasonably describes the level of fixity provided by the hinges. In the actual specimen, the latch side was seated on a *7/8"* door stop with an effective seating width of *3/4"*. This created a condition where the frame provided restraint against out-of-plane translation but provided no restraint against rotational or in-plane displacement. Therefore, the boundary condition along the latch side was idealized in the model by only restraining out-of-plane deformation in the direction of loading, while leaving other degrees of freedom unrestrained. The boundary conditions used in the model are rendered in Figure 3.2 (a). Once boundary conditions were determined, an appropriate mesh size was determined using a mesh sensitivity analysis to ensure the mesh had converged. The maximum global mesh element dimension was specified as *1.9"* and was set not to be smaller than *10%* of this maximum mesh dimension; while *1"* and *0.5"* global maximum mesh dimension sizes were tested, which produced practically

identical results. The larger *1.9”* approximate global mesh dimension was chosen to reduce the time of analysis.

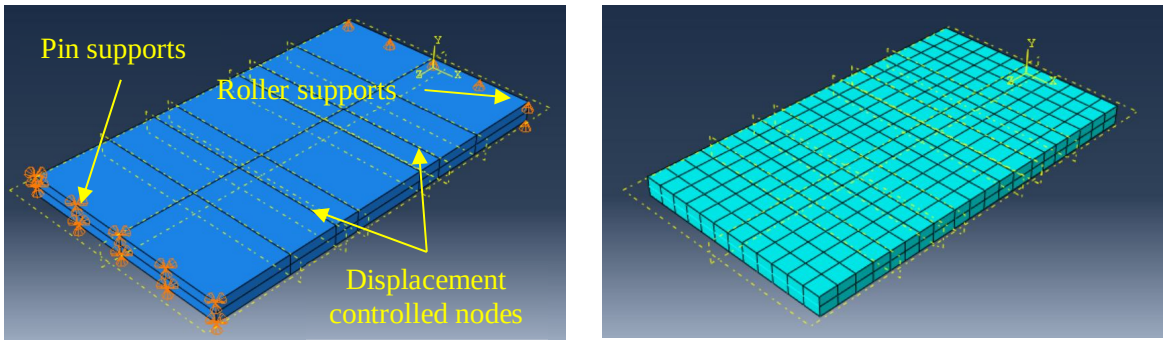

(a) Boundary conditions

(b) Final meshing

Figure 3.2: Boundary conditions and mesh discretization of the skins and stringers for beam-assembly ABAQUS model.

3.2.3 Model Calibration

The finite element resistance curves were empirically calibrated to reasonably match the experimental beam-assembly resistance curves by varying the properties of the bulk material. The beam-assembly test results from Series 2 and 3, presented in Chapter 2, were used to perform the calibration. An elastic-plastic material model was initially used for the bulk material. The yield strength and modulus of elasticity of the idealized bulk material were then altered iteratively until the resistance curve produced an adequate comparison with the test data. The results of calibration are shown in Figure 3.3. It was found that varying the modulus of elasticity of the bulk material altered the initial stiffness of the model while varying the elastic-perfect plastic yield strength altered the onset of nonlinearity and yield strength of the model. Reasonably good agreement was found between the predicted and experimental curves of Series 2 and 3 up to a mid-span displacement of approximately *1.5”* when the bulk material had a modulus of elasticity of *7 ksi* and plastic yield strength of *65 psi* for Series 2 and a modulus of elasticity of *7 ksi* with plastic yield strength of *85 ksi* for Series 3. The difference in plastic yield strength of the idealized bulk material between Series 2 and 3 was attributed to the additional welds which were provided in beam-assemblies constructing using the max. weld specification.

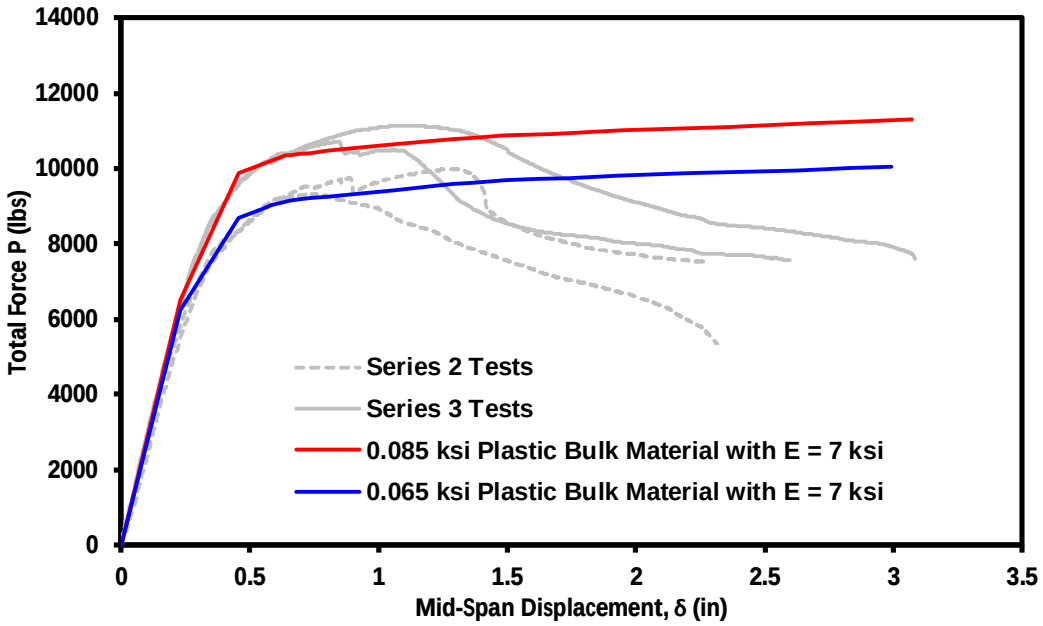

Figure 3.3: Beam-assembly model resistance curve predictions with elastic-plastic bulk materials.

The predicted resistance curves shown in Figure 3.3 were found to not capture the unloading behavior of the beam-assemblies which occurred due to loss of composite action. It was determined that this behavior could be incorporated into the model by prescribing a more detailed stress-strain curve for the bulk material which included an unloading phase. After calibrating the results to the experimental data of Series 2 and 3 separately, it was found that prescribing a general stress-strain relation (shown below in Figure 3.4) to the bulk material for Series 2 and 3 adequately captured unloading after peak load in the resistance curve predictions. The prediction of Series 2 and 3 including unloading can be seen in Figure 3.5.

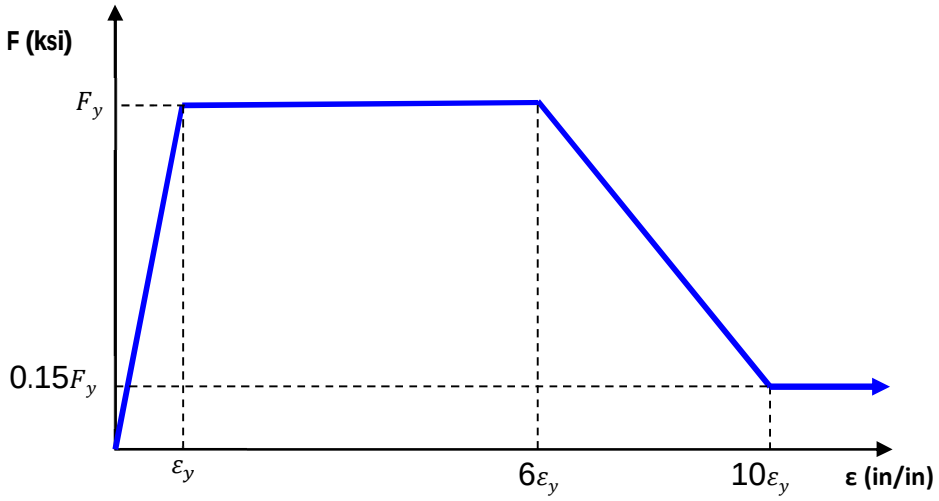

Figure 3.4: Generalized stress-strain curve prescribed to bulk materials of Series 2 and 3 beam-assemblies for modeling resistance curve unloading.

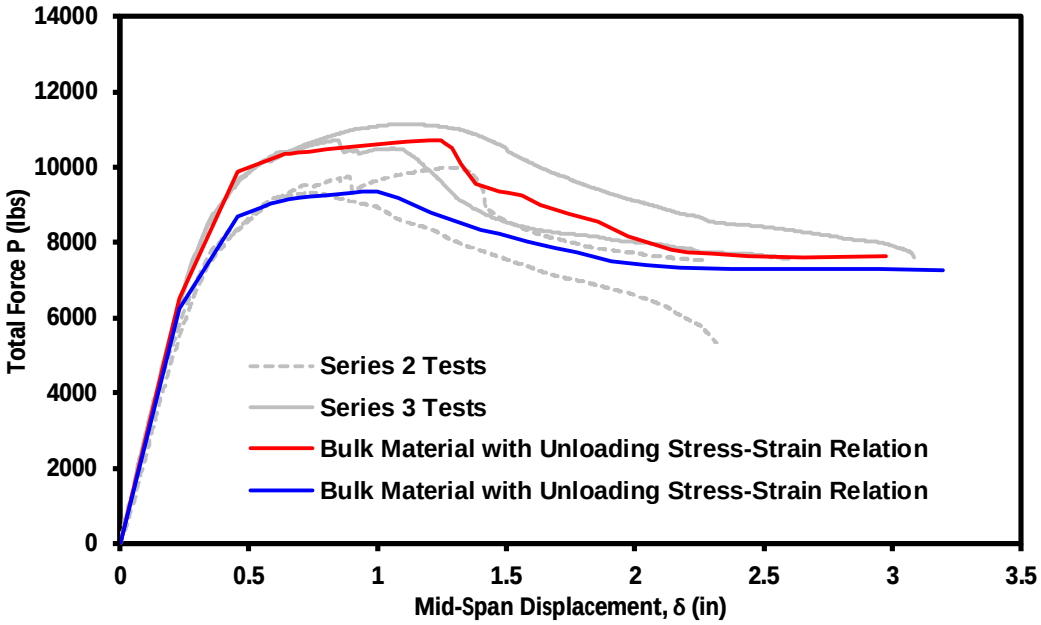

Figure 3.5: Beam-assembly resistance curves predictions with unloading stress-strain relations for bulk material.

A qualitative comparison of the predicted and experimental deformed shapes of the beam-assembly model is shown in Figure 3.6. Generally, the analysis provides a reasonable estimate of the global deformation of door panels. Due to the simplified nature of the model, buckling of the skins and the internal HSS tubes, initiated by weld failure, was not captured. However, the analysis did demonstrate that the modeling approach can be used to capture the global load-deflection

response of the beam-assembly specimens, provided the properties of the bulk material are carefully selected.

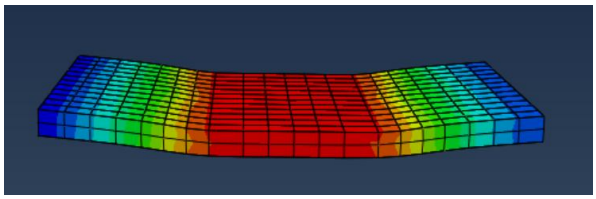

(a) ABAQUS model

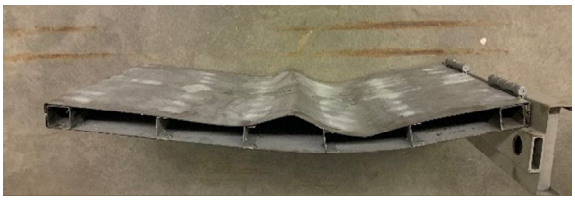

(b) Specimen 3B after testing

Figure 3.6: Deformed shape of the model showing both vertical and horizontal (flexural shortening) deformation.

Lateral shortening of the door panel, which caused the specimens to pull inwards and resulted in a loss of seating on the frame stop, was observed to occur in all beam-assembly tests. Therefore, if the lateral shortening of the door panel exceeded the effective stop width of *3/4"*, the door would slip off the stop and cause global failure. Figure 3.7 shows the experimental resistance curve for specimen 3B, which failed when the door slipped off the stop at a mid-span displacement of *3.1"*. The semi-empirical modeling procedure reasonably captured this behavior and predicted unseating would occur at a mid-span displacement of *3.56"*. It can be seen that the model overpredicts the axial stiffness of the panels at displacements after peak flexural resistance. This is attributed to the properties of the bulk material which do not accurately capture the degradation in strength of the door panel, leading to over predictions in effective axial stiffness, after peak resistance is attained. However, it should also be acknowledged that the model predicts symmetric deformation of the beam-assembly [Figure 3.6 (a)], while test specimens often experienced localized deformation under one of the point loads [Figure 3.6 (b)]. This observation may also contribute to the discrepancy observed between predicted and experimental results. Nonetheless, this comparison of slip off displacement was deemed satisfactory, given the capabilities and limitations of the measurements.

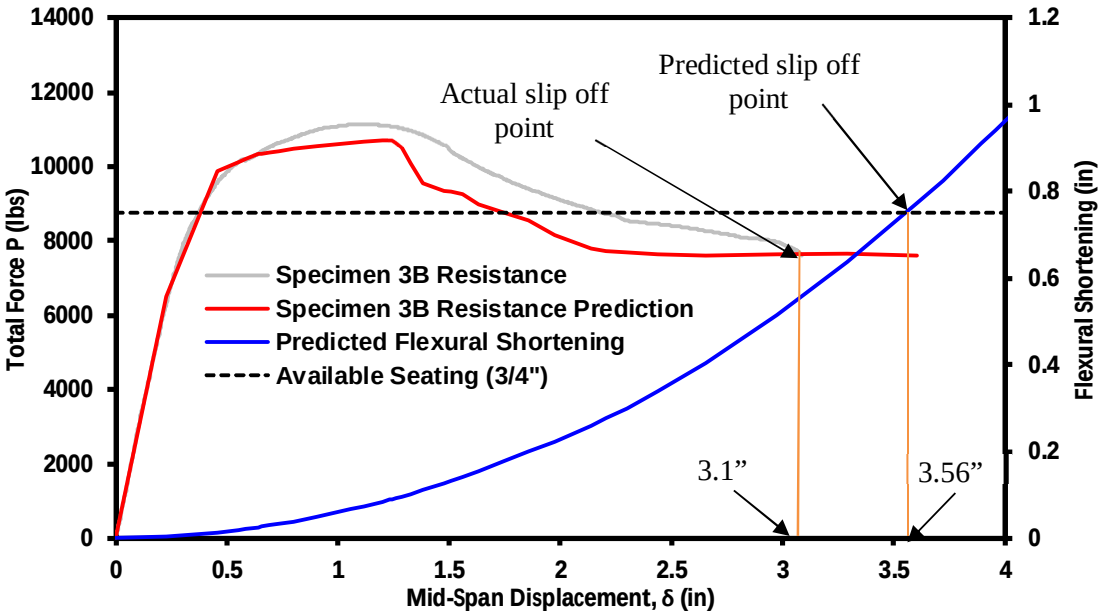

Figure 3.7: Flexural shortening analysis comparison with specimen 3B of the beam-assembly tests.

3.2.4 Discussion of Model

The proposed semi-empirical skin-stringer modeling approach can reasonably capture the non-linearity and gradual loss of composite action observed of the load-deflection response of the welded beam-assemblies (Series 2 and 3), provided the equivalent core properties can be properly calibrated against experimental data. Due to its simplified nature, the model overpredicts post-peak load-deformation as it cannot capture the propagation of weld failure, buckling of HSS tubes, and warping of sheet metal skins. However, this is not regarded as a major limitation since typical blast resistant doors are designed to satisfy ASTM F2927 (ASTM 2012) Category III “Non-catastrophic failure” or better. Doors satisfying this performance criteria are expected to experience some permanent deformations and may even become lodged in the frame, but should not undergo widespread weld failure or component buckling. Therefore, it is expected that the maximum dynamic displacement of a typical blast-resistant door will be at or near peak resistance – a displacement range for which the proposed methodology has been demonstrated to be ideally suited to predicting global load-deformation response.

3.3. Full-Sized Hollow Metal Blast Door Modeling

3.3.1 Overview

The skins and stringers modeling strategy, successfully used to describe the global load-deformation response of the beam-assemblies in Section 3.2, was extended to the case of full-sized hollow metal blast doors. Although full-sized blast doors were not tested as part of this thesis, publically available experimental data (Jacques et al. 2015; Jacques 2016) was used to validate the proposed analysis methodology. Door type ST-9A, a fully-welded structural HSS core door with similar construction to Series 2 and 3 beam-assemblies, (Jacques et al. 2015), was selected due to similarities in construction with doors that will be tested in the future using the Virginia Tech Shock Tube Testing Facility. The finite element resistance curve for ST-9A was calibrated against experimental displacement-time histories using SDOF dynamic analysis to predict displacement response. The objective of the full-size door analysis was to validate the proposed skins and stringer modeling strategy as an adequate means of analysis for future applied research into blast resistant doors.

The following provides a review of the full-size door tests, overview of the finite element and SDOF analyses, presentation of results, and discussion.

3.3.2 Review of Previous Full-size Door Tests

Test Specimen and Setup

Full-size, seated door tests were conducted using the University of Ottawa Shock Tube on door type ST-9A, a fully-welded structural HSS core door (Jacques et al. 2015). Door construction details and dimensions for this door type are illustrated in Figure 3.8. The door was composed of an HSS tube and C-shape stiffener core, that is nominally identical to the beam assemblies core components described in Chapter 2. The door was *84”* in height, *36”* in width, and *2”* thick with a total mass of *217.1 lbs*. Materials used include ASTM A500 Grade B structural steel HSS tubes, *14*-gauge galvanneal steel sheet metal with a zinc-iron coating for its sheet metal skins and *16* gauge steel sheet metal for its channel stiffener elements (Jacques et al. 2015). As previously discussed in Chapter 2, the common practice is such that the central and perimeter tubes were only welded along their depth through the thickness of the door panel, as was photographed in Figure 2.1. The door skins were then formed around the perimeter HSS members to create the external

surface of the door. Cut-outs were prepared in the skins on the hinge side with pre-tapped inserts for hinge hardware, as well as on the latch side for the installment of latch hardware. Assembly of the doors was conducted similar to the welded Series 2 and 3 beam assemblies; where skins were fillet-welded on one side and plug welded on the other to the internal core elements of the door. The doors were installed into heavy-duty steel frames which were anchored to a rigid steel test fixture using *ϕ3/4"* bolts. The doors were seated into the frame with an effective seat width of *3/4"*.

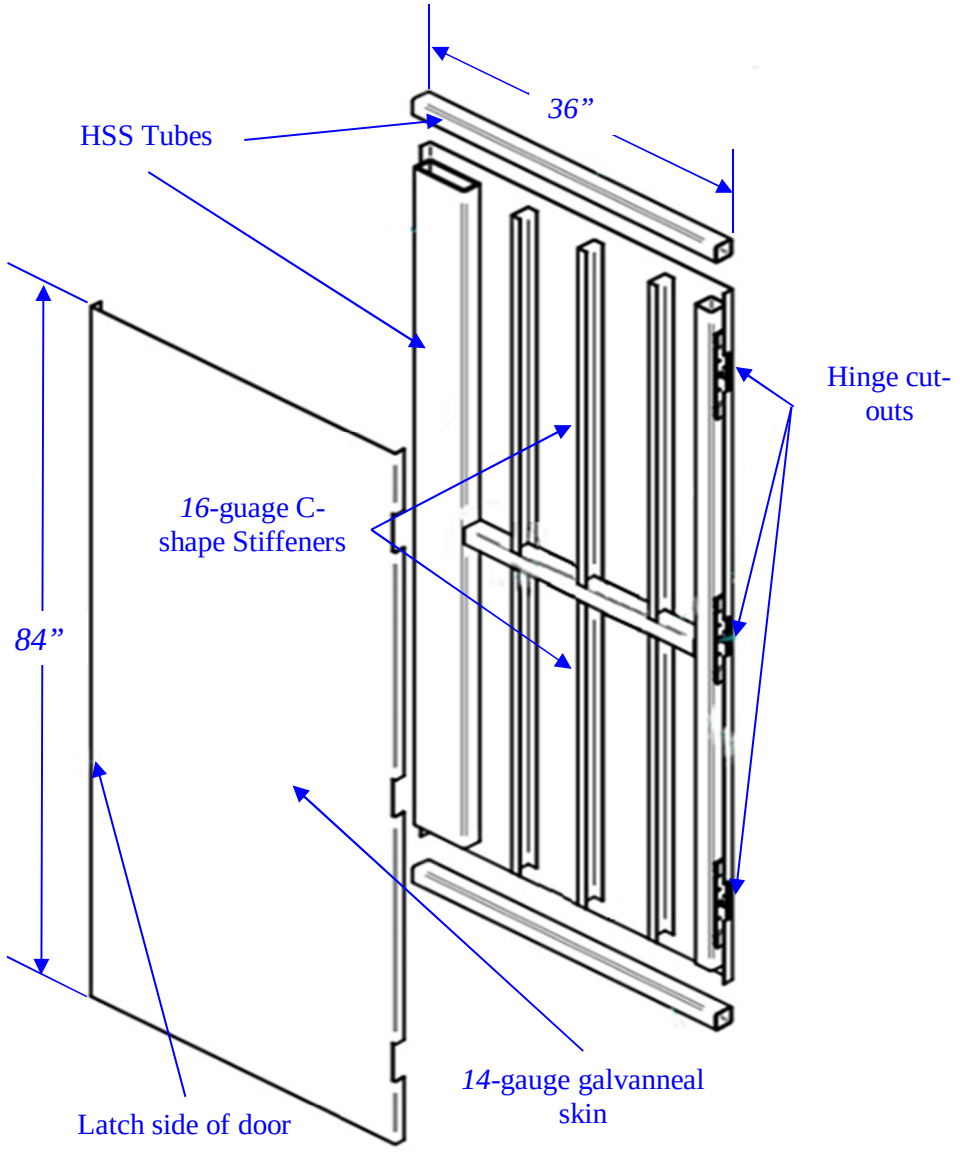

Figure 3.8: Conceptual door construction details for ST-9A blast resistant door (Jacques et al. 2015).

As shown in Figure 3.9, the doors were installed into a rigid steel test fixture and mounted to the shock tube for testing. The fixture included pre-drilled holes for the *¾"* frame bolts of the door frames. The fixture was bolted to the shock tube, and a steel plate cover was fitted over the gaps in framing members to permit full reflection of the shock-wave during testing. Pressure data was measured using piezoelectric pressure sensors located inside the shock-tube along its sidewalls *2"* from the reflecting surface of the test fixture. Five linear potentiometers, shown in Figure 3.9 (b), were used to measure displacements at various locations along the vertical centerline of ST-9A.

(a) Shock tube test fixture for full-size door assemblies.

(b) ST-9A door assembly mounted in test fixture.

Figure 3.9: University of Ottawa shock tube fixture for full-size door testing (Jacques et al., 2015).

Test Results

Door ST-9A was subjected to two progressively increasing pressure-impulse combinations. The first blast test subjected the door to a *13 psi* peak reflected pressure with a reflected impulse of *108 psi-ms* with a positive phase duration of *22.9 ms*. The reflected pressure, reflected impulse, and displacement plotted against time for the first test shot are shown below in Figure 3.10. The displacement data is obtained from an LVDT located at the approximate location of the

geometric center of the door. The maximum displacement at the center of the door during test 1 was *1.81"*, which occurred *11.34 ms* after the blast pressure was first applied.

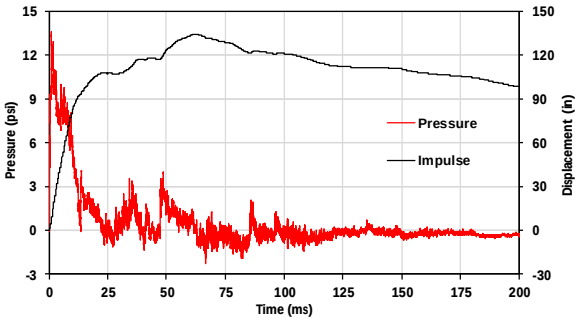

(a) Pressure and Impulse time history

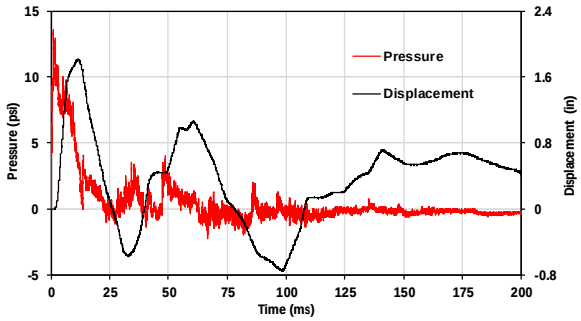

(b) Pressure and displacement-time history

Figure 3.10: Experimental results for ST-9A blast test 1.

The second blast test conducted on ST-9A subjected the door to a peak reflected pressure and reflected impulse of *13.4 psi* and *229.6 psi-ms*, respectively, with a positive phase duration of *55.8 ms*. The reflected pressure, reflected impulse, and displacement plotted against time for the second test shot are shown in Figure 3.11. The maximum displacement at the center of the door during test 2 was *1.54"*which occurred *12.35 ms* after the blast pressure was first applied.

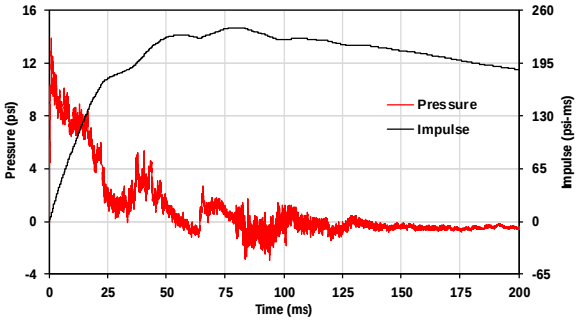

(a) Pressure and impulse time history

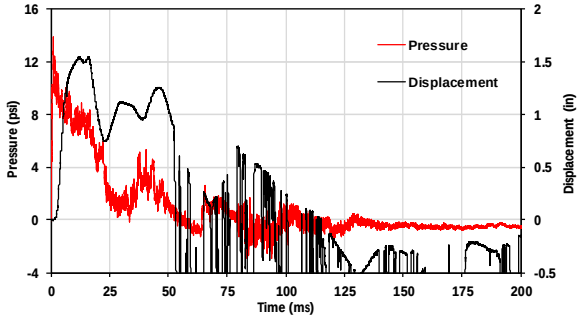

(b) Pressure and displacement-time history

Figure 3.11: Reflected pressure, impulse, and displacement-time history for Test 2 of ST-9A.

For efficiency in analysis; the shock-waves of test 1 and test 2 discussed above were idealized as triangular distributions, as is common practice in dynamic SDOF analysis. The duration of these triangular distributions are summarized in Table 3-1, alongside other key experimental results.

Table 3-1: Summary of experimental and predicted results for door test ST-9A.

	Experimental					Results	
Test	**Reflected pressure P_r (psi)**	**Reflected Impulse I_r (psi-ms)**	**Triangular Positive Phase Duration $t_d = \frac{2I_r}{P_r}$ (ms)**	**Max. displacement δ_m (inch)**	**Time-to-max.-displacement t_m (ms)**	**Max. Displacement predicted (in)**	**Ratio of predicted to experimental displacement (closer to 1 is better)**
1	13.01	108.0	16.60	1.81	11.34	1.28	0.707
2	13.39	230.6	34.29	1.54	12.35	1.91	1.24

3.3.3 Analysis

Finite Element Model Development

A finite element model of ST-9A was created employing the skins and stringers modeling strategy described and calibrated in Section 3.2. A 3D solid of the door was created and partitioned, and the appropriate section properties were associated with the core, HSS tube, stiffener, and skin elements. Materials used for the steel core elements and skins were identical to those used for the analysis of the beam-assemblies discussed in Section 2.2.3. However, the material strengths were increased to account for the anticipated effect of high strain rates which tend to increase the strength and stiffness of materials subjected to short-duration blast loads (Jacques et al. 2013). Empirical dynamic increase factors (DIFs) of *1.19* for the HSS tubes and *1.10* for the galvanneal sheet metals were applied to the yield strengths of steel to account for the dynamic effects of high strain rates (Jacques et al. 2015). The DIF values were applied to the yield strength of the HSS tube and sheet metal materials based on published DIFs for far range blast in ASCE 59-11, Table 3-5 (ASCE 2011). As with the beam-assemblies, the properties of the bulk core material were varied to obtained good correlation between experimental and predicted results. Initially, the bulk material was assumed to have an elasto-plastic stress-strain response with a modulus of elasticity of *3.0 ksi* and yield strength of *75 psi* as these were values that adequately captured results for the beam assembly tests of both Series 2 and 3 on average.

The boundary conditions of the full-size door model were similar to those of the beam-assemblies. The door frame was assumed to be rigid and not respond during loading. The hinge

edge of the door was assumed to be completely fixed against translation but free to rotate. The top and latch edges of the door, which were seated and bearing against the door stop, were restrained against out-of-plane translation and free to rotate and translate in the plane of the door. The bottom edge of the door was unrestrained against translation and rotation. The boundary conditions used in the model are shown in Figure 3.12 (a).

An equivalent static uniform surface pressure was applied on the loaded side of the door, as shown below in Figure 3.12 (a). The model was solved in load control mode, which ramped up to a maximum static pressure of *20 psi* on the door skin. The same procedure for meshing, which was conducted for the beam-assemblies, was conducted for the full-size door. A maximum global mesh dimension of *2"* was chosen, with a limit of no less than *10%* of this global dimension after a mesh sensitivity analysis was conducted to determine convergence of the mesh at this size. Again, the mesh sensitivity analysis was conducted by iteratively solving the model with smaller mesh sizes until the resistance curves generated no-longer changed as a result of this size reduction. Global mesh size limits of *1"* and *0.5"* were solved with no significant change in resistance curve output from the *2"* mesh size; as such, this larger mesh was chosen to save in analysis time. Figure 3.12 (b) shows a qualitative rendering of the typical deformed.

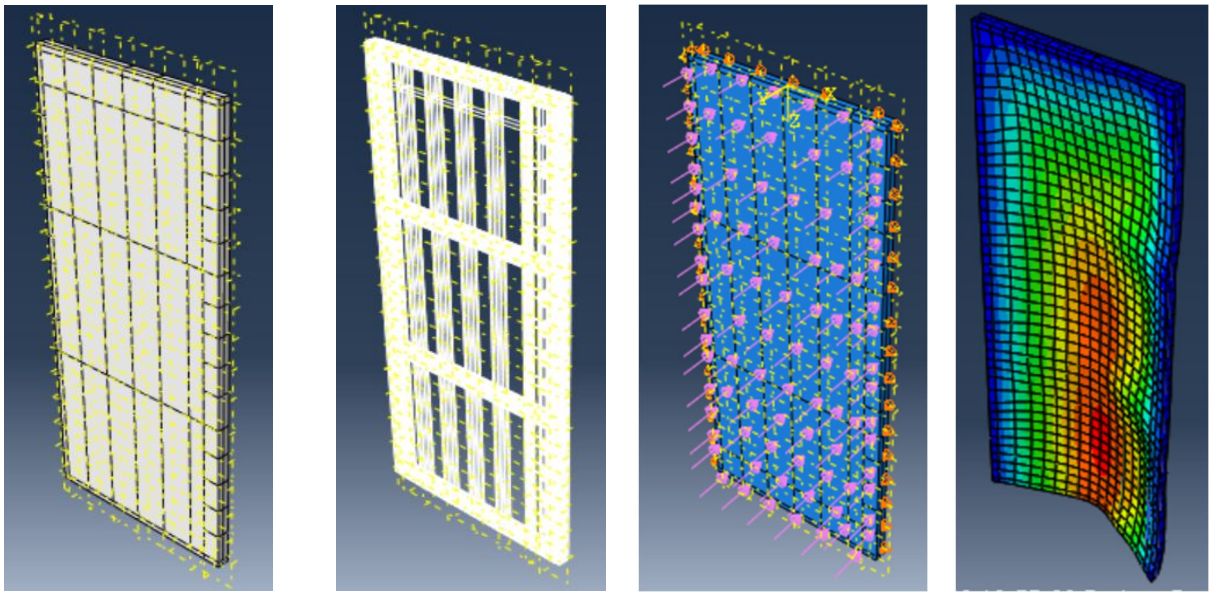

(a) 3D Partitioning (b) Render of beam elements (c) Boundary conditions (d) Deformed shape

Figure 3.12: Boundary conditions and deformed mesh for full-size door assembly FEA.

The model was used to create a resistance curve, R, describing the total static force resisted by the door (applied pressure times loaded area) and corresponding mid-point displacement. This

resistance curve was then used to perform dynamic SDOF analysis to predict the displacement-time history under blast pressure loading. Because the resistance curve is not directly measured during blast testing, calibration of the bulk material was performed through a comparison of the experimental results described in Section 3.3.2, and the SDOF predicted displacement-time history data. Typical resistance curves generated using the proposed skins and stringers methodology for various incremental bulk material properties are illustrated in Figure 3.13.

The following section briefly describes the principles of SDOF dynamic analysis and describes the procedure used to calibrate the bulk material properties of full-size blast resistant doors.

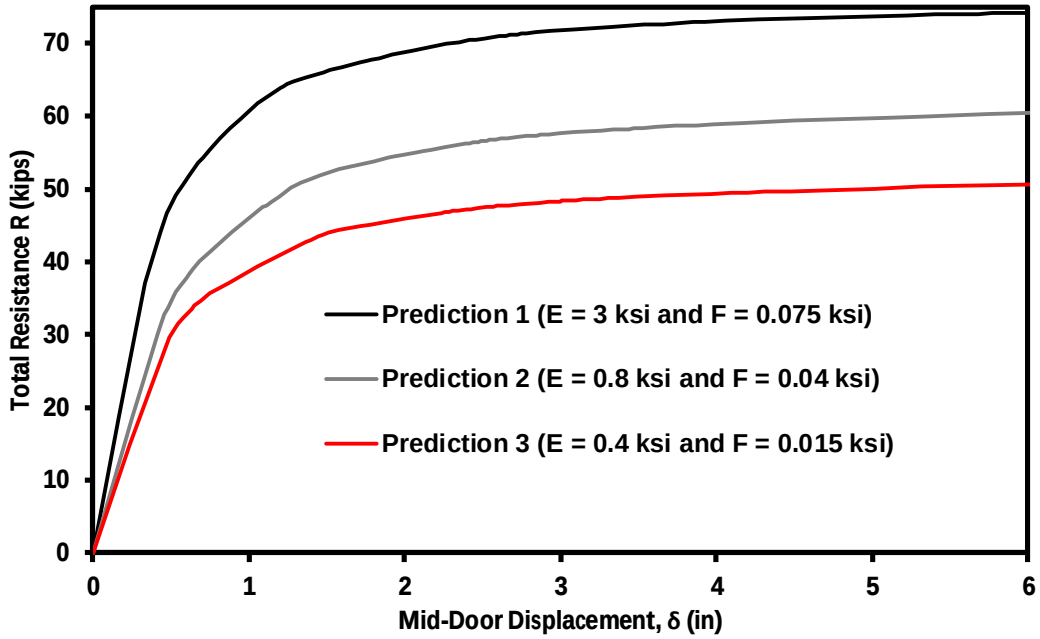

Figure 3.13: FEA model resistance curves with varying bulk material properties.

Dynamic SDOF Analysis

The SDOF dynamic analysis focused on the solution of the dynamic equation of motion presented below:

$$k_{LM}\{u(t)\} \cdot m_t + R\{u(t)\} = P_r(t) \cdot A \qquad (4.1)$$

where:

- $u(t)$ is the displacement of a single degree of freedom taken at the geometric center of the door.
- $R\{u(t)\}$ is the non-linear resistance of the door derived from the finite element model;

- m_t is the total mass of the door, equal to *217.1 lbs*;
- $P_r(t)$ is the equivalent triangular pressure-time history of the shock wave, obtained from the pressure sensor readings of the two test shots presented in Table 3-1;
- A is the loaded area of the door, equal to *36" × 84"*;
- $k_{LM}\{u(t)\}$, is the load mass transformation factor used to transform a system with distributed mass and stiffness into an equivalent SDOF oscillator. The k_{LM} factor used in the analysis was taken as a constant value of *0.73*, based on previous analysis by Jacques et al. (2015).

The software program RCBlast version 0.5.1 (Jacques 2014) was used to solve the SDOF equation of motion given in Eq. (4.1) to obtain the predicted displacement time-history for ST-9A. RCBlast was developed to conduct dynamic inelastic response history analysis of structural components subjected to blast-induced shock waves. The software uses the average acceleration numerical integration technique to solve the equation of motion. The SDOF calculations were performed for the first inbound displacement cycle since the model was developed only to predict maximum displacement and cyclic response was outside the scope of the analysis. Furthermore, damping was ignored as it has a negligible influence on results.

Results

The displacements for ST-9A tests 1 and 2 were generated using SDOF analysis performed with RCBlast. The predicted displacement-time histories were then compared against experimental test data to fine-tune the bulk material properties of the finite element skins and stringers model to obtain a calibrated door resistance curve. Three sample resistance curves for various incremental bulk material properties are shown in Figure 3.13. Initially, the elastic-plastic bulk material properties were assumed to have an elastic modulus of *3 ksi* and *75 psi* yield strength. The resulting dynamic SDOF results for blast tests 1 and 2 using the initial bulk material properties are shown in Figure 3.14 (a) and (b), respectively. It can be observed that the initial bulk properties produce a resistance curve that is substantially stronger than the actual door, resulting in a significant underprediction of the door's displacement response. Further refinements to the bulk material properties were performed by reducing the elastic modulus and yield strength of the idealized solid core. Reasonable comparisons between predicted and experimental displacements were obtained for the idealized core having an elasticity of *400 psi* and strength of *15 psi*. It can be observed from Figure 3.14 (a) that the analysis underpredicted the displacement time history of test 1, while

Figure 3.14 (b) shows an over-estimation in displacement response from test 2. The average ratio of predicted peak displacement to experimental peak displacement listed in Table 3-1 is *0.97*; that is, the model underpredicted the experimental peak displacement of the door by *3%* on average. Ideally, however, a greater quantity of test data should be available to enhance the confidence in the semi-empirical procedure. The results of this comparison suggest that the proposed skins and stringers approach can be used to reasonably capture the dynamic displacement response of full-size doors subjected to blast loading on average, provided sufficient test data is available to calibrate the model beforehand.

An overview of the whole of data from Jacques et al. revealed that tests were conducted on *45* full AMBICO blast resistant door assemblies (Jacques et al. 2015). This work conducted dynamic SDOF analysis using resistance curves derived from a skins and stingers FEA modeling approach similar to the method described in this chapter. The results in this study concluded that the skins and stingers method of modeling created resistance curves that over-estimated and under-estimated the displacement-time histories of the *45* doors tested. However, according to the database developed, the results of analysis predictions generally over-estimated the peak displacement of the doors by around *4%* (Jacques 2016). This overall view of the data provides further validation to this door analysis method and offers reasoning for the perceived inconsistent comparisons observed in Figure 3.14.

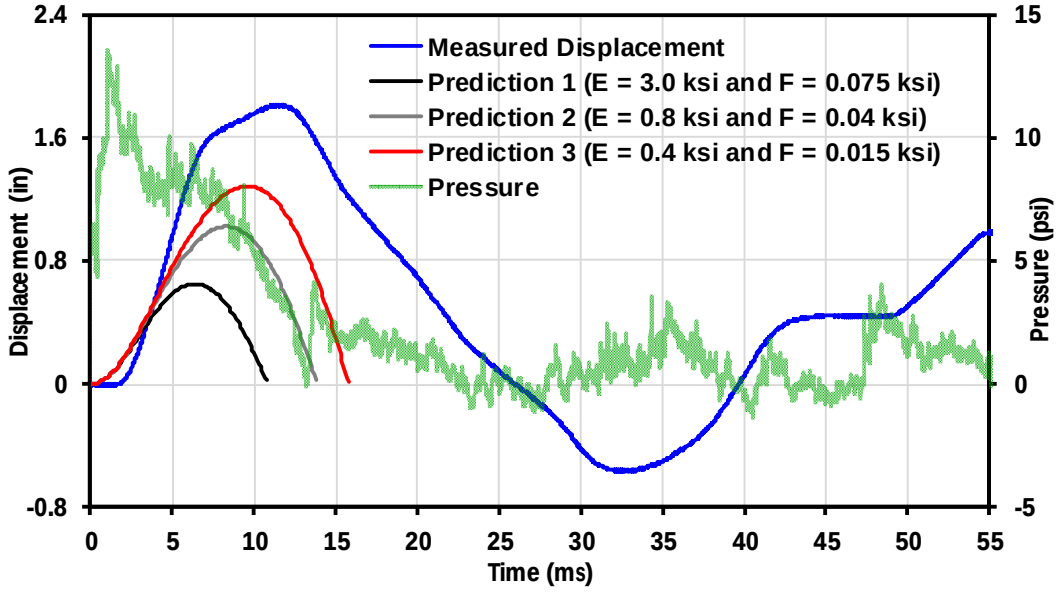

(a) Dynamic SDOF analysis results compared to measured test 1 displacement-time history.

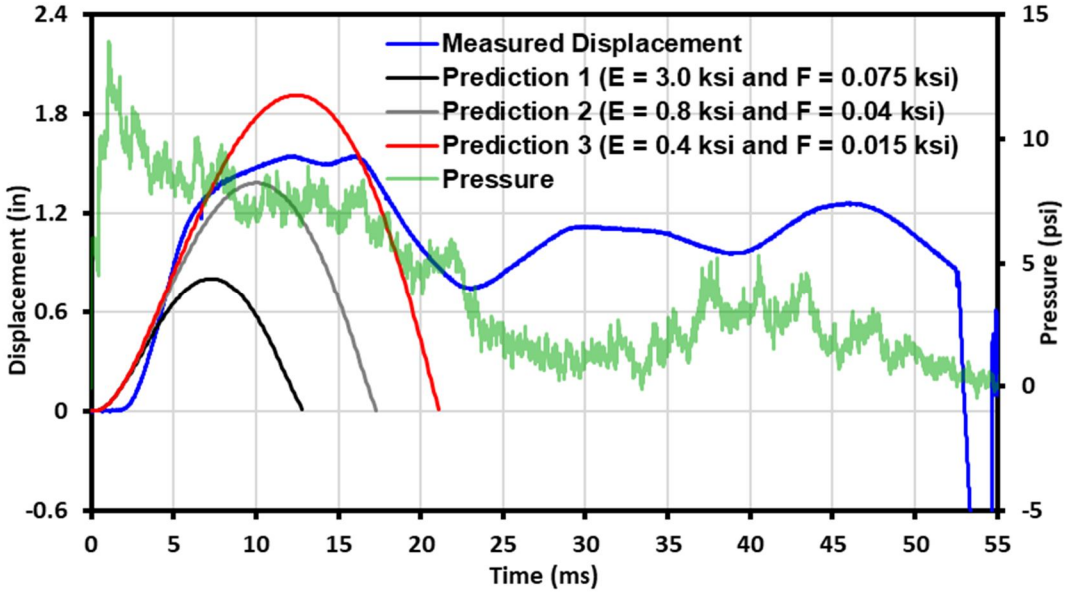

(b) Dynamic SDOF analysis results compared to measured test 2 displacement-time history.

Figure 3.14: Dynamic SDOF solutions for three iterations of bulk material properties compared with ST-9A test 1 and test 2 shock-wave displacement-time histories

Summary

A model created utilizing a skins and stringers approach was developed, which effectively reproduced the resistance curves measured during the static testing of beam-assemblies. The modeling approach developed offers a time-efficient alternative to modeling welds and connections between components in great detail by representing these high-fidelity characteristics

with an idealized bulk material. This was accomplished by calibrating the material properties of the idealized bulk material to match the performance characteristics of the beam-assembly as a whole. The overall response of the beam-assembly data was accurately captured.

The method was expanded and used in modeling a full-sized blast resistant door so that dynamic SDOF analysis could be used to predict the displacement-time response of the door subjected reflected pressure and impulse combinations. The door type (ST-9A) was chosen as its construction closely relates to future doors to be tested at Virginia Tech. Two sets of dynamic displacement-time data were also available from shock tube test results. The door model was used to create resistance curves for use in dynamic SDOF analysis so that the displacement-time predictions could be compared with the dynamic data available; this allowed for calibration of the bulk material until the SDOF analysis results provided an adequate comparison. Inconsistent results were obtained from the displacement-time data comparison; however, on average, the models accurately predicted the overall peak displacement of the door with the average ratio of predicted to experimental peak displacement of *0.97*. The final result of the analysis developed a model that could be used to predict the general dynamic displacement-time behavior of ST-9A subjected to pressure and impulse combinations that are beyond the test results used in calibration.

Chapter 4. Conclusions and Recommendations

4.1. Conclusions

Based on the literature review, experimental results of the beam-assembly tests, and development of a semi-empirical FEA-SDOF analysis procedure presented in this thesis, the following conclusions were reached:

- Skin-core door construction methodologies were observed to have an insignificant effect on the load-deformation performance of beam-assembly specimens prior to the loss of composite action between the skins and the core elements; however, construction was discovered to play a large role in performance post-composite action loss.
- Epoxy constructed beam-assemblies (Series 1) exhibited the lowest peak strength and most variable load-deflection results when compared to the welded specimens (Series 2 and 3); this proves un-conducive in design, as available strength would need to be penalized heavily to account for performance variability.
- During testing of epoxy specimens, once the capacity of the epoxy was reached at the interface between the skins and core elements, an instantaneous failure over the entire shear-span of the beam-assembly specimens was observed to occur. This catastrophic failure resulted in an immediate and wide-spread loss of composite action, which was presumed to cause crack initiation in fillet welds connecting core elements. Because of this wide-spread loss of composite action, it is highly probable that a full-size door constructed with epoxy would result in a high hazard failure.
- Observations were made, that epoxy application was only around 50% on certain areas of the core elements. An improved procedure for epoxy application, where the epoxy would coat the entire surface, would likely improve the inconsistency observed in static load testing.
- Welded specimens (Series 2 and 3) had more localized failures; wherein the welds were observed to arrest the propagating skin-core detachment during loading. This localized failure allowed both welded specimens to attain higher loads while maintaining composite

action. Series 3 specimens (with closest weld attachment specification) achieved the highest loads during testing of all other specimens.

- During testing of both Series 2 and 3 welded specimens; failures in the plug welds on the compression face always occurred. Failures on the tension skin (which was attached via fillet welds) never occurred. It may be beneficial to conduct future testing attaching the compression skins via fillet welds.
- Under blast loading, the maximum weld specification (Series 3) would be expected to perform best when performance characteristics of ASTM F2927-12 are considered. The specimens constructed under this construction achieved higher loads and greater ductility during static testing. However, it should be considered that, under blast loading, the high loads and deformations tested will likely not be reached. Thus, it would be advantageous to focus the higher efforts and cost associated with closer welds in key areas, such as along the central HSS beams of the doors, rather than in less pivotal areas such as along the stiffeners.
- After the evaluation of all hinge hardware tested, Surelock McGill S2HA7 hinges of Series 8 exhibited the best performance considering the criteria of ideal blast characteristics (which are to remain operable and avoid sudden failures). During testing, both specimens of Series 8 remained operable and undeformed. The exceptional performance is attributed to the robust build of the hinges and the integrally connected hinge reinforcement plate connection configuration.
- The frame-pin interlocking retainer system of hinge hardware Series 5 was found to provide the next highest level of protection when analyzed considering blast performance, due to the load-path provided by the interlocking frame-pin system. The blast performances of Series 4 and 9 hinge hardware were indistinguishable, as both suffered from inadequate hinge reinforcement plate connection configurations which were not integrally connected to the core framing elements of the frame and beam-assembly.
- The retainer angle and channel interlocking hinge hardware system of Series 6 failed to perform as well as Series 5, as it relied too much on tack welds that held on the retainer angles.

- Both of the pin and barrel hinge specimens of Series 7 demonstrated poor performance, as both failed catastrophically, leading to the conclusion that their blast performance would be hazardous.
- Development of an ABAQUS finite element analysis methodology utilizing a "skins and stringers" approach to generate a beam-assembly model resulted in a resistance curve which adequately captured the general load-deflection results recorded during beam-assembly testing after calibration of an idealized bulk material which shares a mesh with the stringer (internal core) elements and skins. The model also adequately captured the flexural shortening of the beam-assemblies.
- Further validation of the "skins and stringers" modeling approach was confirmed when the strategy was extended to developing a resistance curve for a full-size door, for which dynamic displacement-time data was available through previous shock tube testing. Dynamic SDOF analysis was performed, which yielded adequate comparisons to the measured data given the limited data available for comparison.

4.2. Recommendations

Based on the results and observations presented in this document, the following recommendations can be made for the development of hollow metal blast resistant doors:

- Whenever possible, blast resistant doors should be constructed with full weld attachment (maximum specification with weld spaced every *3"*) as these doors were found to provide the greatest out-of-plane resistance. However, *50%* weld specification (*6"* weld spacing) could be used for more modest blast loads provided full-scale blast testing is conducted to confirm performance suitability.
- Future testing is recommended to explore the performance of beam-assemblies with compression skins attached with fillet welds.
- Due to their highly variable and sudden failure mode, epoxy skin-core construction is not recommended for use in blast resistant doors at this time.
- Improved quality control and assurance during epoxy application could provide enhanced performance of these specimens; however, further testing with improved epoxy specimens would be required to confirm this is the case.

- Full penetration welds around the perimeter of all perpendicular HSS internal core elements would improve stiffness and strength of intersecting framing element connections; especially in cases such as the epoxy specimens where composite action was lost over a large area.
- Hinge reinforcement plates (which hinge hardware leaves are attached to) should be integrally connected to the frame and door internal reinforcing elements to provide adequate load path for hinge hardware forces and avoid the large deformations observed in tests which included "floating" hinge reinforcement plates.
- Whenever possible, hinges with fully welded knuckles should be used for blast applications as these knuckles limit deformation which is desirable during a blast event for facilitating operability after a blast event.
- As previously stated, based on the static test results, the Surelock S2HA7 hinges of Series 8 are believed to offer the most robust blast protection, followed by, in decreasing order: the externally-mounted interlocking frame-pin system of Series 5; a tie between the 6" PBB hinges of Series 4, the gallery hinges of Series 9A, and the 6" mild steel hinges of Series 9B; the hinge retainer and *4.5"* hinges of Series 6; and, the pin & barrel hinge of Series 7.
- Full-length fillet welds should be used in lieu of tack welds for connecting the retainer angles to the frames when using Series 6 hinge systems.
- Series 7 pin and barrel hinges are not recommended for use in blast resistant applications due to the sudden and unpredictable behavior observed during testing.
- Full-scale shock-tube testing is recommended to confirm all recommendations listed above as the static testing performed in this research does not capture all in-situ behavior of doors, or high strain rate effects.
- Full-scale shock-tube testing is also recommended to provide more data for validation of the finite element modeling strategies developed in Chapter 3 of this thesis.

4.3. Recommendations for Future Research

Based on the research and analysis conducted in this thesis, the following recommendations for research going forward can be made:

- Static testing conducted for purposes of skin-core construction methodologies in the future should incorporate the use of strain gauges on the compression face and tension face so that more information can be obtained relating to the critical stress which causes loss of composite action.
- To conclude more information regarding hinge hardware capacity, it would be useful to develop a test fixture that would test only hinge hardware; as in nearly every case, the beam-assembly failed before the substantial failure of the hinges was observed.
- It may be beneficial to develop a uniform load spreading device that more closely resembles actual blast loading that does not concentrate load at two points (*i.e.*, airbag loading); as it was observed during testing that flexural failure often occurred at load-point locations.
- A high-fidelity finite element modeling approach could be used to generate resistance curves of full-size doors to be compared alongside resistance curves developed using the time-efficient methods developed in this research. Using both models to evaluate the dynamic SDOF displacement-time behavior of full-size doors would be beneficial for determining whether or not the time and effort involved in high-fidelity model development are warranted.

References

ABAQUS. (2013). “ABAQUS/CEA User’s Guide (6.13).” *Dassault Systèmes*, <http://dsk.ippt.pan.pl/docs/abaqus/v6.13/books/usi/default.htm>.

Anderson, M., and Dover, D. (2003). “Lightweight, Blast-Resistant Doors for Retrofit Protection Against the Terrorist Threat.” *Proc. 2nd International Conference on Innovation in Architecture, Engineering and Construction (AEC)*, Loughborough University, London.

Armstrong, J. (2015). “Design of a Free Field Blast Simulating Shock Tube.” M.S. Thesis, Department of Mechanical Engineering, University of Ottawa, Ottawa, Canada. (doi:10.20381/ruor-3904).

ASCE. (2011). *Blast Protection of Buildings*. American Society of Civil Engineers/Structural Engineering Institute, Reston, VA (doi:10.1061/9780784411889).

ASTM. (2012). “Standard Test Method for Door Systems Subject to Airblast Loadings.” *ASTM F2927-12*, West Conshohocken, PA (doi:10.1520/F2927-12.1).

ASTM. (2016). “Test Methods for Tension Testing of Metallic Materials.” *ASTM E8/E8M – 16a*, West Conshohocken, PA (doi:10.1520/E0008_E0008M-16A).

ASTM. (2018). “Standard Test Method for Metal Doors Used in Blast Resistant Applications (Equivalent Static Load Method).” ASTM F2247-18, West Conshohocken, PA (doi:10.1520/F2247-11).

Chen, W., and Hao, H. (2014). “Experimental investigations and numerical simulations of multi-arch double-layered panels under uniform impulsive loadings.” *International Journal of Impact Engineering*, Vol. 63, pp. 140–157 (doi:10.1016/j.ijimpeng.2013.08.012).

Courtney, A. C., Andrusiv, L. P., and Courtney, M. W. (2012). “Oxy-acetylene driven laboratory scale shock tubes for studying blast wave effects.” *Review of Scientific Instruments*, Vol. 83, No. 4 (doi:10.1063/1.3702803).

DoD. (2018). “DoD Minimum Antiterrorism Standards for Buildings.” *UFC 4-010-01*, Arlington, VA.

Gallery Specialty Hardware. (2014). “Gallery Specialty GSH 918.” GSH, Toronto, Canada.

Hager Companies. (1996). “Hager Companies Full Mortise Hinges - 4 1/2" - Template.” Hager Companies, St. Louis, Missouri.

Hsieh, M.-W., Hung, J.-P., and Chen, D.-J. (2008). “Investigation on the Blast Resistance of a Stiffened Door Structure.” *Journal of Marine Science and Technology*, Vol. 16, No. 2, pp. 149–157.

Jacques, E. (2011). “Blast retrofit of reinforced concrete walls and slabs.” M.A.Sc. thesis, Department of Civil Engineering, University of Ottawa, Ottawa, Canada.

Jacques, E. (2013). “OverPressure”, Version 1.0 <http://www.ericjacques.com/overpressure/>.

Jacques, E. (2014). “RCBLAST”, Version. 0.5.1 <http://www.rcblast.ca/>.

Jacques, E. (2016). “AMBICO Blast Door Analysis Software.” Ottawa, Canada.

Jacques, E., Keene, C., and Johnson J. (2019). “Safety Policies for the Shock Tube Testing Facility at Virginia Tech.”, Department of Civil and Environmental Engineering, Virginia Tech, Blacksburg, VA.

Jacques, E., Lloyd, A., and Saatcioglu, M. (2013). “Predicting reinforced concrete response to blast loads.” *Canadian Journal of Civil Engineering*, Vol. 40, No. 5, pp. 427–444 (doi:10.1139/L2012-014).

Jacques, E., Saatcioglu, M., Lloyd, A., Berry, T., and Shinder, J. (2015). “Development of Blast Resistant Steel Doors.” *Proc., 11th International Conference on Shock and Impact Loads on*

*Structures,*14-15 May, Ottawa, Canada.

Lloyd, A. (2010). "Performance of Reinforced Concrete Columns Under Shock Tube Induced Shock Wave Loading." M.S. Thesis, Department of Civil Engineering, University of Ottawa, Ottawa, Canada., (doi:10.20381/ruor-19305).

Lowak, M. J., Idriss, J. S., and Wesevich, J. W. (2011). "Testing and Analytical Evaluation of Doors." *Proc., Structures Congress 2011*, American Society of Civil Engineers, Reston, VA., 1375–1410 (doi:10.1061/41171(401)121).

Lowak, M., Pierorazio, A. J., and Wesevich, J. (2009). *University of Ottawa Shock Tube Operating Guidelines*, Baker Engineering and Risk Consultants, San Antonio, TX.

PBB. (2003). "PBB Full Mortise Heavy Weight Template 4B60." PBB World Class Hinges, Ontario, CA.

Rao, A. A. (1987). "Fuel Air Explosives." *Defence Science Journal*, Vol. 37, No. 1, pp. 23–28 (doi:10.14429/dsj.37.5888).

Ritzel, D. V. (2007). *Upgrade of the DRDC Suffield Blast Tube Facility*. Amherstburg, Canada.

Salomoni, V. A., Mazzucco, G., Xotta, G., Fincato, R., Majorana, C. E., and Schiavon, M. (2013). "Nonlinear modelling, design, and test of steel blast-resistant doors." *Advances in Mechanical Engineering*, Vol. 2013, 15 pg (doi:10.1155/2013/908373).

SDI (Steel Door Institute). (2014). "Testing and Rating of Severe Windstorm Resistant Components for Swinging Door Assemblies." *ANSI A250.13-2014 (R2018)*, Westlake, OH. < https://www.steeldoor.org/T-DOC/ansi-250-13.php>.

SDI. (2016). "Guideline for Specifying Steel Doors and Frames for Blast Resistance." *SDI 133-16*, Westlake, OH.

Select Hinges (2015). "Select Hinges SL200 Concealed Pin & Barrel Hinge." Portage, MI.

Shen, J., Lu, G., Wang, Z., and Zhao, L. (2010). "Experiments on curved sandwich panels under

blast loading." *International Journal of Impact Engineering*, Vol. 37, No. 9, pp. 960–970 (doi:10.1016/j.ijimpeng.2010.03.002).

Surelock McGill. (2016). "Surelock McGill S2HA7 Mortised 5.75" Hinge." Surelock McGill, Lexington, KY.

Tri Tex Co. Inc. (2009). "Tri-Tex Co. Inc. 0379A Adhesive for Doors." Tri Tex Co. Inc., Quebec, Canada.

Veeredhi, L. S. B., and Ramana Rao, N. V. (2015). "Studies on the Impact of Explosion on Blast Resistant Stiffened Door Structures." *Journal of The Institution of Engineers (India): Series A*, Vol. 96, No. 1, pp 11–20 (doi:10.1007/s40030-014-0103-x).

Yuen, S. C. K., and Nurick, G. N. (2005). "Experimental and numerical studies on the response of quadrangular stiffened plates. Part I: Subjected to uniform blast load." *International Journal of Impact Engineering*, Vol. 31, No. 1, pp. 55–83 (doi:10.1016/j.ijimpeng.2003.09.048).

Appendix A: VT Shock Tube Testing Facility

A1. General

This Virginia Tech Shock Tube Testing Facility is a new addition to the Thomas M. Murray Structures Laboratory. This chapter will provide an overview of the facility, beginning with a summary of its primary components and their general construction. The facility site layout is described along with a description of the instrumentation and controls. A detailed description of shock tube operation is outlined, including procedures necessary for safety. A calibration plan is deliberated, and sample data is shown from a previous test shot taken with the shock tube at the manufacturer's plant. Future work is discussed which will serve as a continuation of this research by providing data to be analyzed using the procedures discussed in Chapter 3.

A2. Facility Description

A2.1 Overview

The Virginia Tech Shock Tube, shown in Figure A.1, is designed to generate high pressure, short-duration shock waves similar to those produced by the detonation of high explosives. The equipment is *42'* long by, at its largest cross-section, *12'* wide by *14'* tall and weighs in excess of *80,000 lbs*. The shock tube consists of three main components: (i) a detonation chamber responsible for generating blast energy through the detonation of an oxy-fuel mixture; (ii) a transition section for maintaining shock wave planarity; and, (iii) a reaction frame for mounting test specimens. Planar and non-planar test specimens up to *10' × 10'* square may be mounted to the reaction frame for simulated blast testing. A photograph of the shock tube is shown in Figure A.2. The shock tube is capable of generating reflected blast pressures in excess of *28 psi* with positive phase durations between *15* and *40 ms*. For reference purposes, this represents an equivalent hemispherical detonation of *46,000 lbs* of TNT located *330'* from the target based on Kinnery-Bulmash scaled distance relationships (Jacques 2013)

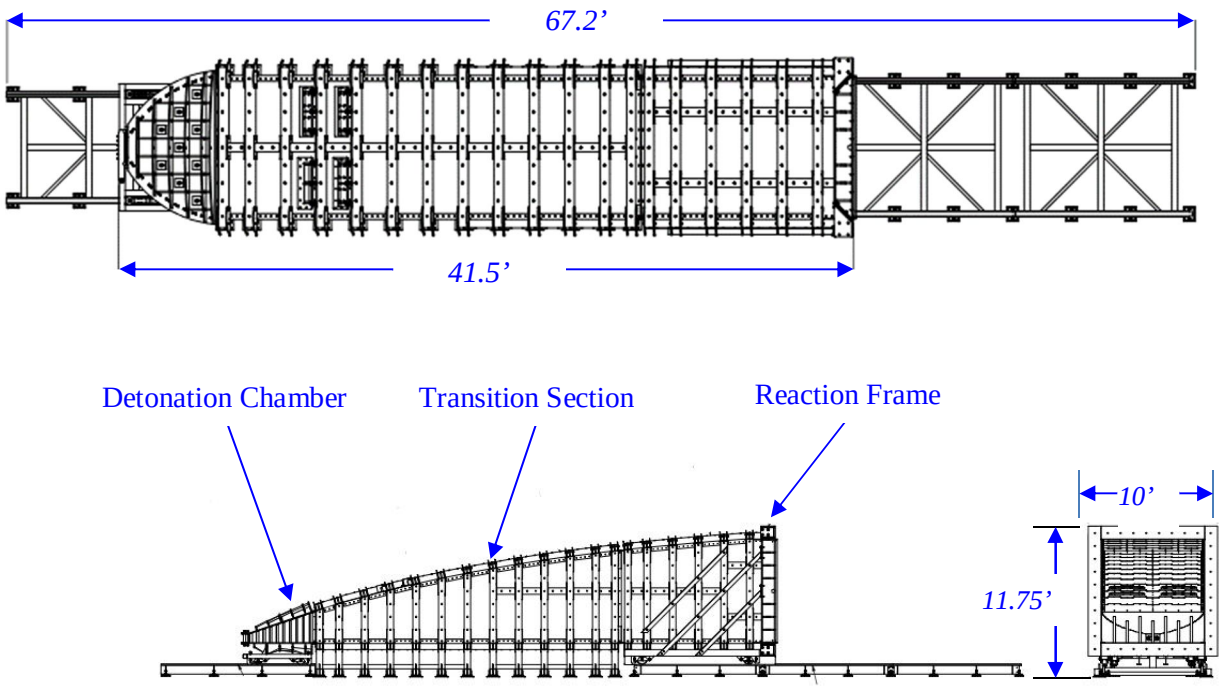

Figure A.1: Overview of the Virginia Tech Shock Tube Testing Facility.

The shock tube is driven by the detonation of a reactive gas mixture, in this case, a stoichiometric mixture of oxygen and acetylene. The driver portion of the shock tube, known as the detonation chamber, is filled with gas contained by a thin barrier material. A small pyrotechnic charge is used to ignite the mixture. One of the key advantages of detonation driven shock tubes is that thin barrier materials used as diaphragms do not impede shock wave propagation as long as there is no differential pressure between the driver and driven sections before ignition (Armstrong 2015). Detonation driven shock tubes also generate more realistic blast profiles than comparable compressed-gas shock tubes since expansion of compressed gas out of the driver creates a “jet effect” that alters the impulse imparted to the target (Courtney et al. 2012). However, there are several drawbacks to detonation driven shock tubes; namely, the additional infrastructure required for storage and handling of combustible gases and the strict safety procedures and personnel training that must be followed.

The Virginia Tech shock tube is designed to simulate blast-induced shock wave loading within a well-defined operating envelope described in terms of peak reflected pressure, reflected

impulse, and positive phase duration. The system is designed to achieve a peak reflected pressure of *30 psi*. Although the operating envelope has yet to be defined experimentally (refer to Section A3 for more details on equipment calibration), the magnitude of shock wave reflected pressure is expected to be controlled by the volume of oxy-fuel gas, while reflected impulse (and by extension, the positive phase duration) is expected to be controlled by the volume and mixture proportions of oxy-fuel gas. The base fuel is acetylene, although other gases such as ethylene or hydrogen may be used. Additional combustible gas clouds, consisting of either separate volumes or discrete gas-filled bags, can be used to increase the positive phase duration when ignited by the main oxy-acetylene charge (Ritzel 2007). However, the shock tube requires modest upgrading to accommodate a second hydrocarbon gas.

Figure A.2: Photograph of Virginia Tech Shock Tube Testing Facility.

A2.2 Shock Tube Construction

Detonation Chamber

The detonation chamber, shown in Figure A.3, is responsible for generating shock wave energy and directing it down the length of the simulator. The combustion products generated by the detonation of a stoichiometric mixture of acetylene and oxygen during are water vapor and carbon dioxide.

The detonation chamber has a clamshell shape that is *4'* long and opens to *8'* wide by *2'-4"* tall with an internal volume of *45* ft^3. The detonation chamber mates to the transition section through a *3"* long slip joint. To withstand the high pressures generated by the detonation of oxy-acetylene, the chamber is constructed with *1"* thick steel plate externally stiffened with interlocking, fully-welded *1"* thick steel stiffeners and internally with $\phi 2"$ steel rods. The detonation chamber is installed on four heavy-duty casters sitting on a track. The track is *22'* long

with a spacing of *6'* between the rails. The detonation chamber is decoupled from the transition section and is allowed to roll away to dissipate energy. When necessary, brakes can be initiated on each of the two heavy-duty casters to aid in energy dissipation and limit the movement of the detonation chamber.

(a) Back view of detonation chamber. (b) Front opening of detonation chamber.

Figure A.3: Detonation Chamber of Virginia Tech Shock tube.

The heavy-duty door on the back of the detonation chamber, shown in Figure A.4, houses the oxy-acetylene filling ports and electric match holder. A cork membrane is installed around the perimeter of the door to provide a good seal. The door is equipped with a sensor that activates a notification light on the control panel that is hardwired to prevent the shock tube from being operated if the door is not fully engaged.

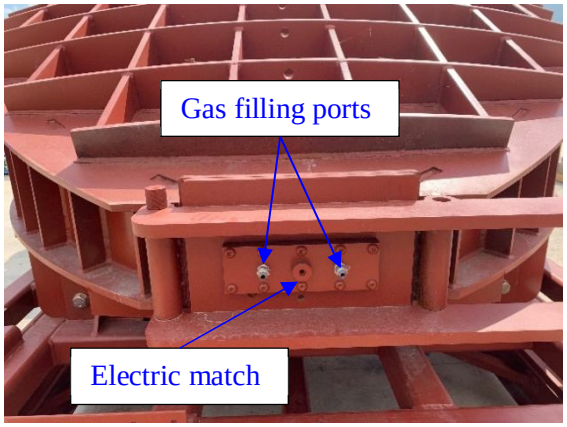

(a) External view of det-chamber door.

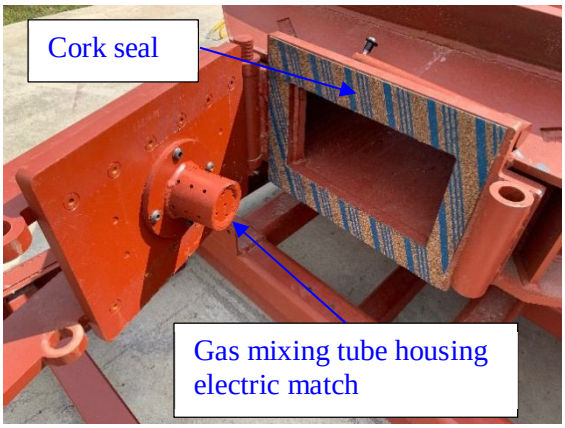

(b) Components of det-chamber door.

Figure A.4: Detonation Chamber components.

The volume of oxy-acetylene in the detonation chamber can be controlled in two ways. For small volumes of gas, typically less than $8\ ft^3$, plastic bags of known volume can be used. The bags are secured using zip ties to the gas mixing tube and inserted in the detonation chamber. For large volumes of gas, a thin barrier material can be placed in the open end of the detonation chamber to contain the gas mixture. The barrier material is sealed to the inside of the chamber using adhesive tape. The barrier material may be composed of a thin plastic film or construction paper. Small slits are made to perforate the barrier or bag to allow ambient air to escape during filling.

Proper placement of the barrier is necessary to ensure the correct volume of detonation gases. Figure A.5 provides a calibration curve that may be used to establish the volume of gas as a function of the distance of the barrier from the back wall of the detonation chamber. The curve was constructed based on the theoretical volume obtained from the shock tube AutoCAD model.

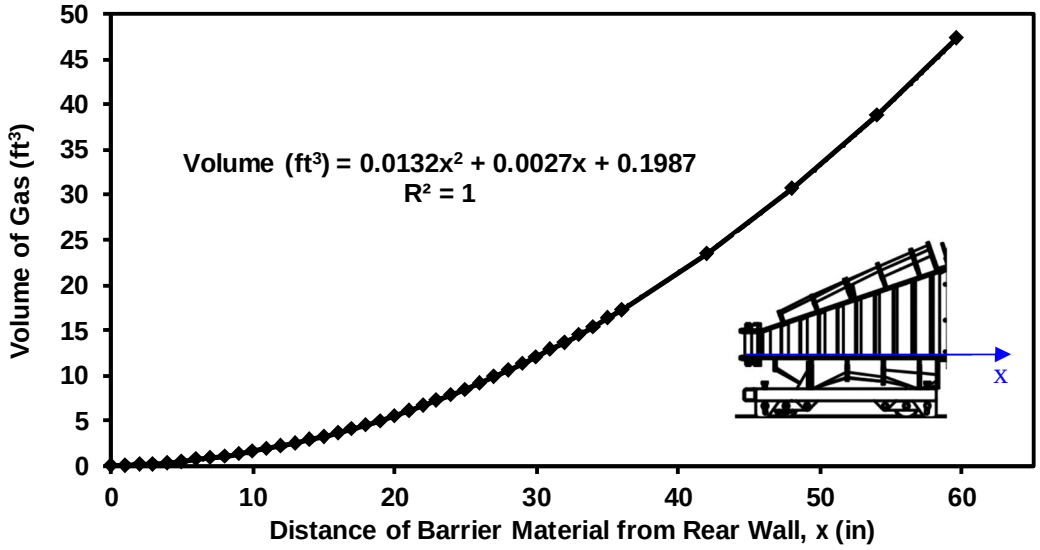

Figure A.5: Volume of gas in detonation chamber as a function of the distance from the rear wall of the detonation chamber.

The Virginia Tech Shock Tube creates a shock wave through the combustion of oxy-acetylene, the chemical reaction of which is provided below:

$$2C_2H_2 + 5O_2 \rightarrow 4CO_2 + 2H_2O + \Delta H \qquad \text{(A.1)}$$

The volume of unburned oxy-fuel in the detonation chamber is consumed and converted into reaction by-products consisting of carbon dioxide, water, and energy. The Chapman Jouget detonation parameters for stochiometric oxy-acetylene fuel-air explosions are *281 psi* pressure, *6115 ft/s* velocity, and *9295°F* temperature (Rao 1987).

Once the barrier material has been installed, shock tube filling is conducted by remotely purging the detonation chamber with oxygen gas to remove ambient nitrogen and carbon dioxide present in the atmosphere. The oxygen-rich chamber is then filled with the desired mixture and proportion of oxy-fuel. Once the desired filling parameters have been achieved, firing is initiated by remotely detonating an electric match which triggers the initiates detonation of the oxy-fuel. The resulting combustion reaction creates a drastic change in pressure, which ruptures and consumes the membrane and allows the shock wave to propagate down the simulator.

Transition Section

The transition section allows the shock wave to expand and remain planer for contact with specimens mounted at the reaction frame; it is this function that warrants its parabolic shape. The

section is *24'* long and stationary, as seen in Figure A.6. It is constructed of *½"* steel plate bolted at every *24"* to a *6×6×5/16* HSS reinforcing frame which is attached to the base plates that are anchored to the concrete pad. At the end closest to the detonation chamber, the transition section opens up to an *8'* wide by *2'-4"* tall opening and expands along its section, following a parabolic shape until it mates with the reaction cart at an *8'* wide and *7'-3"* tall opening.

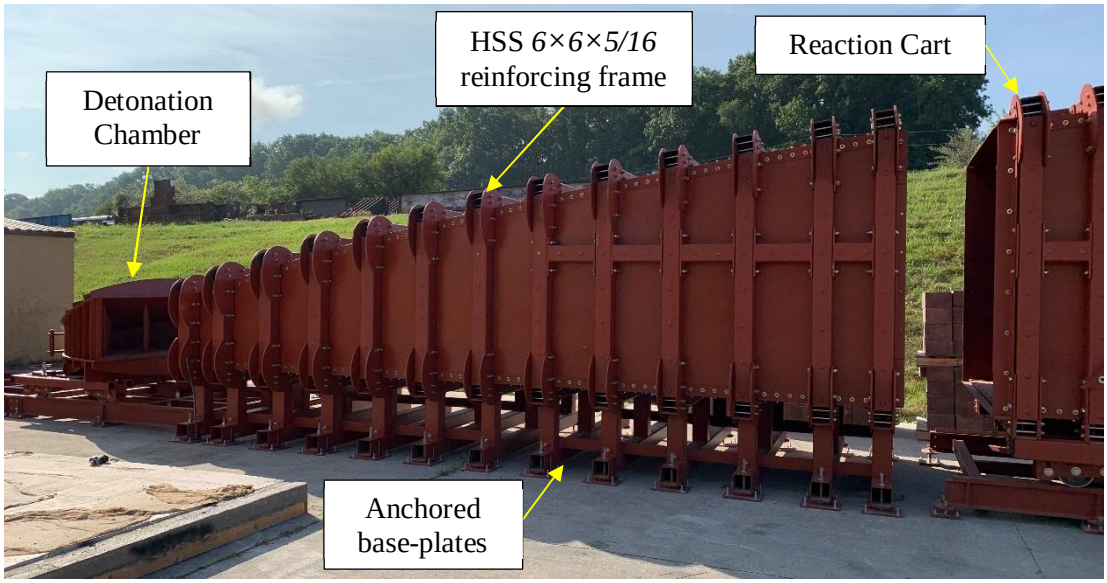

Figure A.6: Photograph of the transition section of the shock tube.

Reaction Frame

The reaction frame, shown in Figure A.7 below, is a heavily ballasted specimen mounting area, as it sits upon six forged steel casters atop a *30'* track with rails that are *7'-6"* apart. The reaction frame is attached to the transitions section via a slip joint and is allowed to roll up to *15'* after the event of a blast to dissipate energy, analogous to the detonation chamber. The sidewalls of this portion of the shock tube are also constructed of *1/2"* thick steel plate bolted at every *24"* to a *6×6×5/16* HSS reinforcing frame, only this time, the reinforcing frames are reinforced by diagonally positioned angles. The reaction frame opens to an *8'×8'* test area where specimens are attached via pre-drilled bolt holes spaced at *12"* on center to a *1"* thick steel plate surface stiffened around its perimeter at every *12"* with *1"* thick interlocking stiffener plates. At the front of the reaction cart, an extended steel frame fixture serves as both an instrumentation mounting location, and a bumper which stops the cart upon contact with the rubber bumper stoppers at the end of the track.

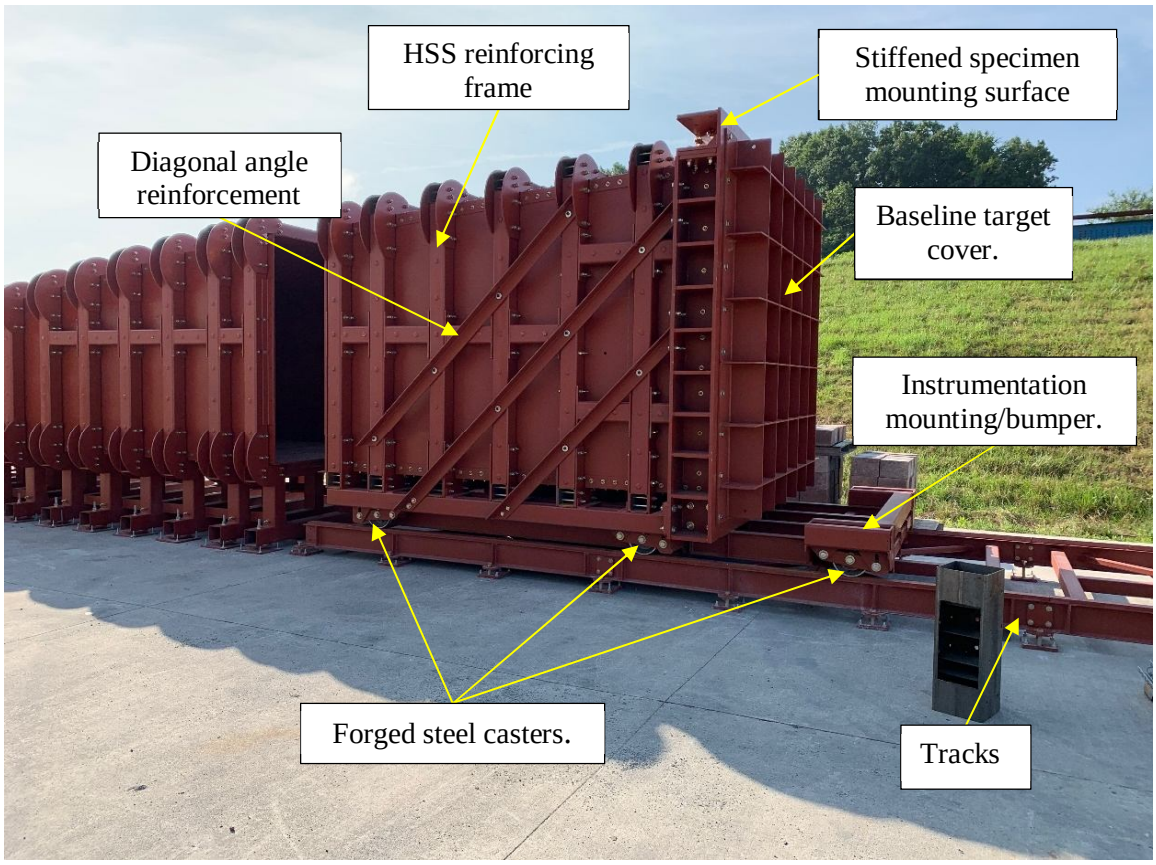

Figure A.7: Photograph of the reaction frame of the Virginia Tech Shock Tube.

A2.3 Location

The shock tube is located outdoors on the concrete apron behind the Thomas M. Murray Structures Laboratory in Blacksburg, Virginia. A plan view of the shock tube site is presented in Figure A.8. The shock tube faces away from the building in a westerly orientation. Shock tube operation is remotely monitored and controlled from a control building located adjacent to the shock tube. Compressed gas bottles and fueling manifold are located in a dedicated fueling station attached to the main laboratory building. During operation, one *310 ft^3* tank of acetylene and *200 ft^3* tank of oxygen on a cylinder cart, as well as a *200 ft^3* tank of nitrogen attached to the wall are located in the fueling station. An additional *310 ft^3* tank of acetylene and *200 ft^3* tank of oxygen are stored in the fuel storage room. Hoses and control cables are run from the fueling manifold, located in the fueling station, to the shock tube. Additional control cables are run from the fueling manifold to the control building. Hoses and cables are stored in the fueling station when not in use.

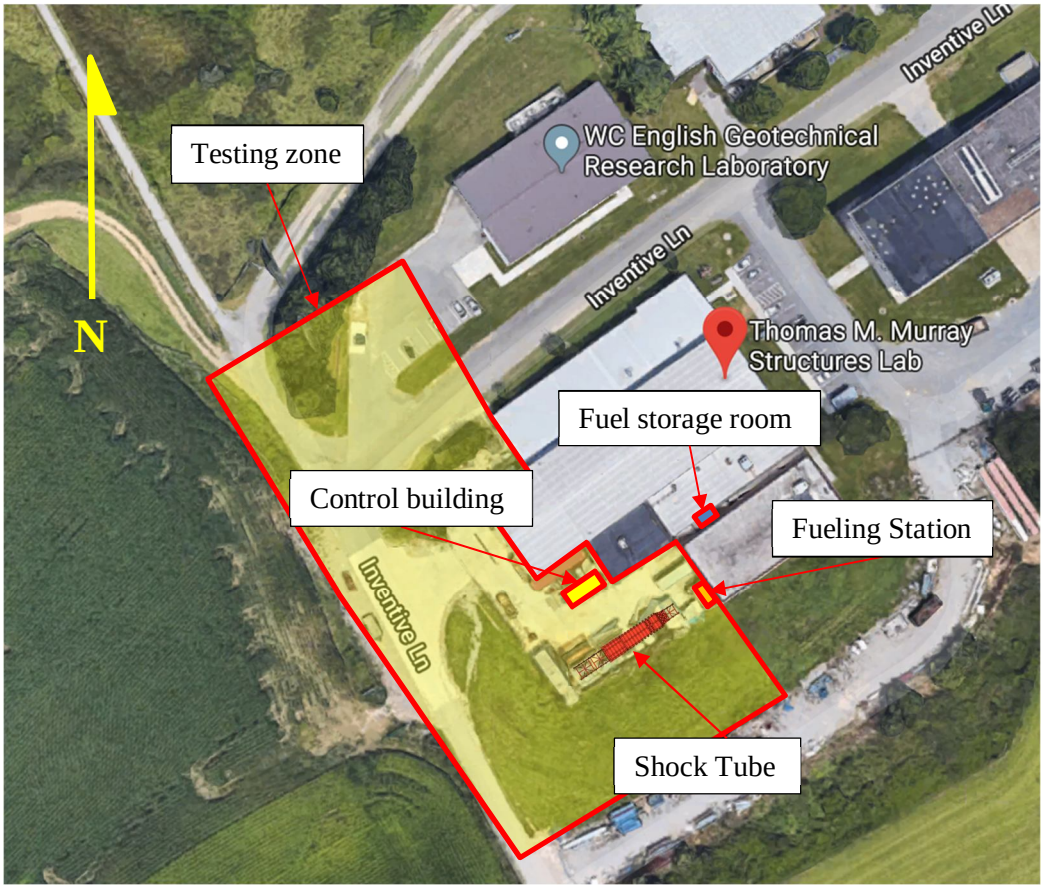

Figure A.8: Site layout of the Virginia Tech Shock Tube Testing Facility.

A2.4 Instrumentation and Control

Experimental data is monitored and recorded using an eighteen channel AstroNova TMX-18 high-speed digital oscilloscope capable of recording at *800,000* samples per second per channel. The TMX-18 consists of an integrated data acquisition system and built-in PC with a *17"* touch screen and can accommodate a wide variety of sensors and transducers. The system is triggered when one of the pressure sensors records a pressure in excess of a predetermined threshold. Data is typically recorded for *10 seconds*, with a *0.1-second* pre-trigger time. Depending on sensor requirements, excitation can be supplied by either a Kistler 24V 16-channel signal conditioner or Eventek KPS305D variable DC power supply.

Blast pressures are recorded using Endevco 8530C-100 piezoresistive pressure transducers with a range of *100 psia*. The pressure transducers are installed into 3D printed adaptors which are then mounted into the steel walls of the shock tube. The pressure transducers may be installed anywhere along the driven length of the shock tube to obtain incident pressure measurements, or they may be installed into the reflecting surface to obtain reflected pressure measurements. Specimen displacements are monitored using an array of *14"* and *28"* stroke linear potentiometers. Quarter bridge *350Ω* strain gauges are used to monitor component strains. The TMX-18 requires external bridge completion, which is provided using Campbell Scientific 4WFBS350 bridge terminals. A Photron Fastcam Mini AX50 high-speed camera is used to record specimen response in full-color at *1024×1024* resolution at frames rates up to *2,000 fps.*

Below, in Figure A.9, is a schematic of the instrumentation and operating system that is used for calibration and testing at the shock tube facility. Shock tube operation and instrumentation monitoring and recording are conducted from the control building. A control room PC and control panel, located in the control building, must be used in tandem to conduct filling operations. An electronic match is controlled used to initiate the explosive reaction in the detonation chamber. Both the control panel and the control room PC have the capability to directly shut down the gas filling operation in case of an emergency. The control room PC will be used to remotely operate the PC in the fueling station, the room behind the shock-tube which houses the Alicat Scientific flow regulator, and gases required for detonation. This computer inside the fueling station directly operates the flow regulator during the gas filling process. As previously eluded to, instrumentation operation is also conducted in the control building. The TMX-18 data acquisition system,

discussed above, collects data from the previously discussed measurement devices and triggers the high-speed camera during testing; while the computer is used to operate the camera directly.

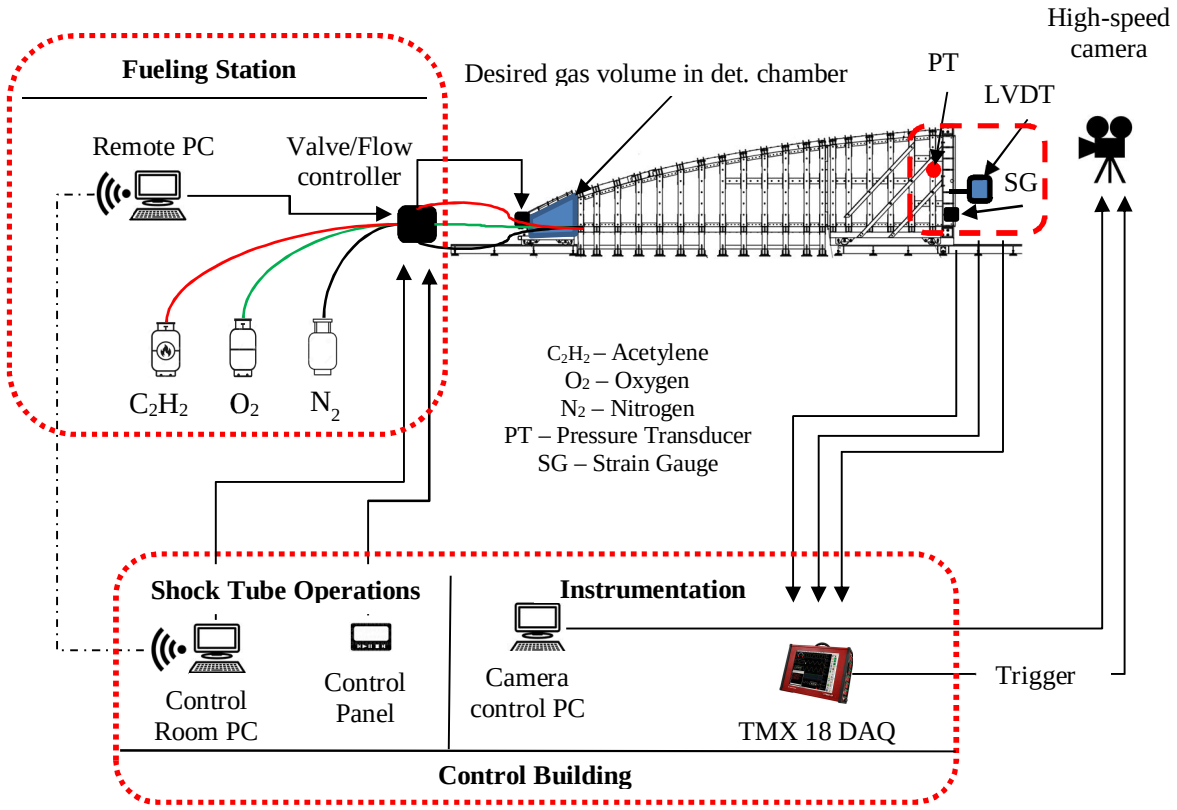

Figure A.9: Instrumentation and operations schematic for shock tube facility.

A2.5 Operating Procedure

Shock tube operation must follow a strict operating procedure to ensure a safe and repeatable firing procedure. The Virginia Tech Shock Tube Safety Document (Jacques et al. 2019) outlines the safety protocols that must be followed to ensure the safety of students, staff, faculty, and personnel at the test site. The safety procedure includes pre-test and post-test activities designed to mitigate the primary risks of combustible compressed gas, pre-mature detonation, loud noises, and potential for flying debris from test specimens. The operating procedure and safety requirements described in the following sections are based on similar procedures for the University of Ottawa Shock Tube (Lowak et al. 2009).

One Week Prior to Testing

The first portion of the safety procedure is related to notifying certain groups and personnel prior to testing such as surrounding Virginia Tech facilities, apartment complexes, and police, to avoid confusion regarding the noise disturbance accompanied by testing. These groups are to be notified of upcoming tests one-week prior to the scheduled test date. The following details must be communicated to these groups: the dates of testing, the number of tests to be conducted on each test date, a brief description of the noise generated by the shock tube and contact information for those people or facilities which have concerns or questions. The following provides a summary of the typical test procedure which is involved beginning on the day of testing.

On the Day of Testing

Three key personnel are involved in shock tube operation: the safety manager, test operator, and safety spotters.

The safety manager is responsible for maintaining contact with all other personnel involved with testing and within the test site. They have the ability to suspend testing operations if it is deemed necessary to maintain safety. The test operator, typically a trained graduate student, is in charge of operating the shock tube. The safety spotters are responsible for keeping the roads and areas immediately adjacent to the test area clear of pedestrians and traffic. They are equipped with safety vests and are in constant contact via cellphone with the safety manager throughout testing. The safety spotters are also available to answer any questions from the public regarding testing operation.

1. Prepare shock tube and instrumentation for tests according to the test plan. Check that:
    i. Test specimen or baseline target cover is properly installed.
    ii. Shock tube vents and cart sections are in the proper position for firing.
    iii. Instrumentation, including pressure gauges, structural instrumentation, and high-speed video equipment, are properly configured.
    iv. Shock tube firing parameters in the control software are correctly input.
    v. Proper fuel-air supply is connected to the filling station.
    vi. Diaphragm/air bag is properly set-up.
2. The Test Operator and Safety Manager will verify that the shock tube is ready for testing. This will include a walk-around inspection to ensure/confirm that:

i. Shock tube, test specimen, and instrumentation are properly prepared.
ii. All personnel in the Structures Laboratory have been notified and are wearing appropriate hearing protection.
iii. All personnel in the Testing Zone and the Structures Laboratory are accounted for and in sight of the control station and other safe areas.
iv. Warning signs have been posted on all doors entering the testing zone as well as the control room. These doors should not be opened during testing.

3. The Test Operator and Safety Manager will be located in the control station and watch for personnel approaching the shock tube or any other unsafe condition.
4. The Safety Manager will verify that all personnel in the control station are aware that testing is about to begin, and that proper PPE is being used.
5. The Safety Spotters will take the position at the designated location in (Figure A.8) and perform a communication check with the Safety Manager by handheld radio or cellphone.
6. The Safety Spotters will confirm that the area is clear of vehicles and pedestrians.
7. The Test Operator will report the expected size of the detonation to all personnel and explain the commands and warnings he will give prior to firing. The Test Operator will explain that only they or other appointed personnel can approach the shock tube prior to giving the "all clear" signal.
8. The Test Operator will connect fuel-air fill lines.
9. The Test Operator will man the operating controls and fill the detonation chamber with oxy-acetylene gas per the requirements of the test plan following the shock tube filling procedure.
10. Immediately prior to firing the shock tube:
    i. The Safety Spotters will confirm that the area is clear of vehicles and pedestrians by communicating with the Safety Manager via handheld radio or cellphone.
    ii. The Safety Manager will confirm that the site is secure, all personnel is accounted for, and that the shock tube is ready for firing.
    iii. The Safety Manager will give the Test Operator permission to proceed with firing.
    iv. The Test Operator will emit one loud 2-second burst from a compressed gas marine horn to notify the laboratory that the test is about to begin. After signaling with the

horn, the Test Operator will wait 10 seconds before firing the shock tube to allow personnel time to prepare for firing.

11. Immediately after firing the shock tube:
    i. The Test Operator and/or Safety Manager will approach the shock tube, disconnect gas lines, and inspect the test specimen.
    ii. The fuel-air lines will be manually turned off at the regulator, and the shock tube controls will be locked out.
    iii. The Safety Manager will brief all personnel on any hazards present and the rules for inspecting the shock tube.
12. At this point, the Safety Manager will give the "all clear" signal, close the vent valves on the driver and lock out the shock tube controls by disconnecting the control wiring.
13. The Safety Spotters will proceed to return to the Structures Laboratory from their designated positions.
14. Data collection will take place according to the limits set forth by the Test Operator or Safety Manager.
15. After the completion of data collection, the shock tube can be prepared for the next test.

Test Abort and Purging Procedures

1. In the event a test must be aborted, all personnel shall remain in a location outside the testing zone until the Safety Manager gives the all-clear signal.
2. The Test Operator will purge the gas in the detonation chamber by filling the chamber with nitrogen that is injected through the fuel line. The volume of nitrogen used to purge the shock tube must exceed the volume of oxy-acetylene by a factor of *1.25*.
3. Once the nitrogen purge has been completed, the Test Operator will open the detonation driver.
4. The "all clear" signal shall not be given until the detonation chamber is purged entirely; no one should be inside the testing zone.
5. The Test Operator shall report to the Safety Manager the issue causing a test abort. Possible issues requiring a test abort include the following:

    i. Unauthorized individuals enter the testing zone.
    ii. The testing zone is not properly secured.

iii. Failure of the diaphragm/air bag inside the detonation chamber.

6. Once the issue is corrected, and the detonation chamber is fully purged, personnel shall proceed to the Operating Procedure start.

A3. Calibration Plan

The Virginia Tech Shock Tube Testing Facility requires calibration to establish critical information about reflected pressure and impulse combinations that can be generated using the shock tube, as well as the planarity of the shock-wave that makes contact with a given target. Calibration will require performing a number of detonations using progressively increasing volumes of oxy-acetylene gas and measuring the resulting reflected pressure and impulse at the stiffened reflecting calibration plate. Other parameters that must be measured during the calibration tests are the planarity of the shock wave as well as the movement of both the reaction cart and the detonation chamber cart. Several replicate tests will be performed to establish repeatability of the system. The following sections outline the calibration plan.

A3.1 Simulator Calibration Curves

The results of the calibration tests will be used to establish calibration curves that will be used to determine the effect of varying the volume of oxy-acetylene on reflected pressure, reflected impulse, and cart movement during shock tube operation. To create the pressure and impulse calibration curves, a pressure gauge mounted *2"* from the surface of the calibration plate will record the pressure-time history. Ten volumes of gas will be tested, in increments of *1* ft^3 from *1* ft^3 up to *10* ft^3. Three replicate tests will be taken for each oxy-fuel volume to establish consistency and repeatability of operation. A plot of the peak reflected pressure against volume of gas, created using the average peak reflected pressure at each volume increment, will serve as the peak reflected pressure calibration curve. The pressure-time histories collected during these shots will then be integrated to determine the average peak impulse for each gas increment. Once average impulse values are determined at each volume increment, a plot should be created of average peak impulse against volume of gas, which will serve as the peak impulse calibration curve. During these shots, measurements will also be taken of both detonation chamber and reaction cart movement with

large deflection laser displacement transducers. All measurements for the above-mentioned calibrations can be collected in a table format, which follows Table A-1.

Table A-1: Sample calibration data for Peak Reflected Pressure, Impulse, and Cart Movement Calibration Curve Values.

Volume Increment (ft^3)	Actual Volume (ft^3)	Peak Reflected Pressure P_r (psi)	Peak Reflected Impulse I_r (psi-ms)	Test Area Cart Movement (in)	Detonation Cart Movement (in)
1	Vol. 1	Pressure 1	Impulse 1	Distance 1	Distance 1
	Vol. 2	Pressure 2	Impulse 2	Distance 2	Distance 2
	Vol. 3	Pressure 3	Impulse 3	Distance 3	Distance 3
…1 ft^3 increments	…	…	…	…	…
…10	Vol. 1	Pressure 1	Impulse 1	Distance 1	Distance 1
	Vol. 2	Pressure 2	Impulse 2	Distance 2	Distance 2
	Vol. 3	Pressure 3	Impulse 3	Distance 3	Distance 3

A3.2 Determination of Planarity of the Shock Wave

To determine the planarity of the shock wave generated by the system, three shots are to be taken with *3 ft^3*, *6 ft^3* and *10 ft^3* of oxy-acetylene. The shots will target the reflecting calibration plate mounted at the testing area which will be instrumented with *12* piezoresistive dynamic pressure gauges arranged in the pattern shown in Figure A.10, similar to the shock wave planarity analysis performed by (Lloyd 2010, Jacques 2011) at the University of Ottawa. The pressure gauges will record the reflected pressure-time history of each shot; from this, the reflected impulse at each shot will be found. The reflected pressure data recorded at each point will then be compared with respect to arrival time and magnitude in Table A-2 below to analyze the shape of the shock wave generated.

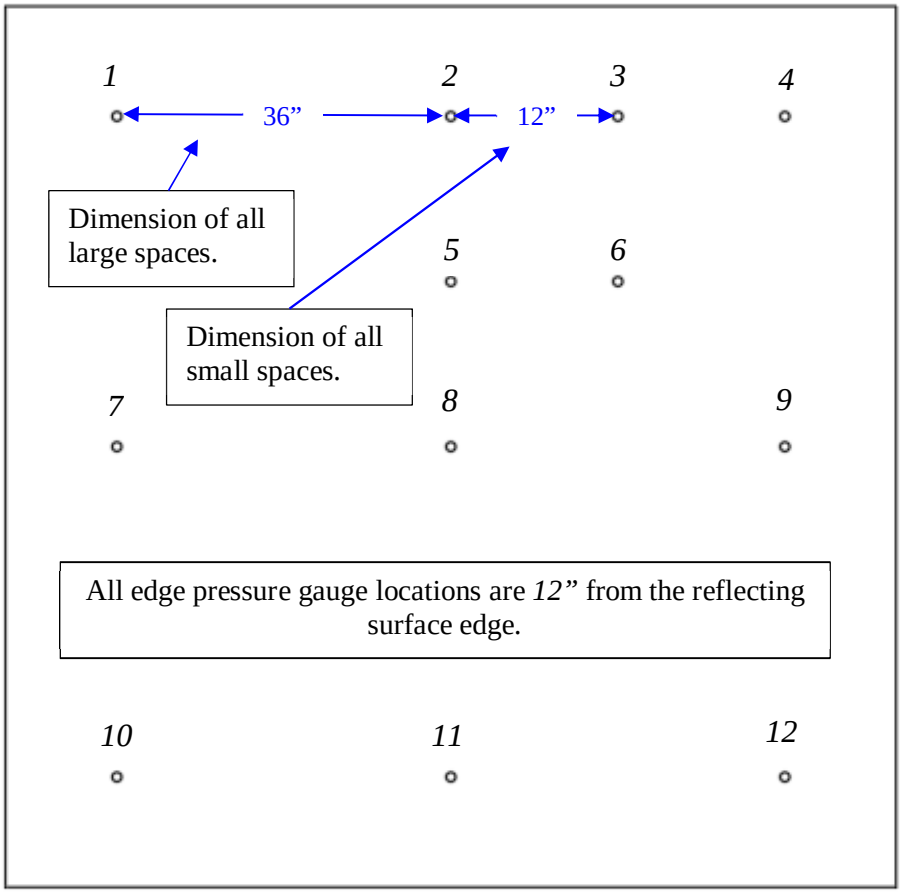

Figure A.10: *10'×10'* Steel Calibration Plate Reflecting Surface with Gauge Mount Locations (Shown from Inside shock-tube).

Table A-2: Properties for Analysis of Shock Wave Planarity on the Reflecting Calibration surface.

Gauge Number	Gauge Location		Reflected Pressure	Reflected Impulse	Positive Phase	Relative Time of	Positive Phase	Reflected Pressure	Reflected Impulse
	x (in)	y (in)	P_r (psi)	I_r (psi-ms)	t_d (ms)	t_a (ms)	$T_d/t_{d,max}$	$P_r/P_{r,max}$	$I_r/I_{r,max}$
1									
…									
12									

A4. Sample Test Data

The following discussion provides an example of how test pressure data will be processed per the calibration plan. The shock tube was operated at the manufacturer's facility on *April 19, 2019*. A volume of *7.8* ft^3 of oxy-acetylene was detonated during the test, which is about *17%* of the total maximum volume in the detonation chamber. A pressure transducer mounted at position *8* of the calibration plate, shown in Figure A.10, was used to record the pressure-time history. The pressure- and impulse-time history recorded during the test are plotted in Figure A.11. Inspection of the data revealed that the peak reflected pressure was around *21 psi* with a positive phase duration of *25 ms* and a peak reflected impulse of around *135 psi-ms*.

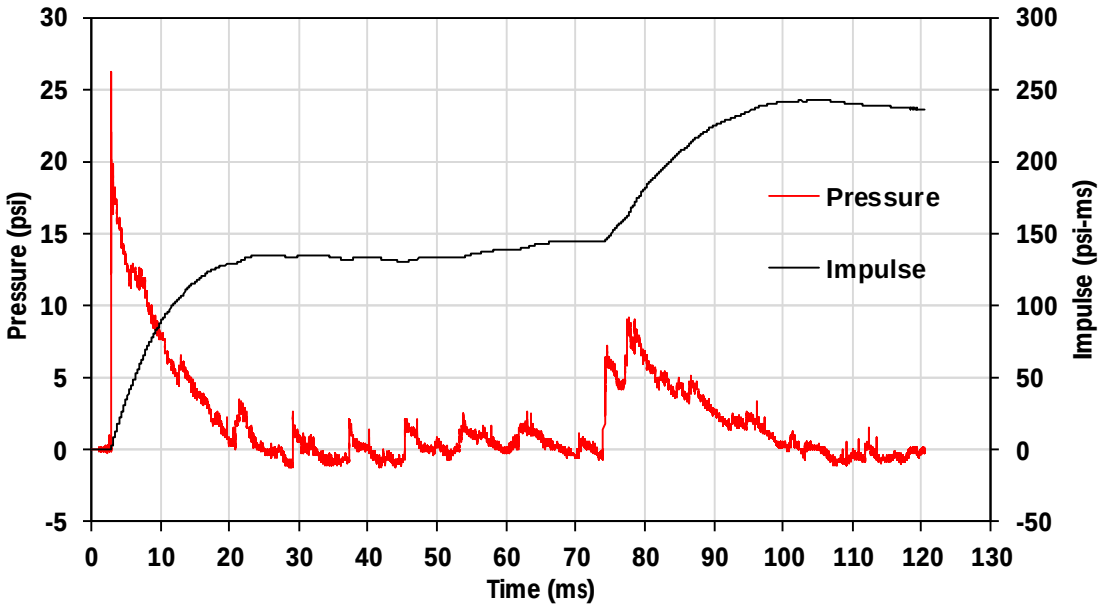

Figure A.11: Pressure and impulse-time histories for test shot 1 using the Virginia Tech Shock Tube.

Inspection of the pressure curve of Figure A.11 reveals a series of reoccurring pressure spikes are the initial shockwave has passed. These repeated spikes, which occur every *8 ms*, are believed to have been caused by the vibration of the calibration plate which is picked up by the pressure transducer. The pressure curve shown in Figure A.11 can also be used to approximate the velocity of the shock wave. The second pressure spike at *78 ms* occurs after the initial reflected wave propagates down the length of the shock tube and back. Using the length of the shock tube, $L = 41.5\, ft$, and the time between the initial and secondary reflected waves, $\Delta t \approx 75\, ms$, the average shock front velocity can be established as $v_o = 2L/\Delta t = 1{,}213\, ft/s$, or *Mach 1.08*.

A5. Future Work

The Virginia Tech Shock Tube Testing Facility will be used to conduct the next phase of work for AMBICO through the testing of full-size door assemblies. A test fixture has been designed and constructed at the facility, shown in Figure A.12 below, to accommodate three full-size door assembly models. A total of ten blast resistant door assemblies are to be tested using the Virginia Tech Shock-Tube Testing Facility (sized *3'×7'*, *4'×7'* and *6'×7'*). Displacement-time data collected during testing and FEA modeling strategies developed in Figure A.12 will be used to develop resistance curves for inclusion in a database for AMBICO blast-resistant design software.

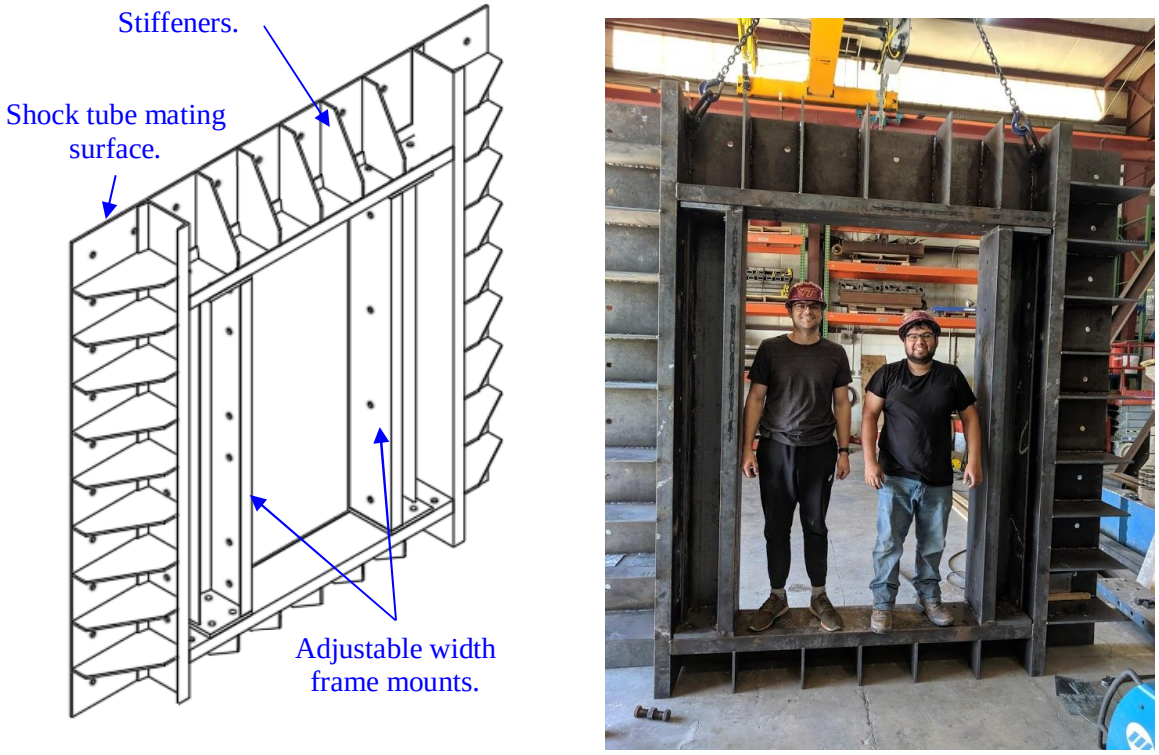

(a) Conceptual rendering of blast resistant door assembly test fixture.

(b) Photograph of the completed test fixture prior to painting.

Figure A.12: Shock tube test fixture for full-size door assembly testing.